FREE VIBRATION ANALYSIS

OF TAPERED COMPOSITE BEAMS

USING HIERARCHICAL FINITE ELEMENT METHOD

Lin Chen

A Thesis

in

The Department

of

Mechanical and Industrial Engineering

Presented in Partial Fulfillment of the Requirements

for the Degree of Master of Applied Science at

Concordia University

Montreal, Quebec, Canada

November 2004

Your file Votre référence
ISBN: 0-494-04415-2
Our file Notre référence
ISBN: 0-494-04415-2

ABSTRACT

Free vibration analysis of tapered composite beams using hierarchical finite element method

Lin Chen

Compared with the conventional finite element method, hierarchical finite element method has the advantages of using fewer elements and obtaining better accuracy in the calculation of natural frequencies, buckling loads, displacements and stresses. These advantages are also shown in the analysis for uniform or thickness-tapered composite beams. In many of the existing works on the dynamic response, the effect on the mechanical behavior of plies in the tapered composite beam caused by the taper angle is ignored if the angle is small. In the present thesis, this effect is always considered and quantified based on the three-dimensional ply stiffness analysis. The free vibration response of tapered composite beam with different taper angles is studied. Also, based on the ply stiffness analysis, the response of the taper configuration and laminate configuration on the stiffness and vibration response of the tapered beam are studied. Because of the complicated mechanical behavior of the tapered composite beam and the complexity of the analysis, no exact solution is available at present and therefore, Ritz method and hierarchical finite element method have been used for the calculation of free vibration response. The free vibration response of different types of tapered composite beams with and without axial force are analyzed first using Ritz method. Then the

developed hierarchical finite element formulation is applied to the same analysis. Both the classical laminate theory and first-order shear deformation theory are considered in the analysis. The efficiency and accuracy of the developed formulation are established in comparison with available solutions, where applicable, as well as with the results obtained using Ritz method and conventional finite element formulation. Finally, a detailed parametric study encompassing the influences of boundary conditions, laminate configuration, taper angle, taper model and axial force on the natural frequencies of the beam is performed. The NCT301 graphite-epoxy composite material is considered in the study.

ACKNOWLEDGMENTS

I would like to express my gratitude to all those who gave me the possibility to complete this thesis. First and foremost, I want to express my most sincere gratitude to my supervisor Dr. Rajamohan Ganesan, not only for his guidance in writing this thesis, but also for his advice, concern, patience, and encouragement during my study and research in Concordia University.

Needless to say, that I am grateful to all of my colleagues in our small lab: Karun Nayyar, Daiying Liu, Shashank Venugopal and Vijay Kowda. Not only are they the ideal officemates, but are also good friends.

Here, I would also like to express my heartfelt appreciation to my wife Li Zhang. Without her support and encouragement this work would not have been possible.

CONTENTS

List of Figures

List of Tables

Nomenclature

α	Taper angle in tapered beam
θ	Orientation of ply
ε_{ij}	Strain corresponding to coordinate system $x_1x_2x_3$
σ_{ij}	Stress corresponding to coordinate system $x_1x_2x_3$
S_{ij}	Coefficient of compliance matrix
C_{ij}	Coefficient of stiffness matrix
ε'_{ij}	Strain corresponding to coordinate system $x'y'z'$
σ'_{ij}	Stress corresponding to coordinate system $x'y'z'$
$\{\varepsilon^{123}\}$	Strain vector corresponding to coordinate system $x_1x_2x_3$
$\{\sigma^{123}\}$	Stress vector corresponding to coordinate system $x_1x_2x_3$
$[T_{\sigma\theta}]$	Stress transformation matrix of ply due to angle θ
$[T_{\varepsilon\theta}]$	Strain transformation matrix of ply due to angle θ
$[T_{\sigma\alpha}]$	Stress transformation matrix of ply due to angle α
$[T_{\varepsilon\alpha}]$	Strain transformation matrix of ply due to angle α
$[\ ]^{-1}$	Inverse of the matrix
$[\ ]^{T}$	Transverse of the matrix
$\overline{S}_{ij}$	Coefficient of the transformed ply compliance matrix
$\overline{C}_{ij}$	Coefficient of the transformed ply stiffness matrix

$\overline{Q}_{ij}$	Coefficient of the reduced ply stiffness matrix
φ_x	Rotation about y-axis
w	Displacement in thickness direction
L	Length of the beam
b	Width of the beam
H	Height of the beam
h	Ply height in z-direction
ρ	Density
ρ_r	Density of the resin
E_1	Modulus of elasticity in fiber direction
E_2	Modulus of elasticity in transverse direction
ν_{21}	Poisson ratio of ply
G_{23}	Out-of-plane shear modulus
G_{13}	In-plane shear modulus
E	Modulus of elasticity of resin
ν	Poisson ratio of resin
G	Shear modulus of resin
u	Displacement in x-direction
v	Displacement in y-direction
u_o	Mid-plane displacement in x-direction
v_o	Mid-plane displacement in y-direction
w_o	Mid-plane displacement in z-direction

κ_x^o Curvature of the mid-plane

M_x Bending moment per unit width

N_x Axial force per unit width

A_{ij} Coefficients of stretching stiffness matrix of composite beam

B_{ij} Coefficients of bending-stretching coupling matrix of composite beam

D_{ij} Coefficients of bending stiffness matrix of composite beam

I Moment of inertia

A Cross-section area

z_k Coordinate of the top surface of the k^{th} layer of composite beam

U Strain energy

T Kinetic energy

t Time variable

W Magnitude of vibration

H_L Total height of laminate

H_r Total height of resin

ρ_L Density of laminate

c_i Undetermined coefficient in Ritz method

ϕ_i Interpolation function in Ritz method

$[K]$ Stiffness matrix of beam

$[M]$ Mass matrix of beam

w_i Displacement at i^{th} node

θ_i Rotation at i^{th} node

N_i^w Interpolation function for the deflection

N_i^θ Interpolation function for the rotation in the Euler-Bernoulli beam theory

N_i^ψ Interpolation function for the rotation in the Timoshenko beam theory

$\{u\}$ Vector containing nodal displacements and rotations

N_{cr} Critical buckling load

Ψ Total rotation of the cross-section in Timoshenko beam

k Shear correction factor used in Timoshenko beam theory

ω Natural frequency of the beam

Chapter 1

Introduction, Literature Survey and Scope of the Thesis

1.1 Dynamic analysis in mechanical design

Concern for vibration phenomena can have various motivations. Safety considerations require that we identify situations that cause excessive motions, for they will result in the generation of large stress. Even if a vibration does not damage a system, it might be a source of physical discomfort.

There are two general types of vibration: free and forced. In the case of a free vibration, there are no externally applied forces during vibration, but an external force may have caused an initial displacement or velocity in the system. If the external force is then removed, the body continues to vibrate because of the action of elasticity and mass. Natural frequency, which is a property of an elastic system, is a frequency of the system when it undergoes a free vibration without friction. If the frequency of exciting force gets close to the frequency band of the natural frequencies of the structure, the mechanical component experiences severe vibration due to resonance. The resonance will decrease the lifetime of the structure and causes unpredictable failures. It is, therefore, essential to carry out vibration analysis as an inherent part of mechanical design.

1.2 Composite materials and structures

A composite material consists of two or more materials of different nature but with complementing mechanical properties and allows us to obtain a material that the performance characteristics of which are greater than that of the components taken separately [1]. The major reason for the success of composite materials is that no homogeneous structural material can fulfill all the requirements for a given application. Originally, structural composites were developed for the aerospace industry as they offered attractive properties of stiffness and strength, compared to their weight. Thus, they replaced previously used aluminum alloys, which also combined quite good mechanical properties with low specific weight. Furthermore, fiber composites provide the unique opportunity to simultaneously optimize structure configuration, material make-up, fabrication process and structural integrity.

Today, composites have found their way into a much more wide range of applications than simply the aerospace sector. Fiber reinforced composite materials are the engineering materials which are most commonly used in modern industries and composite beam is one of the most widely used structural elements. They are made by stacking together many plies of fiber-reinforced layers in different orientations to achieve the desired properties. Then these stacked layers are permanently bonded together under heat and pressure using a hot press or autoclave. Some specific applications of composite beams need to be stiff at one end and flexible at the other end. Such beams can be made by dropping off some plies at discrete locations to reduce the stiffness of the beams. This

results in a tapered shape, which is to be discussed in the present thesis.

1.3 Finite element method

The finite element method (FEM) is one of the most powerful numerical procedures for solving the mathematical problems of engineering and physics. Its application ranges from static analysis of a simple component to a complicated fluid flowing system. In FEM, any continuous quantity, such as temperature, pressure or displacement, can be approximated by a discrete model composed of a set of piecewise continuous functions defined over a finite number of subdomains. FEM has been widely used and developed. Nowadays, some advanced formulations have been introduced, among them is the hierarchical FEM (HFEM). In conventional FEM, a beam element is modeled using two nodes at the ends where each node has two degrees of freedom. Therefore, a large number of elements are needed to achieve an acceptable accuracy. In HFEM, some polynomial or trigonometric terms are added to the displacement and rotation functions in order to obtain extra degrees of freedom. Thus, the same accuracy can be achieved by using much less number of elements. This results in rapid convergence. The present thesis investigates the capability of the HFEM to provide the desired accuracy and speed of convergence for free vibration analysis of tapered composite beams.

1.4 Literature survey

In this section a comprehensive literature survey is presented on the vibration of composite beams and on the application of the finite element method to composite beams. Important works done on the dynamic analysis of uniform and thickness-tapered composite beams by finite element methodologies have been chronicled. The majority of works done on the HFEM analysis of beams and plates are limited to homogeneous material or based on the Classical Laminate Theory (CLT). The works on the HFEM analysis of composite beams are presented at the end, though the quantity of such works is of course very limited.

1.4.1 Dynamic analysis of composite beams

Most of the analysis works on composites are limited to static analysis. At the same time, the works on dynamic analysis of composite plates or shells have concentrated on uniform laminates. Study on the dynamic analysis of tapered laminated beams has been scarce despite their applicability in important structures.

Reddy [1] used virtual work principles, and variational methods to study the static and dynamic response of laminated composite plates based on the classical and first-order shear deformation theories of laminated plates. Whitney [2] derived the foundation in the theory of uniform laminated anisotropic plates and beams, including the problems of bending under transverse load, stability, and free-vibration. Bertholet [3] and Jones [4] described the exact solutions for free vibrations of laminated composite beams. Krishnaswamy *et al* [5] derived the governing equations of laminated composite beams using the Hamilton's principle and presented the analytical solutions. Noor [6] studied

the free vibration of simply supported symmetric laminated plate based on classical laminate theory, which neglects the effects of the rotary inertia and shearing deformation. Miller and Adams [7] studied the vibration characteristic of orthotropic fixed-free beams based on the classical laminate theory. Teoh and Huang [8] made a theoretical analysis of the vibration of fiber reinforced composite beams based on a Timoshenko beam theory. Chen and Yang [9] carried out static and dynamic analysis of symmetrically laminated beams. Chandrashekhara *et al* [10] presented the exact solutions for the free vibration of symmetrically laminated composite beams with arbitrary boundary conditions. First-order shear deformation and rotary inertia have been included in the analysis. Abramovich [11] obtained exact solutions based on high-order shear deformation theory for symmetrical composite beams. Shear deformation and rotary inertia are included in the analysis. Exact expressions for the frequency equation and mode shapes of composite Timoshenko beams with cantilever end conditions are derived by Banerjee [12] in explicit analytical form by using symbolic computation. He [13] also studied the free vibration of Timoshenko beams with axial force. In Cortinez and Piovan's [14] paper, a theoretical model is developed for the dynamic analysis of composite thin-walled beams with open or closed cross-sections. Hodges *et al* [15] studied the free vibration of composite beams using exact integration method and mixed finite element method. They discuss the influences of laminate configuration on the natural frequencies.

Reddy and Khdeir [16] dealt with the free vibration behavior of cross-ply composite laminates under various boundary conditions considering the shear deformation laminate theory. Chandrashekhara and Bangera [17] studied the free vibration characteristics of laminated composite beams using a third order shear

deformation theory. Eisenberger *et al* [18] obtained the exact vibration frequencies of generally laminated beams, considering the effect of rotary inertia and shear deformations. They concluded that the effect of shear in laminated beams is more significant than in homogenous beams, due to the fact that the ratio of extensional stiffness to the transverse shear stiffness is high. Hjela and Teboub [19] used symbolic computations to analyze generally orthotropic composite beams based on the first order shear deformation theory. Singh and Abdelnassar [20] studied the forced vibration response of composite beams considering a third order shear deformation theory. Zappe and Lesiutre [21] used a smeared laminate model to study the dynamic analysis of laminated beams including the effects of transverse shear and rotatory inertia.

Few researchers have investigated tapered composite beams. Farghaly and Gadelrab [22] studied the natural frequency of a one-span composite beam with a stepwise variable cross-section. They concluded that in addition to the results obtained for the conventional beams, the stiffness to mass ratio for the composite stepped cantilever beam may give higher natural frequencies than those made of conventional materials. Rao and Ganesan [23] investigated the harmonic response of tapered composite beams using finite element method based on a higher order shear deformation theory, considering uniaxial bending and ignoring the interlaminar shear stresses. Nabi and Ganesan [24] developed a general finite element based on a first-order deformation theory to study the free vibration characteristics of laminated composite beams. They also conducted a parametric study on the influence of beam geometry and boundary conditions on natural frequencies. Karabalis and Beskos [25] used finite element method based on an exact flexural and axial stiffness matrix and approximate consistent mass and

geometric stiffness matrices to study a linearly tapered beam with constant width. Tong *et al* [26] obtained an analytic solution for free and forced vibrations of stepped Timoshenko beams. He, Hoa and Ganesan [27] presented a review of recent developments in the analysis of tapered laminated composite structures with an emphasis on interlaminar stress analysis and delamination analysis. Recently, Abd EL-Maksoud [28] studied the dynamic analysis of uniform and mid-plane tapered composite beams by using conventional and higher order finite element formulations. Zabihollah [29] presents the vibration and buckling analysis of uniform and tapered composite beams using conventional and advanced finite element methods based on the classical laminate theory and the first-order shear deformation theory.

1.4.2 Hierarchical finite element method

The finite element method is a powerful tool for the analysis of structures. The standard finite element method is to divide the domain of interest into a number of smaller – although not necessarily identical – sub-domains called Finite Elements. The solution is then approximated by locally admissible polynomial functions. Various procedures have been developed to achieve more accuracy and rapid convergence of solutions. Broadly these fall into two categories: The most common procedure is to increase the number of elements while keeping the degrees of freedom of each element fixed. This is termed as the *h*-version of the finite element method, or simply the finite element method. The other procedure involves keeping the mesh size constant and letting the degree of the approximating polynomial to tend to infinity [30,31]. This approach is

better known as the *p*-version of the finite element method or the Hierarchical Finite Element Method (HFEM).

Many researchers have applied conventional FEM to study the vibration of beams. Cook [32], Zienkiewicz [33] and Reddy [34] investigated the vibration of Euler-Bernoulli beams made of conventional materials. Similar works have been done on the dynamic analysis of Timoshenko beams [35,36,37]. Some researchers extended the study to tapered beams. Thomas and Dokumaci [38] treated the dynamic analysis of tapered beams by using an internal node element considering the total deflection and bending slope as the co-ordinates at the two terminal nodes and two internal nodes giving eight degrees of freedom to the element. Thomas and Abbas [39] considered four degrees of freedom per node and two nodes at the ends to obtain stiffness and mass matrices for tapered beams based on the Euler-Bernoulli beam element. In this model, the deflection, rotation, curvature and gradient of curvature are considered as degrees of freedom. Cleghorn and Tabarrok [40] presented a finite element model for free vibration of lineary-tapered Timoshenko beams.

Some research works have been carried out on the dynamic analysis of composite beams or plates using conventional FEM. Shi *et al* [41] presented a finite element model for higher order plate theories for the vibration analysis of composite beams and plates. Ramtekkar *et al* [42] used a mixed finite element formulation to calculate the natural frequencies of laminated beams. Rao and Ganesan [43] studied the natural frequencies of tapered composite beams considering the shear deformation.

The works on the dynamic analysis of beams using HFEM are very few. With regards to the HFEM, Han and Petyt [44, 45] used the popular Legendre polynomials in

the Rodrigues form to study the free and forced vibration of laminated rectangular plates. They [46-50] also conducted the non-linear dynamic analysis of plates using HFEM. West *et al* [51] discussed the limitations associated with the use of polynomials in hierarchical versions because of the ill-conditioned higher order polynomials. Some researchers preferred trigonometric functions to polynomial functions. Houmat [52] investigated linear plate vibration by the HFEM and compared trigonometric shape functions with Legendre polynomials. He concluded that trigonometric HFEM yields better accuracy in some cases. Leung and Chan [53] and Krahula and Polhemus [54] used the Fourier series to increase the internal degree of freedom. Barrette *et al* [55] presented the vibration analysis of stiffened plates using hierarchical finite elements with a set of local trigonometric interpolation functions. The trigonometric functions showed great numerical stability. Recently, Nigam [56] used hierarchical finite element method to investigate the static and dynamic response of uniform laminated composite beams. He used both polynomial and trigonometric functions and compared the convergences and accuracies. He found that the latter one performs better than the former one. Zabihollah [29] extended Nigam's work to tapered composite beams. He presented the vibration and buckling analysis of uniform and tapered composite beams using conventional and advanced finite element method based on the classical laminate theory and the first-order shear deformation theory. He concluded that the advanced formulation gives more accurate results by using fewer elements, which is a good advantage in terms of computational expenses and discretization errors.

1.5 Objectives of the thesis

The objectives of the present thesis are, (1) to derive the formulations for tapered laminates considering the effect on the stiffness of plies caused be the taper angle; (2) to analyze the thickness-tapered composite beams for dynamic response using the developed hierarchical finite element formulation based on both the Classical Laminate Theory (CLT) and the First-order Shear Deformation Theory (FSDT); and, (3) to conduct a detailed parametric study of tapered composite beams. Tapered composite beams with axial forces are also considered.

The formulation using Ritz method and hierarchical finite element formulation are developed. The formulations are analyzed for their performance in the dynamic analysis of uniform and thickness-tapered composite beams based on both the classical laminate theory and the first-order shear deformation theory. These formulations are then used to analyze the free vibration response of tapered composite beams subjected to axial forces. The hierarchical formulation gives more accurate results by using fewer elements compared with the conventional FEM. Finally, a detailed parametric study of thickness-tapered composite beams is conducted.

1.6 Layout of the thesis

The present chapter provided a brief introduction and literature survey on the hierarchical finite element method and the dynamic analysis of uniform and tapered composite beams.

Chapter 2 provides the formulation of off-axis behavior of an arbitrary oblique ply in a tapered composite beam. Then the formulations of elastic behavior of different tapered beam models are developed considering the effect on the stiffness of plies due to the taper angle.

In Chapter 3, formulation based on Ritz method and the hierarchical finite element method are developed and applied to the dynamic analysis of uniform and tapered composite beams based on the classical laminate theory and the first-order shear deformation theory. The effect on the stiffness of plies due to the taper angle is considered. Then a detailed comparison is made between the conventional and the hierarchical finite element formulations.

Chapter 4 extends the analysis of Chapter 3 to uniform and tapered composite beams subjected to axial forces. Similar derivations, examples and comparisons are given.

Chapter 5 is devoted to the parametric study, which includes the effects of the boundary conditions, laminate configurations, taper angle, taper model and axial forces on the natural frequencies of the tapered beams.

Chapter 6 brings the thesis to its end by providing an overall conclusion of the present work and some recommendations for future work.

Chapter 2

Mechanical Behavior of Tapered Laminated Composite Beam

2.1 Introduction

Composite structures are increasingly being used in a variety of structural components in aerospace and automobile industries due to their high strength to weight and stiffness to weight ratios. Interest in laminated beams as movable elements of machines that have uniform and non-uniform configurations, and tapered and stepped configurations, is growing as they are finding a number of applications in modern industries, such as turbine blades, helicopter blades and robot arms. In this thesis, we will consider tapered composite beams. In this chapter, the mechanical behavior of tapered composite beam will be considered. For a composite beam with a small taper angle, the effect of the tapered angle can be ignored. As the tapered angle increases, the effect is not negligible. Then it is essential to develop the appropriate formulation for tapered laminate.

2.2 Off-axis Behavior of Composite Ply

2.2.1 Formulation of Off-axis Behavior

The tapered beam may have different configurations. First of all, a tapered beam model without resin pocket is considered, as shown in Figure 2.1:

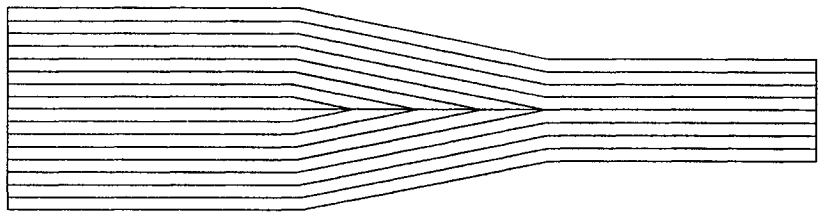

Figure 2.1 Tapered beam without resin pocket

This beam is constituted of different orthotropic layers at different orientations. The reference coordinate system for the structure is xyz system, while the principal directions of each layer are x_1, x_2 and x_3. We can derive the relation between the stress-strain relations in the principal material directions and those in the reference system.

We take the tapered portion for our study object, called Model F (see Appendix), as shown in Figure 2.2.

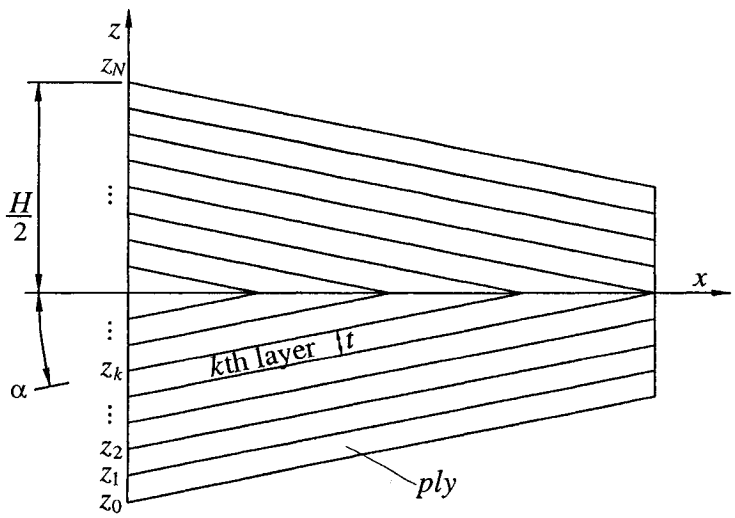

Figure 2.2 Tapered beam Model F

All the layers below the midline have a positive oblique angle α and the others above the midline have a negative oblique angle $-\alpha$.

The first step is to consider a layer of unidirectional material with principal directions x_1, x_2 and x_3. We can characterize the elastic properties of this layer, expressing them in a temporary reference coordinate system $x'y'z'$. The interpretation is given in reference [2]. The principal axis x_1 makes an angle θ with axis x'. Axes x_3 and z' are overlapped, as shown in Figure 2.3.

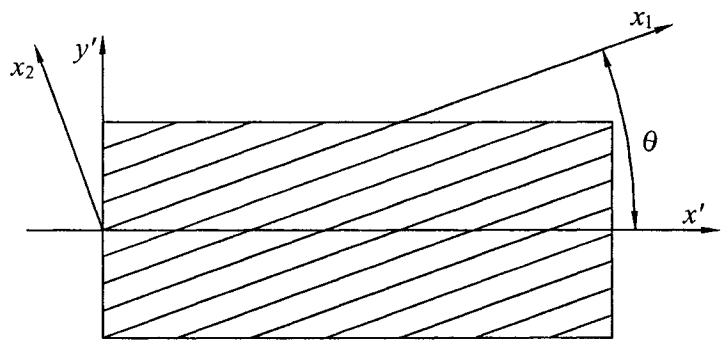

Figure 2.3 Rotation of axes x_1x_2 to $x'y'$

In the principal $x_1x_2x_3$ coordinate system of each orthotropic ply, we have the stress-strain relations from reference [2]:

$$\begin{Bmatrix} \varepsilon_{11} \\ \varepsilon_{22} \\ \varepsilon_{33} \\ \gamma_{23} \\ \gamma_{13} \\ \gamma_{12} \end{Bmatrix} = \begin{bmatrix} S_{11} & S_{12} & S_{13} & 0 & 0 & 0 \\ & S_{22} & S_{23} & 0 & 0 & 0 \\ & & S_{33} & 0 & 0 & 0 \\ & & & S_{44} & S_{45} & 0 \\ & & & & S_{55} & 0 \\ sym & & & & & S_{66} \end{bmatrix} \begin{Bmatrix} \sigma_{11} \\ \sigma_{22} \\ \sigma_{33} \\ \tau_{23} \\ \tau_{13} \\ \tau_{12} \end{Bmatrix} \tag{2.1}$$

where ε_{ij} and σ_{ij} are the strain and stress in coordinate system $x_1x_2x_3$. S_{ij} is the

corresponding compliance coefficient.

Equation 2.1 can be expressed as

$$\{\varepsilon^{123}\}=[S]\{\sigma^{123}\} \tag{2.2}$$

The stresses in the reference $x'y'z'$ coordinate system can be expressed with respect to stresses in $x_1x_2x_3$ coordinates as:

$$\begin{Bmatrix}\sigma_{x'}\\ \sigma_{y'}\\ \sigma_{z'}\\ \tau_{y'z'}\\ \tau_{x'z'}\\ \tau_{x'y'}\end{Bmatrix}=\begin{bmatrix}\cos^2\theta & \sin^2\theta & 0 & 0 & 0 & 2\cos\theta\sin\theta\\ \sin^2\theta & \cos^2\theta & 0 & 0 & 0 & -2\cos\theta\sin\theta\\ 0 & 0 & 1 & 0 & 0 & 0\\ 0 & 0 & 0 & \cos\theta & -\sin\theta & 0\\ 0 & 0 & 0 & \sin\theta & \cos\theta & 0\\ -\cos\theta\sin\theta & \cos\theta\sin\theta & 0 & 0 & 0 & \cos^2\theta-\sin^2\theta\end{bmatrix}\begin{Bmatrix}\sigma_{11}\\ \sigma_{22}\\ \sigma_{33}\\ \tau_{23}\\ \tau_{13}\\ \tau_{12}\end{Bmatrix} \tag{2.3}$$

That is:

$$\{\sigma'\}=[T_{\sigma\theta}]\{\sigma^{123}\} \tag{2.4}$$

where θ is defined in Figure 2.3. $\{\sigma'\}$ is the stress vector in coordinate system $x'y'z'$. $[T_{\sigma\theta}]$ is the stress transformation matrix due to angle θ and $\{\sigma^{123}\}$ is the stress vector in coordinate system $x_1x_2x_3$.

Similarly, we have the expression of the strains:

$$\begin{Bmatrix}\varepsilon_{x'}\\ \varepsilon_{y'}\\ \varepsilon_{z'}\\ \gamma_{y'z'}\\ \gamma_{x'z'}\\ \gamma_{x'y'}\end{Bmatrix}=\begin{bmatrix}\cos^2\theta & \sin^2\theta & 0 & 0 & 0 & \cos\theta\sin\theta\\ \sin^2\theta & \cos^2\theta & 0 & 0 & 0 & -\cos\theta\sin\theta\\ 0 & 0 & 1 & 0 & 0 & 0\\ 0 & 0 & 0 & \cos\theta & -\sin\theta & 0\\ 0 & 0 & 0 & \sin\theta & \cos\theta & 0\\ -2\cos\theta\sin\theta & 2\cos\theta\sin\theta & 0 & 0 & 0 & \cos^2\theta-\sin^2\theta\end{bmatrix}\begin{Bmatrix}\varepsilon_1\\ \varepsilon_2\\ \varepsilon_3\\ \gamma_{23}\\ \gamma_{13}\\ \gamma_{12}\end{Bmatrix} \tag{2.5}$$

This can be expressed as:

$$\{\varepsilon'\} = [T_{\varepsilon\theta}]\{\varepsilon^{123}\} \tag{2.6}$$

Likewise, $[T_{\varepsilon\theta}]$ is the strain transformation matrix due to angle θ. And we have the relations [2]:

$$[T_{\sigma\theta}]^{-1} = [T_{\varepsilon\theta}]^T \tag{2.7}$$

$$[T_{\varepsilon\theta}]^{-1} = [T_{\sigma\theta}]^T \tag{2.8}$$

Substituting Equations 2.2 and 2.4 into Equation 2.6, we can get the relation between stresses and strains in the reference coordinate system $x'y'z'$:

$$\{\varepsilon'\} = [T_{\varepsilon\theta}]\,[S]\,[T_{\sigma\theta}]^{-1}\{\sigma'\} \tag{2.9}$$

Considering that, the strain-stress relation in $x'y'z'$ coordinate system can be written as

$$\{\varepsilon'\} = [S']\,\{\sigma'\} \tag{2.10}$$

Thus the compliance matrix in $x'y'z'$ system can be expressed by:

$$[S'] = [T_{\varepsilon\theta}]\,[S]\,[T_{\sigma\theta}]^{-1} \tag{2.11}$$

The compliance matrix can be written in the form:

$$[S'] = \begin{bmatrix} S'_{11} & S'_{12} & S'_{13} & 0 & 0 & S'_{16} \\ & S'_{22} & S'_{23} & 0 & 0 & S'_{26} \\ & & S'_{33} & 0 & 0 & S'_{36} \\ & & & S'_{44} & S'_{45} & 0 \\ & & & & S'_{55} & 0 \\ sym & & & & & S'_{66} \end{bmatrix} \tag{2.12}$$

Similarly,

$$\{\sigma'\} = [T_{\sigma\theta}]\,[C]\,[T_{\varepsilon\theta}]^{-1}\{\varepsilon'\} \tag{2.13}$$

The stiffness matrix is:

$$[C'] = [T_{\sigma\theta}]\,[C]\,[T_{\varepsilon\theta}]^{-1} \tag{2.14}$$

It has the same form as $[S']$.

Hereafter, we can consider this layer, having an orientation θ, in another reference coordinate system xyz. The axis x' has an angle α with axis x while axes y' and y are overlapped, as shown in Figure 2.4:

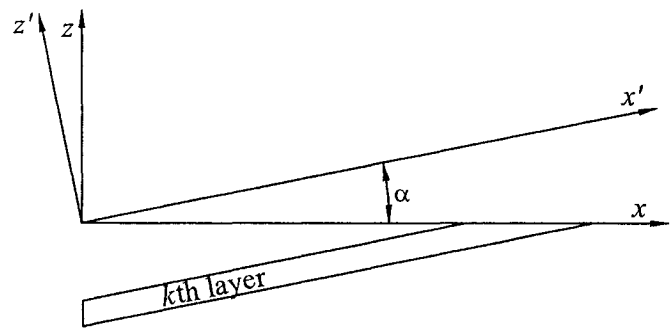

Figure 2.4 Rotation of axes x'y' to xy

In the coordinate system xyz, the direction cosines can be written as:

Table 2.1 Direction Cosines

	x'	y'	z'
x	$\cos\alpha$	0	$\sin\alpha$
y	0	1	0
z	$-\sin\alpha$	0	$\cos\alpha$

Note that, all the layers below the midline have a positive oblique angle α and the others above the midline have a negative oblique angle $-\alpha$.

From the above table, we can get the stress relations between these two coordinate

systems:

$$\begin{Bmatrix}\sigma_x\\ \sigma_y\\ \sigma_z\\ \tau_{yz}\\ \tau_{xz}\\ \tau_{xy}\end{Bmatrix}=\begin{bmatrix}\cos^2\alpha & 0 & \sin^2\alpha & 0 & 2\cos\alpha\sin\alpha & 0\\ 0 & 1 & 0 & 0 & 0 & 0\\ \sin^2\alpha & 0 & \cos^2\alpha & 0 & -2\cos\alpha\sin\alpha & 0\\ 0 & 0 & 0 & \cos\alpha & 0 & -\sin\alpha\\ -\cos\alpha\sin\alpha & 0 & \cos\alpha\sin\alpha & 0 & \cos^2\alpha-\sin^2\alpha & 0\\ 0 & 0 & 0 & \sin\alpha & 0 & \cos\alpha\end{bmatrix}\begin{Bmatrix}\sigma_{x'}\\ \sigma_{y'}\\ \sigma_{z'}\\ \tau_{y'z'}\\ \tau_{x'z'}\\ \tau_{x'y'}\end{Bmatrix} \tag{2.15}$$

It can be written as:

$$\{\sigma\}=[T_{\sigma\alpha}]\{\sigma'\} \tag{2.16}$$

where $\{\sigma\}$ is the stress vector in coordinate system xyz. $[T_{\sigma\alpha}]$ is the stress transformation matrix due to taper angle α.

Similarly, the strain relations are:

$$\begin{Bmatrix}\varepsilon_x\\ \varepsilon_y\\ \varepsilon_z\\ \gamma_{yz}\\ \gamma_{xz}\\ \gamma_{xy}\end{Bmatrix}=\begin{bmatrix}\cos^2\alpha & 0 & \sin^2\alpha & 0 & \cos\alpha\sin\alpha & 0\\ 0 & 1 & 0 & 0 & 0 & 0\\ \sin^2\alpha & 0 & \cos^2\alpha & 0 & -\cos\alpha\sin\alpha & 0\\ 0 & 0 & 0 & \cos\alpha & 0 & -\sin\alpha\\ -2\cos\alpha\sin\alpha & 0 & 2\cos\alpha\sin\alpha & 0 & \cos^2\alpha-\sin^2\alpha & 0\\ 0 & 0 & 0 & \sin\alpha & 0 & \cos\alpha\end{bmatrix}\begin{Bmatrix}\varepsilon_{x'}\\ \varepsilon_{y'}\\ \varepsilon_{z'}\\ \gamma_{y'z'}\\ \gamma_{x'z'}\\ \gamma_{x'y'}\end{Bmatrix} \tag{2.17}$$

It is abbreviated as:

$$\{\varepsilon\}=[T_{\varepsilon\alpha}]\{\varepsilon'\} \tag{2.18}$$

Likewise, $\{\varepsilon\}$ is the strain vector in coordinate system xyz. $[T_{\varepsilon\alpha}]$ is the strain transformation matrix due to angle α, and we have the relations:

$$[T_{\sigma\alpha}]^{-1}=[T_{\varepsilon\alpha}]^T \tag{2.19}$$

$$[T_{\varepsilon\alpha}]^{-1} = [T_{\sigma\alpha}]^{T} \tag{2.20}$$

Substituting Equations 2.10 and 2.16 into Equation 2.18, we can get:

$$\{\varepsilon\} = [T_{\varepsilon\alpha}]\,[S']\,[T_{\sigma\alpha}]^{-1}\{\sigma\} = [\bar{S}]\{\sigma\} \tag{2.21}$$

Then, the compliance matrix in the reference coordinate system *xyz* can be written as:

$$[\bar{S}] = [T_{\varepsilon\alpha}]\,[S']\,[T_{\sigma\alpha}]^{-1} \tag{2.22}$$

It can be written in the form:

$$[\bar{S}] = \begin{bmatrix} \bar{S}_{11} & \bar{S}_{12} & \bar{S}_{13} & \bar{S}_{14} & \bar{S}_{15} & \bar{S}_{16} \\ & \bar{S}_{22} & \bar{S}_{23} & \bar{S}_{24} & \bar{S}_{25} & \bar{S}_{26} \\ & & \bar{S}_{33} & \bar{S}_{34} & \bar{S}_{35} & \bar{S}_{36} \\ & & & \bar{S}_{44} & \bar{S}_{45} & \bar{S}_{46} \\ & & & & \bar{S}_{55} & \bar{S}_{56} \\ sym & & & & & \bar{S}_{66} \end{bmatrix} \tag{2.23}$$

Similarly, we can get the stiffness matrix in the reference coordinate system *xyz* as following:

$$[\bar{C}] = [T_{\sigma\alpha}]\,[C']\,[T_{\varepsilon\alpha}]^{-1} \tag{2.24}$$

$[\bar{C}]$ has the same form as $[\bar{S}]$. Each term of $[\bar{C}]$ can be nonzero.

With the notations:

$p = \cos\alpha$

$q = \sin\alpha$

The expanded compliance coefficients are:

$$\bar{S}_{11} = p^4 S'_{11} + 2p^2q^2 S'_{13} + q^4 S'_{33} + p^2q^2 S'_{55} \tag{2.25}$$

$$\bar{S}_{12} = p^2 S'_{12} + q^2 S'_{23} \tag{2.26}$$

$$\bar{S}_{13} = p^2q^2S'_{11} + \left(p^4 + q^4\right)S'_{13} + p^2q^2S'_{33} - p^2q^2S'_{55} \tag{2.27}$$

$$\bar{S}_{14} = q\left(-p^2S'_{16} - q^2S'_{36} + p^2S'_{45}\right) \tag{2.28}$$

$$\bar{S}_{15} = pq\left[-2p^2S'_{11} + 2\left(p^2 - q^2\right)S'_{13} + 2q^2S'_{33} + \left(p^2 - q^2\right)S'_{55}\right] \tag{2.29}$$

$$\bar{S}_{16} = p\left(p^2S'_{16} + q^2S'_{36} + q^2S'_{45}\right) \tag{2.30}$$

$$\bar{S}_{22} = S'_{22} \tag{2.31}$$

$$\bar{S}_{23} = q^2S'_{12} + p^2S'_{23} \tag{2.32}$$

$$\bar{S}_{24} = -qS'_{26} \tag{2.33}$$

$$\bar{S}_{25} = 2pq\left(-S'_{12} + S'_{23}\right) \tag{2.34}$$

$$\bar{S}_{26} = pS'_{26} \tag{2.35}$$

$$\bar{S}_{33} = q^4S'_{11} + 2p^2q^2S'_{13} + p^4S'_{33} + p^2q^2S'_{55} \tag{2.36}$$

$$\bar{S}_{34} = -q\left(q^2S'_{16} + p^2S'_{36} + p^2S'_{45}\right) \tag{2.37}$$

$$\bar{S}_{35} = pq\left[-2q^2S'_{11} - 2\left(p^2 - q^2\right)S'_{13} + 2p^2S'_{33} - \left(p^2 - q^2\right)S'_{55}\right] \tag{2.38}$$

$$\bar{S}_{36} = p\left(q^2S'_{16} + p^2S'_{36} - q^2S'_{45}\right) \tag{2.39}$$

$$\bar{S}_{44} = p^2S'_{44} + q^2S'_{66} \tag{2.40}$$

$$\bar{S}_{45} = p\left[2q^2S'_{16} - 2q^2S'_{36} + \left(p^2 - q^2\right)S'_{45}\right] \tag{2.41}$$

$$\bar{S}_{46} = pq\left(S'_{44} - S'_{66}\right) \tag{2.42}$$

$$\bar{S}_{55} = 4p^2q^2S'_{11} - 8p^2q^2S'_{13} + 4p^2q^2S'_{33} + \left(p^2 - q^2\right)^2S'_{55} \tag{2.43}$$

$$\bar{S}_{56} = q\left[-2p^2S'_{16} + 2p^2S'_{36} + \left(p^2 - q^2\right)S'_{45}\right] \tag{2.44}$$

$$\bar{S}_{66} = q^2S'_{44} + p^2S'_{66} \tag{2.45}$$

The stiffness coefficients are:

$$\overline{C}_{11} = p^4 C'_{11} + 2p^2 q^2 C'_{13} + q^4 C'_{33} + 4p^2 q^2 C'_{55} \tag{2.46}$$

$$\overline{C}_{12} = p^2 C'_{12} + q^2 C'_{23} \tag{2.47}$$

$$\overline{C}_{13} = p^2 q^2 C'_{11} + \left(p^4 + q^4\right) C'_{13} + p^2 q^2 C'_{33} - 4p^2 q^2 C'_{55} \tag{2.48}$$

$$\overline{C}_{14} = q\left(-p^2 C'_{16} - q^2 C'_{36} + 2p^2 C'_{45}\right) \tag{2.49}$$

$$\overline{C}_{15} = pq\left[-p^2 C'_{11} + \left(p^2 - q^2\right) C'_{13} + q^2 C'_{33} + 2\left(p^2 - q^2\right) C'_{55}\right] \tag{2.50}$$

$$\overline{C}_{16} = p\left(p^2 C'_{16} + q^2 C'_{36} + 2q^2 C'_{45}\right) \tag{2.51}$$

$$\overline{C}_{22} = C'_{22} \tag{2.52}$$

$$\overline{C}_{23} = q^2 C'_{12} + p^2 C'_{23} \tag{2.53}$$

$$\overline{C}_{24} = -qC'_{26} \tag{2.54}$$

$$\overline{C}_{25} = pq\left(-C'_{12} + C'_{23}\right) \tag{2.55}$$

$$\overline{C}_{26} = pC'_{26} \tag{2.56}$$

$$\overline{C}_{33} = q^4 C'_{11} + 2p^2 q^2 C'_{13} + p^4 C'_{33} + 4p^2 q^2 C'_{55} \tag{2.57}$$

$$\overline{C}_{34} = -q\left(q^2 C'_{16} + p^2 C'_{36} + 2p^2 C'_{45}\right) \tag{2.58}$$

$$\overline{C}_{35} = pq\left[-q^2 C'_{11} - \left(p^2 - q^2\right) C'_{13} + p^2 C'_{33} - 2\left(p^2 - q^2\right) C'_{55}\right] \tag{2.59}$$

$$\overline{C}_{36} = p\left(q^2 C'_{16} + p^2 C'_{36} - 2q^2 C'_{45}\right) \tag{2.60}$$

$$\overline{C}_{44} = p^2 C'_{44} + q^2 C'_{66} \tag{2.61}$$

$$\overline{C}_{45} = p\left[q^2 C'_{16} - q^2 C'_{36} + \left(p^2 - q^2\right) C'_{45}\right] \tag{2.62}$$

$$\overline{C}_{46} = pq\left(C'_{44} - C'_{66}\right) \tag{2.63}$$

$$\overline{C}_{55} = p^2 q^2 C'_{11} - 2p^2 q^2 C'_{13} + p^2 q^2 C'_{33} + \left(p^2 - q^2\right)^2 C'_{55} \tag{2.64}$$

$$\overline{C}_{56} = q\left[-p^2 C'_{16} + p^2 C'_{36} + \left(p^2 - q^2\right) C'_{45}\right] \tag{2.65}$$

$$\overline{C}_{66} = q^2 C_{44}^{'} + p^2 C_{66}^{'} \tag{2.66}$$

Note that every term in matrices $[\overline{S}]$ and $[\overline{C}]$ may be nonzero.

Substituting Equations 2.9 and 2.16 into Equation 2.18, we can get:

$$\{\varepsilon\} = [T_{\varepsilon\alpha}]\,[T_{\varepsilon\theta}]\,[S]\,[T_{\sigma\theta}]^{-1}[T_{\sigma\alpha}]^{-1}\{\sigma\} = [\overline{S}]\{\sigma\} \tag{2.67}$$

Thus, the compliance matrix in the reference coordinate system *xyz* can be expressed by the compliance matrix in the principal coordinate system $x_1x_2x_3$ and the transformation matrices:

$$[\overline{S}] = [T_{\varepsilon\alpha}]\,[T_{\varepsilon\theta}]\,[S]\,[T_{\sigma\theta}]^{-1}[T_{\sigma\alpha}]^{-1} \tag{2.68}$$

Similarly,

$$[\overline{C}] = [T_{\sigma\alpha}]\,[T_{\sigma\theta}]\,[C]\,[T_{\varepsilon\theta}]^{-1}[T_{\varepsilon\alpha}]^{-1} \tag{2.69}$$

Because the expression of $\overline{S}_{ij}$ expressed by S_{ij} is too long and difficult to simplify, it is not convenient to present it here. Instead, an example is given in section 2.2.2.

For plane stress assumption, we have the following stress-strain relationship:

$$\begin{Bmatrix} \varepsilon_x \\ \varepsilon_y \\ \varepsilon_z \\ \gamma_{yz} \\ \gamma_{xz} \\ \gamma_{xy} \end{Bmatrix} = \begin{bmatrix} \overline{S}_{11} & \overline{S}_{12} & \overline{S}_{13} & \overline{S}_{14} & \overline{S}_{15} & \overline{S}_{16} \\ & \overline{S}_{22} & \overline{S}_{23} & \overline{S}_{24} & \overline{S}_{25} & \overline{S}_{26} \\ & & \overline{S}_{33} & \overline{S}_{34} & \overline{S}_{35} & \overline{S}_{36} \\ & & & \overline{S}_{44} & \overline{S}_{45} & \overline{S}_{46} \\ & & & & \overline{S}_{55} & \overline{S}_{56} \\ sym & & & & & \overline{S}_{66} \end{bmatrix} \begin{Bmatrix} \sigma_x \\ \sigma_y \\ 0 \\ 0 \\ 0 \\ \tau_{xy} \end{Bmatrix} \tag{2.70}$$

Condensing out ε_z, γ_{yz} and γ_{xz}, the reduced Equation is:

$$\begin{Bmatrix} \varepsilon_x \\ \varepsilon_y \\ \gamma_{xy} \end{Bmatrix} = \begin{bmatrix} \overline{S}_{11} & \overline{S}_{12} & \overline{S}_{16} \\ & \overline{S}_{22} & \overline{S}_{26} \\ sym & & \overline{S}_{66} \end{bmatrix} \begin{Bmatrix} \sigma_x \\ \sigma_y \\ \tau_{xy} \end{Bmatrix} \tag{2.71}$$

Note that, because $\bar{S}_{14}$, $\bar{S}_{15}$, $\bar{S}_{24}$, $\bar{S}_{25}$, $\bar{S}_{34}$, and $\bar{S}_{35}$ are nonzero, σ_x, σ_y, and τ_{xy} have some contributions to ε_{zz}, γ_{yz}, and γ_{xz}. That means ε_{zz}, γ_{yz}, and γ_{xz} can be nonzero although σ_{zz}, τ_{yz}, and τ_{xz} are zero. This differs from the behavior of uniform laminated plate. For a uniform laminated plate, each ply is parallel to the middle plane, and its principal axis x_3 and the axis z of the reference coordinate system are overlapped. As a direct consequence of this some terms of $[\bar{S}]$ are zero, i.e., $\bar{S}_{14}$, $\bar{S}_{15}$, $\bar{S}_{24}$, $\bar{S}_{25}$, $\bar{S}_{34}$, and $\bar{S}_{35}$. Then, if plane stress state is assumed, ε_{zz}, γ_{yz}, and γ_{xz} must be zero.

Inverting the reduced stiffness matrix, we can get the reduced compliance matrix as below:

$$\begin{Bmatrix} \sigma_x \\ \sigma_y \\ \tau_{xy} \end{Bmatrix} = \begin{bmatrix} \bar{Q}_{11} & \bar{Q}_{12} & \bar{Q}_{16} \\ & \bar{Q}_{22} & \bar{Q}_{26} \\ sym & & \bar{Q}_{66} \end{bmatrix} \begin{Bmatrix} \varepsilon_x \\ \varepsilon_y \\ \gamma_{xy} \end{Bmatrix} \tag{2.72}$$

2.2.2 Example Applications

Example 2.1 Off-axis behavior of a ply

A tapered composite beam with the configuration shown in Figure 2.5 is constituted by graphite-epoxy plies (NCT301). The properties of this unidirectional composite material are given in Table 2.2.

This tapered beam has ply configurations $[(\pm 30)_{12}]_S$ and $[\pm 30/30]_S$ at the left and right ends respectively. The layer number drops from forty-eight to six. The length of the beam is $L = 0.0366\,\text{m}$. The individual ply thickness $t = 0.0001524\,\text{m}$ and the individual ply height in z direction is $h = 0.000152986\,\text{m}$. The taper angle of this beam

is $\alpha = 5^o$. We consider the 13^{th} ply and its orientation is $\theta = 30^o$. Figure 2.5 shows the left part of this beam.

Table 2.2 Material Properties of NCT301

Composite	E_1	144 GPa
	E_2, E_3	12.14 GPa
	ν_{21}, ν_{31}	0.017
	ν_{23}	0.458
	G_{12}, G_{13}	4.48 GPa
	G_{23}	3.2 GPa
	ρ	1660.8 kg/m^3
Resin	E	3.93 GPa
	ν	0.37
	G	1.034 GPa
	ρ_r	1000 kg/m^3

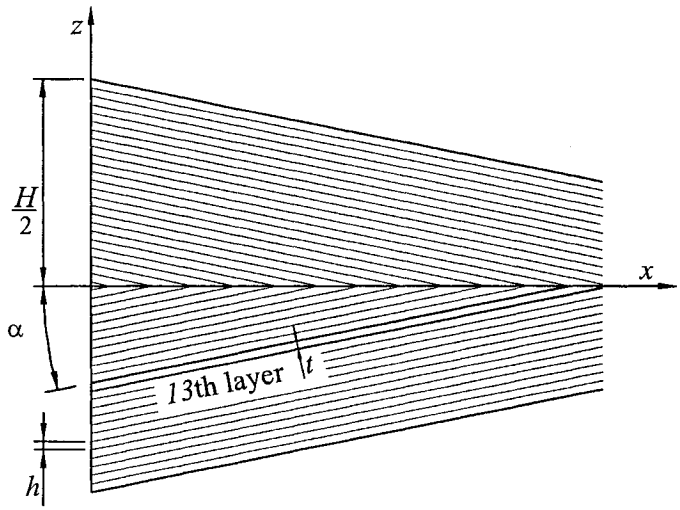

Figure 2.5 An oblique ply in a tapered laminate

After two transformations, the compliance and stiffness matrices of this layer in coordinate system *xyz* are given below:

$$[\bar{S}]=\begin{bmatrix} 513.2 & -260.0 & -111.7 & -19.15 & 106.3 & 604.0 \\ & 881.0 & -286.2 & -3.728 & -4.626 & 42.62 \\ & & 828.2 & -6.634 & -50.73 & -309.3 \\ & & & 2889 & 393.3 & 143.5 \\ & & & & 2428 & -126.8 \\ sym & & & & & 1261 \end{bmatrix} TPa^{-1}$$

$$[\bar{C}]=\begin{bmatrix} 869.5 & 295.8 & 58.02 & 36.01 & -64.21 & -422.7 \\ & 229.1 & 67.05 & 11.93 & -20.16 & -136.3 \\ & & 154.8 & 2662 & 1.197 & 8.000 \\ & & & 37.19 & -8.758 & -22.69 \\ & & & & 47.37 & 37.48 \\ sym & & & & & 294.6 \end{bmatrix} GPa$$

Note that, none of these terms is zero. This differs from the matrices for the uniform composite beam. The material property is similar to that of anisotropic material but symmetric.

The reduced stiffness matrix for the ply is:

$$[\bar{Q}]=\begin{bmatrix} 743.4 & 237.0 & -364.0 \\ & 189.3 & -119.9 \\ sym & & 257.6 \end{bmatrix} GPa$$

2.3 Elastic Behavior of Tapered Composite Laminate

2.3.1 Formulation of Elastic Behavior

For a thin plate, because the magnitudes of the stresses acting on the surface parallel to the middle plane are much smaller than the bending stresses, an approximate state of plane stress exists.

For a tapered composite beam as shown in Figure 2.2, some basic assumptions are imposed:

1. The beam is constructed of an arbitrary number of layers of orthotropic sheets bonded together. However, the orthotropic axes of material symmetry of an individual layer need not coincide with the xyz axes of the beam.

2. The beam is thin, i.e., the thickness H is much smaller than the length L and width b.

3. Small deformation is assumed.

4. In order to include in-plane force effects, nonlinear terms in the equations of motion involving products of stress and slope are retained. All other nonlinear terms are neglected.

5. Transverse shear strains γ_{xz} and γ_{yz} are negligible.

6. In-plane displacements u and v are linear functions of the z coordinate.

7. The transverse strain ε_z is negligible.

8. Each ply obeys Hooke's law.

9. Rotary inertia moments are negligible.

10. There are no body forces.

11. Transverse shear stresses τ_{xz} and τ_{yz} vanish on the surfaces $z = \pm H/2$.

In this thesis, Classical Laminate Theory (CLT) is applied to tapered composite beam. CLT has been introduced in reference [2].

CLT uses a first-order model. From assumption 5, γ_{xz} and γ_{yz} are zero, then the displacements u, v and w can be written as:

$$u(x,y,z) = u^o(x,y) - z\frac{\partial w^o(x,y)}{\partial x} \tag{2.73}$$

$$v(x,y,z) = v^o(x,y) - z\frac{\partial w^o(x,y)}{\partial y} \tag{2.74}$$

$$w(x,y,z) = w^o(x,y) \tag{2.75}$$

where, u, v and w are displacements in x, y and z directions respectively. u^o, v^o and w^o are the displacements of an arbitrary point in the mid-plane.

The expression for the strain field in xyz coordinate system is

$$\epsilon_x(x,y,z) = \epsilon_x^o(x,y) + z\kappa_x^o(x,y) \tag{2.76}$$

$$\epsilon_y(x,y,z) = \epsilon_y^o(x,y) + z\kappa_y^o(x,y) \tag{2.77}$$

$$\gamma_{xy}(x,y,z) = \gamma_{xy}^o + z\kappa_{xy}^o \tag{2.78}$$

$$\varepsilon_z = 0$$

$$\gamma_{yz} = 0$$

$$\gamma_{xz} = 0$$

where, ϵ_x^o, ϵ_y^o and γ_{xy}^o are the strains of an arbitrary point in the mid-plane. κ_x^o, κ_y^o and κ_{xy}^o are the curvatures of the mid-plane.

Substituting Equations 2.76 to 2.78 into Equation 2.72, we can get the stress field:

$$\begin{Bmatrix} \sigma_x \\ \sigma_y \\ \tau_{xy} \end{Bmatrix} = \begin{bmatrix} \overline{Q}_{11} & \overline{Q}_{12} & \overline{Q}_{16} \\ & \overline{Q}_{22} & \overline{Q}_{26} \\ sym & & \overline{Q}_{66} \end{bmatrix} \begin{Bmatrix} \epsilon_x^o + z\kappa_x^o \\ \epsilon_y^o + z\kappa_y^o \\ \gamma_{xy}^o + z\kappa_{xy}^o \end{Bmatrix} \tag{2.79}$$

The force resultants, N_x, N_y, N_{xy} and moment resultants M_x, M_y, M_{xy} are defined as:

$$\begin{Bmatrix} N_x \\ N_y \\ N_{xy} \end{Bmatrix} = \int_{-\frac{H}{2}}^{\frac{H}{2}} \begin{Bmatrix} \sigma_x \\ \sigma_y \\ \tau_{xy} \end{Bmatrix} dz = \sum_{k=1}^{n} \int_{z_{k-1}}^{z_k} \begin{Bmatrix} \sigma_x \\ \sigma_y \\ \tau_{xy} \end{Bmatrix} dz \tag{2.80}$$

$$\begin{Bmatrix} M_x \\ M_y \\ M_{xy} \end{Bmatrix} = \int_{-\frac{H}{2}}^{\frac{H}{2}} \begin{Bmatrix} \sigma_x \\ \sigma_y \\ \tau_{xy} \end{Bmatrix} z dz = \sum_{k=1}^{n} \int_{z_{k-1}}^{z_k} \begin{Bmatrix} \sigma_x \\ \sigma_y \\ \tau_{xy} \end{Bmatrix} z dz \tag{2.81}$$

where, n is the number of layers at a certain section. It varies within the tapered domain.

Finally, as in the case of uniform plate, we can get the following equation:

$$\begin{Bmatrix} N \\ M \end{Bmatrix} = \begin{bmatrix} A & B \\ B & D \end{bmatrix} \begin{Bmatrix} \varepsilon^o \\ \kappa^o \end{Bmatrix} \tag{2.82}$$

where,

$$A_{ij} = \int_{-\frac{H}{2}}^{\frac{H}{2}} \overline{Q}_{ij} dz \tag{2.83}$$

$$B_{ij} = \int_{-\frac{H}{2}}^{\frac{H}{2}} \overline{Q}_{ij} z dz \tag{2.84}$$

$$D_{ij} = \int_{-\frac{H}{2}}^{\frac{H}{2}} \overline{Q}_{ij} z^2 dz \tag{2.85}$$

with i, j = 1, 2, 6

2.3.2 Elastic Behavior of Tapered Beam Model F

2.3.2.1 Formulation of Elastic Behavior of Tapered Beam Model F

Because some plies drop off regularly, none of A, B or D matrices are continuous within the whole tapered length. But they are continuous within each small

domain, and we can express them by continuous functions of x within each small domain.

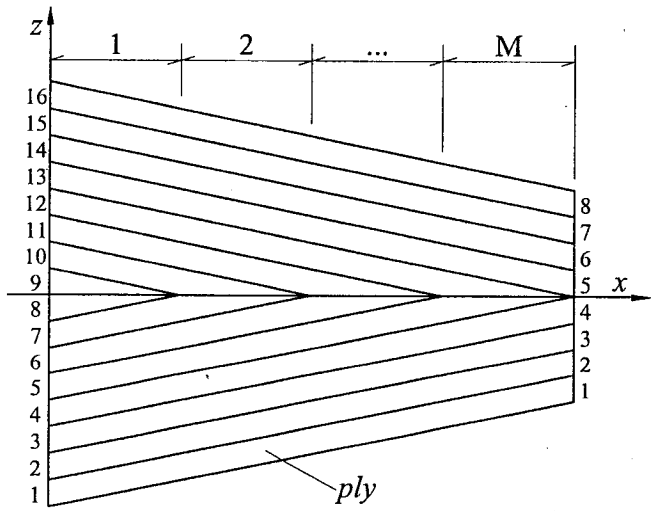

Figure 2.6 Discretization for taper Model F

For the above example, suppose that there are 2M layers dropped above or below the mid-plane, there will be M small domains. At each section, we can integrate from the bottom to top to get A, B and D matrices.

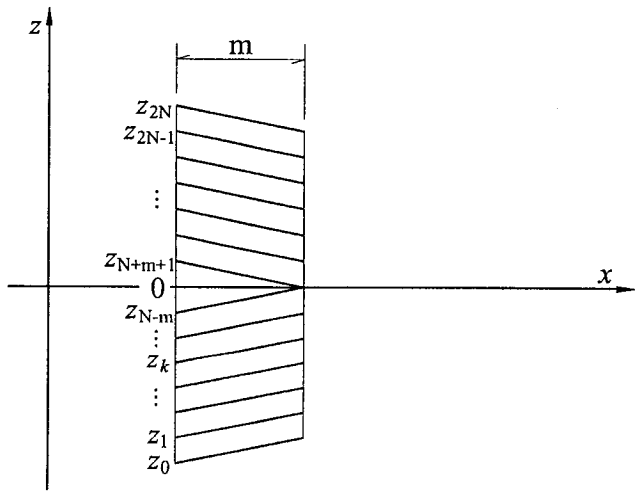

Figure 2.7 The m^{th} domain of Model F

For the m[th] domain shown in Figure 2.7, the stretching stiffness coefficient can be integrated as:

$$
\begin{aligned}
A_{ij} &= \int_{-\frac{H}{2}}^{\frac{H}{2}} \overline{Q}_{ij} dz \\
&= \sum_{k=1}^{N-m} \overline{Q}_{ij_k}(z_k - z_{k-1}) + \sum_{k=N+m+1}^{2N} \overline{Q}_{ij_k}(z_k - z_{k-1}) + \int_{z_{N-m}}^{0} \overline{Q}_{ij_{N-m+1}} dz + \int_{0}^{z_{N+m+1}} \overline{Q}_{ij_{N+m}} dz \\
&= \sum_{k=1}^{N-m} \overline{Q}_{ij_k}(z_k - z_{k-1}) + \sum_{k=N+m+1}^{2N} \overline{Q}_{ij_k}(z_k - z_{k-1}) + \int_{z_{N-m}}^{0} \overline{Q}_{ij_{N-m+1}} dz + \int_{0}^{z_{N-m}} \overline{Q}_{ij_{N+m}} dz \qquad (2.86) \\
&= \sum_{k=1}^{N-m} \overline{Q}_{ij_k}(z_k - z_{k-1}) + \sum_{k=N+m+1}^{2N} \overline{Q}_{ij_k}(z_k - z_{k-1}) - \overline{Q}_{ij_{N-m+1}} z_{N-m} - \overline{Q}_{ij_{N+m}} z_{N-m} \\
&= h\left(\sum_{k=1}^{N-m} \overline{Q}_{ij_k} + \sum_{k=N+m+1}^{2N} \overline{Q}_{ij_k} \right) - \left(\overline{Q}_{ij_{N-m+1}} + \overline{Q}_{ij_{N+m}} \right) z_{N-m}
\end{aligned}
$$

i, j = 1, 2, 6

where, t is the thickness of individual ply and h is the height of individual ply in z direction. α is the tapered angle and is defined in Section 2.2.1. The relation between h and t is:

$$h = \frac{t}{\cos\alpha}$$

The coordinate of the top surface of the k^{th} ply can be expressed by a function of x as following:

$$z_k = x\tan\alpha + h(k - N)$$

$$\tan\alpha = \frac{(N - R)h}{L}$$

where, N and R are half layer numbers at the left and right ends respectively.

Similarly,

$$
\begin{aligned}
B_{ij} &= \int_{-\frac{H}{2}}^{\frac{H}{2}} \overline{Q}_{ij} z dz \\
&= \frac{1}{2}\sum_{k=1}^{N-m} \overline{Q}_{ij\,k}\left(z_k^2 - z_{k-1}^2\right) + \frac{1}{2}\sum_{k=N+m+1}^{2N} \overline{Q}_{ij\,k}\left(z_k^2 - z_{k-1}^2\right) + \int_{z_{N-m}}^{0} \overline{Q}_{ij\,N-m+1} z dz + \int_{0}^{z_{N+m+1}} \overline{Q}_{ij\,N+m} z dz \\
&= \frac{1}{2}\sum_{k=1}^{N-m} \overline{Q}_{ij\,k}\left(z_k^2 - z_{k-1}^2\right) + \frac{1}{2}\sum_{k=N+m+1}^{2N} \overline{Q}_{ij\,k}\left(z_k^2 - z_{k-1}^2\right) + \int_{z_{N-m}}^{0} \overline{Q}_{ij\,N-m+1} z dz + \int_{0}^{-z_{N-m}} \overline{Q}_{ij\,N+m} z dz \\
&= \frac{1}{2}\left[\sum_{k=1}^{N-m} \overline{Q}_{ij\,k}\left(z_k^2 - z_{k-1}^2\right) + \sum_{k=N+m+1}^{2N} \overline{Q}_{ij\,k}\left(z_k^2 - z_{k-1}^2\right) - \overline{Q}_{ij\,N-m+1} z_{N-m}^2 + \overline{Q}_{ij\,N+m} z_{N-m}^2\right] \\
&= \frac{1}{2}\left[\sum_{k=1}^{N-m} \overline{Q}_{ij\,k}\left(z_k^2 - z_{k-1}^2\right) + \sum_{k=N+m+1}^{2N} \overline{Q}_{ij\,k}\left(z_k^2 - z_{k-1}^2\right) - \left(\overline{Q}_{ij\,N-m+1} - \overline{Q}_{ij\,N+m}\right) z_{N-m}^2\right]
\end{aligned}
$$

(2.87)

i, j = 1, 2, 6

The bending stiffness coefficient is:

$$
\begin{aligned}
D_{ij} &= \int_{-\frac{H}{2}}^{\frac{H}{2}} \overline{Q}_{ij} z^2 dz \\
&= \frac{1}{3}\sum_{k=1}^{N-m} \overline{Q}_{ij\,k}\left(z_k^3 - z_{k-1}^3\right) + \frac{1}{3}\sum_{k=N+m+1}^{2N} \overline{Q}_{ij\,k}\left(z_k^3 - z_{k-1}^3\right) + \int_{z_{N-m}}^{0} \overline{Q}_{ij\,N-m+1} z^2 dz + \int_{0}^{z_{N+m+1}} \overline{Q}_{ij\,N+m} z^2 dz \\
&= \frac{1}{3}\sum_{k=1}^{N-m} \overline{Q}_{ij\,k}\left(z_k^3 - z_{k-1}^3\right) + \frac{1}{3}\sum_{k=N+m+1}^{2N} \overline{Q}_{ij\,k}\left(z_k^3 - z_{k-1}^3\right) + \int_{z_{N-m}}^{0} \overline{Q}_{ij\,N-m+1} z^2 dz + \int_{0}^{-z_{N-m}} \overline{Q}_{ij\,N+m} z^2 dz \\
&= \frac{1}{3}\left[\sum_{k=1}^{N-m} \overline{Q}_{ij\,k}\left(z_k^3 - z_{k-1}^3\right) + \sum_{k=N+m+1}^{2N} \overline{Q}_{ij\,k}\left(z_k^3 - z_{k-1}^3\right) - \overline{Q}_{ij\,N-m+1} z_{N-m}^3 - \overline{Q}_{ij\,N+m} z_{N-m}^3\right] \\
&= \frac{1}{3}\left[\sum_{k=1}^{N-m} \overline{Q}_{ij\,k}\left(z_k^3 - z_{k-1}^3\right) + \sum_{k=N+m+1}^{2N} \overline{Q}_{ij\,k}\left(z_k^3 - z_{k-1}^3\right) - \left(\overline{Q}_{ij\,N-m+1} + \overline{Q}_{ij\,N+m}\right) z_{N-m}^3\right]
\end{aligned}
$$

(2.88)

i, j = 1, 2, 6

A, B and D matrices differ from domain to domain. For each small domain, every nonzero term of A is linear function of x, of B is quadratic, and of D is cubic.

For plane stress assumption, we have the strain-stress relation:

$$\begin{Bmatrix} \varepsilon_x \\ \varepsilon_y \\ \gamma_{xy} \end{Bmatrix} = \begin{bmatrix} \overline{S}_{11} & \overline{S}_{12} & \overline{S}_{16} \\ & \overline{S}_{22} & \overline{S}_{26} \\ sym & & \overline{S}_{66} \end{bmatrix} \begin{Bmatrix} \sigma_x \\ \sigma_y \\ \tau_{xy} \end{Bmatrix} \tag{2.89}$$

Now, recall the expressions of these six compliance coefficients from Equations 2.25 to 2.45. We can find that all of these six coefficients are even functions of α. That means for symmetric laminate, both the upper and lower symmetric sub-laminates have the same compliance matrix, even though their tapered angles are α and $-\alpha$ respectively. We invert the compliance matrix to get stiffness matrix:

$$\begin{Bmatrix} \sigma_x \\ \sigma_y \\ \tau_{xy} \end{Bmatrix} = \begin{bmatrix} \overline{Q}_{11} & \overline{Q}_{12} & \overline{Q}_{16} \\ & \overline{Q}_{22} & \overline{Q}_{26} \\ sym & & \overline{Q}_{66} \end{bmatrix} \begin{Bmatrix} \varepsilon_x \\ \varepsilon_y \\ \gamma_{xy} \end{Bmatrix} \tag{2.90}$$

We can expect that both the upper and lower sub-laminates have the same stiffness matrix, just like that of the uniform laminate.

Therefore, for each section of a tapered symmetric laminate, A, B and D matrices have similar forms for $\alpha \neq 0$ or $\alpha = 0$. A_{ij}, B_{ij} and D_{ij} are also zeros in the case of $\alpha \neq 0$ if they are zeros in the case of $\alpha = 0$. For any tapered symmetric laminate, $A \neq 0$, $B = 0$, $D \neq 0$, just like those of the uniform laminate.

$$\begin{Bmatrix} N_x \\ N_y \\ N_{xy} \end{Bmatrix} = \begin{bmatrix} A_{11} & A_{12} & A_{16} \\ A_{12} & A_{22} & A_{26} \\ A_{16} & A_{26} & A_{66} \end{bmatrix} \begin{Bmatrix} \varepsilon_x^o \\ \varepsilon_y^o \\ \gamma_{xy}^o \end{Bmatrix}, \quad \begin{Bmatrix} M_x \\ M_y \\ M_{xy} \end{Bmatrix} = \begin{bmatrix} D_{11} & D_{12} & D_{16} \\ D_{12} & D_{22} & D_{26} \\ D_{16} & D_{26} & D_{66} \end{bmatrix} \begin{Bmatrix} \kappa_x^o \\ \kappa_y^o \\ \kappa_{xy}^o \end{Bmatrix} \tag{2.91}$$

Note that, A_{ij}, B_{ij} and D_{ij} are functions of x. They differ from the constant coefficients A_{ij}, B_{ij} and D_{ij} for a uniform plate.

In addition, for other models, A, B and D matrices are similar.

In this thesis, we limit our discussion to symmetric laminate.

2.3.2.2 Example Applications

Example 2.2 Elastic behavior of Model F beam

A Model F composite beam as shown in Figure 2.5 is made up of NCT301 graphite-epoxy. Its mechanical properties are shown in Table 2.2.

The geometric properties of the beam are: length $L = 0.03048\,\text{m}$; individual ply thickness $t = 0.0001524\,\text{m}$. There are 32 and 28 plies at the left and right ends of the laminate and the configurations are $[(0/90)_8]_S$ and $[(0/90)_7]_S$ respectively. The taper angle $\alpha = 1.146°$.

There are four layers that are dropped, so there will be four small domains and in each domain, the A, B and D matrices are different. These four domains are $0 \sim 0.00762\,\text{m}$, $0.00762 \sim 0.01524\,\text{m}$, $0.01524 \sim 0.02286\,\text{m}$, $0.02286 \sim 0.03048\,\text{m}$.

The four A matrices are

$$\begin{bmatrix} 377.976-487.196x & 11.9710-98.2418x & 0 \\ 11.9710-98.2418x & 382.118-5780.97x & 0 \\ 0 & 0 & 21.8507-179.236x \end{bmatrix} MN\cdot m^{-1}$$

$$\begin{bmatrix} 417.798-5713.20x & 11.9701-98.1325x & 0 \\ 11.9701-98.1325x & 341.781-487.383x & 0 \\ 0 & 0 & 21.8505-179.207x \end{bmatrix} MN\cdot m^{-1}$$

$$\begin{bmatrix} 338.154-487.196x & 11.9718-98.2418x & 0 \\ 11.9718-98.2418x & 422.455-5780.97x & 0 \\ 0 & 0 & 21.8509-179.236x \end{bmatrix} MN\cdot m^{-1}$$

$$\begin{bmatrix} 457.620-5713.20x & 11.9693-98.1325x & 0 \\ 11.9693-98.1325x & 301.444-487.383x & 0 \\ 0 & 0 & 21.8503-179.207x \end{bmatrix} MN \cdot m^{-1}$$

A_{16}, A_{26}, A_{61} and A_{62} are zeros because of the 0/90 configuration. This is as same as that of the uniform plate. The other terms in A matrix are linear functions because of the tapered shape.

The values of A_{11} corresponding to the four A matrices are plotted in Figure 2.8.

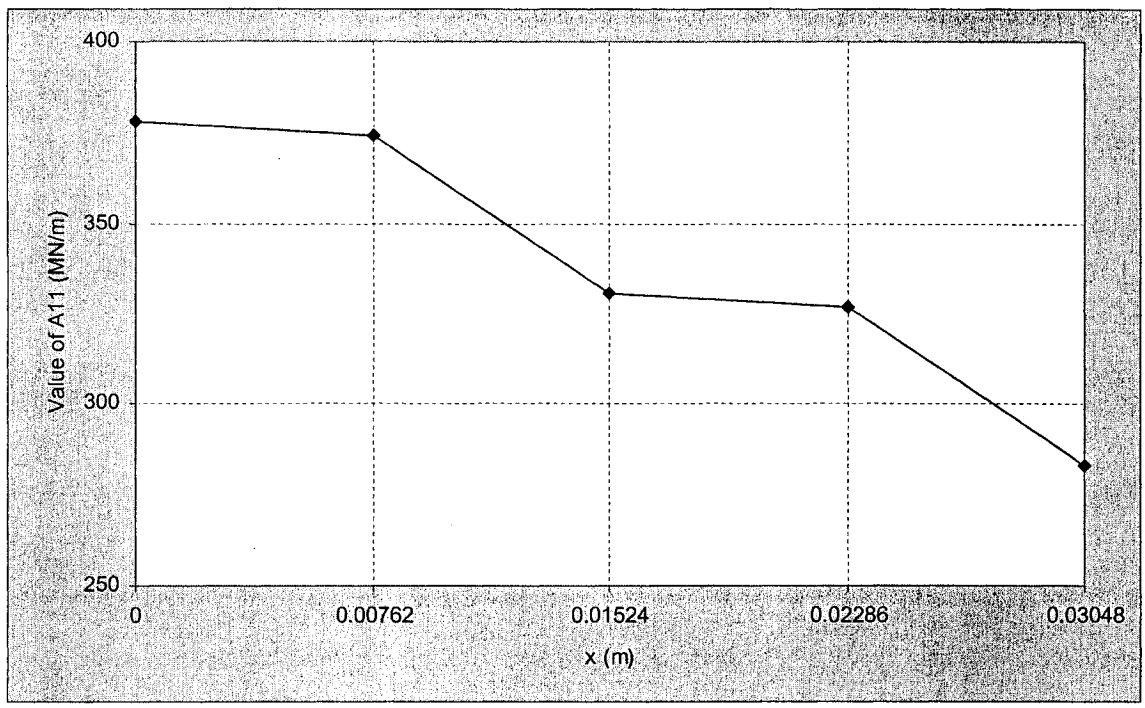

Figure 2.8 Coefficient A_{11} of tapered composite beam

As can be seen, these four straight lines have different slopes and intercepts. In each domain, the line is straight because two layers are dropped off and the other layers

are kept. Segment one and three have the same slope, because in both domains the dropped layers have same orientations. So do segment two and four.

All the four B matrices are zero because of symmetry.

The four D matrices are

$$\begin{bmatrix} 809-19412x+151251x^2-64986x^3 & 24-584x+4790x^2-13104x^3 & 0 \\ 24-584x+4790x^2-13104x^3 & 698-17659x+152908x^2-771103x^3 & 0 \\ 0 & 0 & 43-1066x+8744x^2-23908x^3 \end{bmatrix} N\cdot m$$

$$\begin{bmatrix} 809-19533x+167186x^2-762062x^3 & 24-584x+4790x^2-13090x^3 & 0 \\ 24-584x+4790x^2-13089x^3 & 697-17536x+136767x^2-65010x^3 & 0 \\ 0 & 0 & 43-1066x+8744x^2-23904x^3 \end{bmatrix} N\cdot m$$

$$\begin{bmatrix} 806-19048x+135316x^2-64986x^3 & 24-584x+4791x^2-13104x^3 & 0 \\ 24-584x+4791x^2-13104x^3 & 700-18028x+169050x^2-771103x^3 & 0 \\ 0 & 0 & 43-1066x+8744x^2-23908x^3 \end{bmatrix} N\cdot m$$

$$\begin{bmatrix} 815-20141x+183121x^2-762062x^3 & 24-584x+4790x^2-13090x^3 & 0 \\ 24-584x+4790x^2-13089x^3 & 691-16921x+120626x^2-65010x^3 & 0 \\ 0 & 0 & 43-1066x+8744x^2-23904x^3 \end{bmatrix} N\cdot m$$

D_{16}, D_{26}, D_{61} and D_{62} are also zeros because of the 0/90 configuration. This is as same as that of the uniform plate. The other terms in D matrix are cubic functions because of the tapered shape.

The values of D_{11} corresponding to the four D matrices are plotted in Figure 2.9.

As can be seen from this figure, the entire curve looks like a straight line. In fact, each line is curved but the curvatures are very small as can be seen from the matrices. That is because of the small tapered angle. The curvature increases along with the tapered

angle.

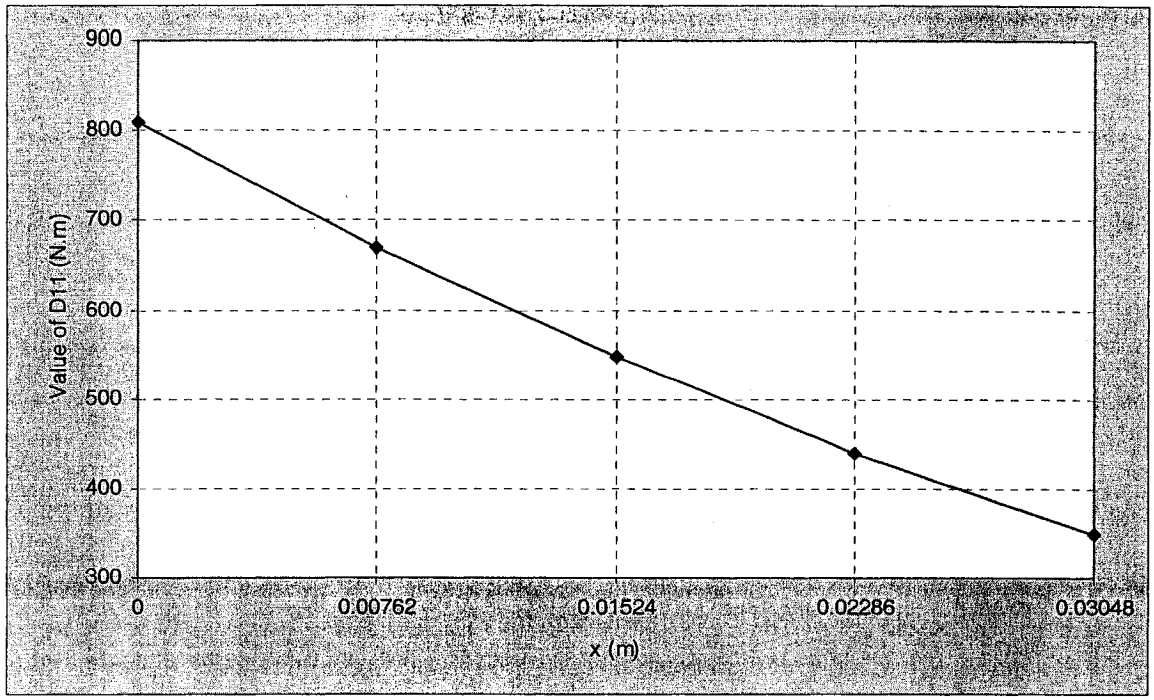

Figure 2.9 Coefficient D_{11} of tapered composite beam

2.3.3 Elastic Behavior of Tapered Beam Models A, B, C, D, and M

In this thesis, we will also discuss the elastic behavior of other tapered beam models as well as Model F. In Zabihollah's thesis [29], he has done a similar work for different models but ignored the effect on the stiffness coefficients caused by the tapered angle α.

2.3.3.1 Formulation of Elastic Behavior of Tapered Beam Models A, B, C, D, and M

Following the same procedure as in the previous section, we can derive the formulations for the other models A, B, C, D and M (see Appendix).

Model M (Mid-plane) is shown in Figure 2.10.

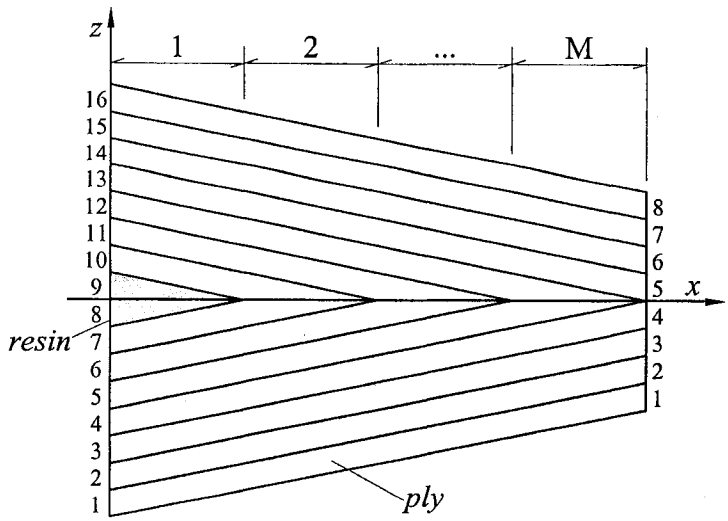

Figure 2.10 Discretization for taper Model M

As can be seen, the first part has a block of resin and differs from the others. We need to integrate from the bottom to top including the resin pocket. Thus, this part is integrated individually. That is:

When $m=1$,

$$
\begin{aligned}
D_{ij} &= \int_{\frac{H}{2}}^{\frac{H}{2}} \overline{Q}_{ij} z^2 dz \\
&= \frac{1}{3}\sum_{k=1}^{N-m} \overline{Q}_{ij_k}\left(z_k^3 - z_{k-1}^3\right) + \frac{1}{3}\sum_{k=N+m+1}^{2N} \overline{Q}_{ij_k}\left(z_k^3 - z_{k-1}^3\right) + \int_{z_{N-m}}^{z_{N+m+1}} \overline{Q}_{rij} z^2 dz \\
&= \frac{1}{3}\sum_{k=1}^{N-m} \overline{Q}_{ij_k}\left(z_k^3 - z_{k-1}^3\right) + \frac{1}{3}\sum_{k=N+m+1}^{2N} \overline{Q}_{ij_k}\left(z_k^3 - z_{k-1}^3\right) + \int_{z_{N-m}}^{z_{N-m}} \overline{Q}_{rij} z^2 dz \\
&= \frac{1}{3}\left[\sum_{k=1}^{N-m} \overline{Q}_{ij_k}\left(z_k^3 - z_{k-1}^3\right) + \sum_{k=N+m+1}^{2N} \overline{Q}_{ij_k}\left(z_k^3 - z_{k-1}^3\right) - 2\overline{Q}_{rij} z_{N-m}^3\right]
\end{aligned}
\tag{2.92}
$$

where z_k and N are defined in the previous section for taper Model F.

When $m = 2,3,...M$, the bending stiffness coefficients are as same as that of the taper model without resin, Model F. The integration is given by Equation 2.88.

Model C (Overlapped) is shown in Figure 2.11. Every part has a resin pocket.

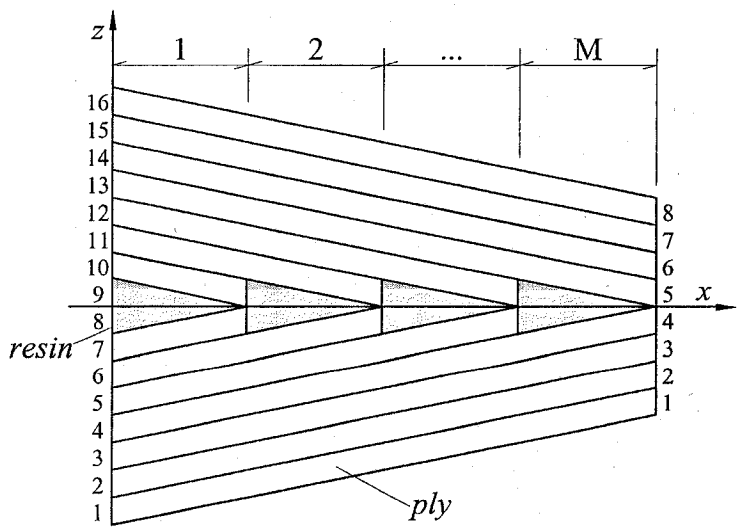

Figure 2.11 Discretization for taper Model C

Similar to the first part of Model M, all the bending stiffness coefficients are:

$$
\begin{aligned}
D_{ij} &= \int_{\frac{H}{2}}^{\frac{H}{2}} \overline{Q}_{ij} z^2 dz \\
&= \frac{1}{3}\sum_{k=1}^{N-m} \overline{Q}_{ij_k}\left(z_k^3 - z_{k-1}^3\right) + \frac{1}{3}\sum_{k=N+m+1}^{2N} \overline{Q}_{ij_k}\left(z_k^3 - z_{k-1}^3\right) + \int_{z_{N-m}}^{z_{N+m+1}} \overline{Q}_{rij} z^2 dz \\
&= \frac{1}{3}\sum_{k=1}^{N-m} \overline{Q}_{ij_k}\left(z_k^3 - z_{k-1}^3\right) + \frac{1}{3}\sum_{k=N+m+1}^{2N} \overline{Q}_{ij_k}\left(z_k^3 - z_{k-1}^3\right) + \int_{z_{N-m}}^{z_{N-m}} \overline{Q}_{rij} z^2 dz \\
&= \frac{1}{3}\left[\sum_{k=1}^{N-m} \overline{Q}_{ij_k}\left(z_k^3 - z_{k-1}^3\right) + \sum_{k=N+m+1}^{2N} \overline{Q}_{ij_k}\left(z_k^3 - z_{k-1}^3\right) - 2\overline{Q}_{rij} z_{N-m}^3\right]
\end{aligned}
\tag{2.93}
$$

where z_k and N are as same as those defined in the previous section for taper Model F.

Model A is shown in Figure 2.12. For this model, D_{ij} is a continuous cubic

function of x throughout the whole beam because there is only one big resin pocket. We do not need to divide the beam into M parts.

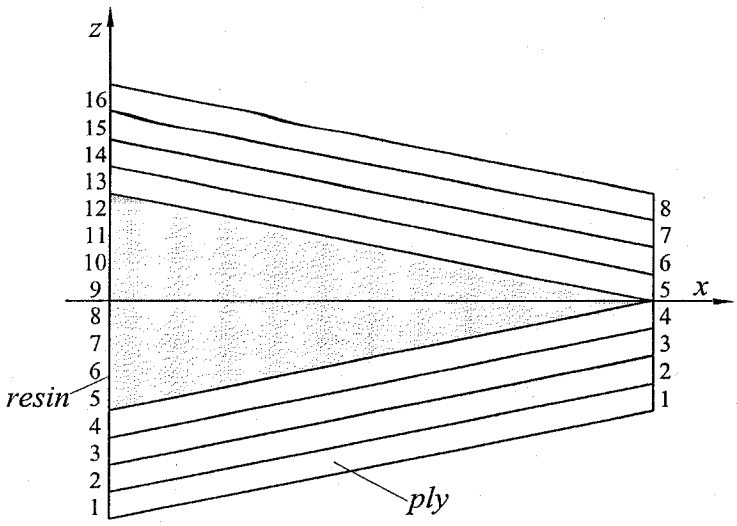

Figure 2.12 Discretization for taper Model A

$$
\begin{aligned}
D_{ij} &= \int_{-\frac{H}{2}}^{\frac{H}{2}} \overline{Q}_{ij} z^2 dz \\
&= \frac{1}{3}\sum_{k=1}^{R} \overline{Q}_{ij_k}\left(z_k^3 - z_{k-1}^3\right) + \frac{1}{3}\sum_{k=2N-R+1}^{2N} \overline{Q}_{ij_k}\left(z_k^3 - z_{k-1}^3\right) + \int_{z_R}^{-z_R} \overline{Q}_{rij} z^2 dz \\
&= \frac{1}{3}\left[\sum_{k=1}^{R} \overline{Q}_{ij_k}\left(z_k^3 - z_{k-1}^3\right) + \sum_{k=2N-R+1}^{2N} \overline{Q}_{ij_k}\left(z_k^3 - z_{k-1}^3\right) - 2\overline{Q}_{rij} z_R^3\right]
\end{aligned}
\tag{2.94}
$$

where z_k and N are as same as those defined in the previous section for taper Model F.

Model B is shown in Figure 2.13.

This type of taper model differs from the previous models. The external layers are kept and the internal layers are dropped off one by one. Meanwhile, each part has a resin

pocket. Therefore, we need to integrate from bottom to top including three parts, resin, oblique and horizontal plies.

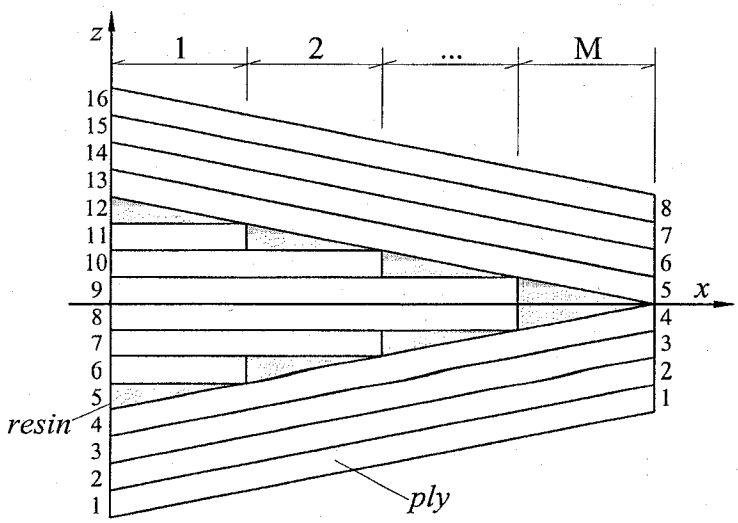

Figure 2.13 Discretization for taper Model B

The expression of bending stiffness coefficient differs from domain to domain.

$$
\begin{aligned}
D_{ij} &= \int_{-\frac{H}{2}}^{\frac{H}{2}} \overline{Q}_{ij} z^2 dz \\
&= \frac{1}{3}\sum_{k=1}^{R} \overline{Q}_{ij_k}\left(z_k^3 - z_{k-1}^3\right) + \frac{1}{3}\sum_{k=R+m+1}^{2N-R-m} \overline{Q}_{ij_k}\left(z_k^3 - z_{k-1}^3\right) + \frac{1}{3}\sum_{k=2N-R+1}^{2N} \overline{Q}_{ij_k}\left(z_k^3 - z_{k-1}^3\right) \\
&+ \int_{z_R}^{z_{R+m}} \overline{Q}_{rij} z^2 dz + \int_{z_{R+m}}^{z_R} \overline{Q}_{rij} z^2 dz \\
&= \frac{1}{3}\left[\sum_{k=1}^{R} \overline{Q}_{ij_k}\left(z_k^3 - z_{k-1}^3\right) + \sum_{k=R+m+1}^{2N-R-m} \overline{Q}_{ij_k}\left(z_k^3 - z_{k-1}^3\right) + \sum_{k=2N-R+1}^{2N} \overline{Q}_{ij_k}\left(z_k^3 - z_{k-1}^3\right) + 2\overline{Q}_{rij}\left(z_{R+m}^3 - z_R^3\right)\right]
\end{aligned}
\tag{2.95}
$$

where, for the external oblique layers, the height of individual ply is

$$h = \frac{t}{\cos\alpha}$$

$$z_k = x\tan\alpha - t(N-R) + h(k-R),\ 1 \le k \le R$$

$$\tan\alpha = \frac{t(N-R)}{L}$$

For the internal horizontal layers,

$$z_k = t(k-N),\ R < k \le N$$

Model D is shown in Figure 2.14.

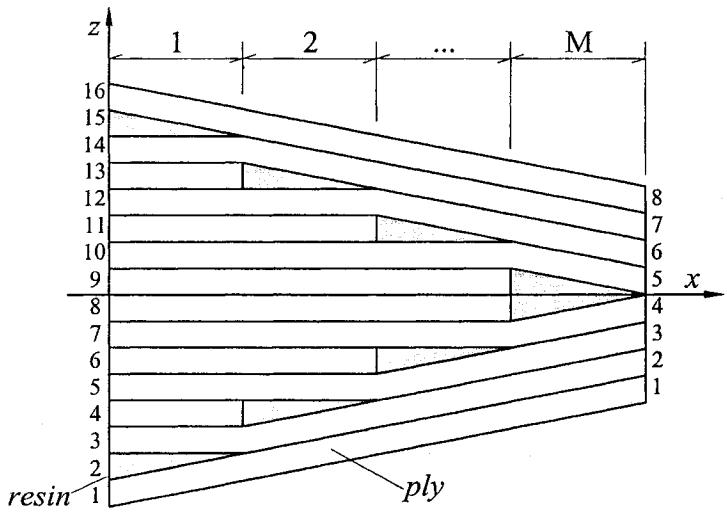

Figure 2.14 Discretization for taper Model D

The expression of D_{ij} is a little more complicated than the others.

$$D_{ij} = \int_{\frac{H}{2}}^{\frac{H}{2}} \overline{Q}_{ij} z^2 dz$$

$$= \frac{1}{3}\sum_{n=1}^{m}\left[\left(\overline{Q}_{ij\,2n-1} + \overline{Q}_{ij\,2N-2n+2}\right)\left(z_{2n-1}^3 - z_{2n-2}^3\right)\right] + \frac{1}{3}\sum_{k=2m+1}^{2N-2m}\overline{Q}_{ij\,k}\left(z_k^3 - z_{k-1}^3\right)$$

$$+ \int_{z_{2m-1}}^{z_{2m}} \overline{Q}_{rij} z^2 dz + \int_{z_{2m}}^{z_{2m-1}} \overline{Q}_{rij} z^2 dz$$

$$= \frac{1}{3}\left\{\sum_{n=1}^{m}\left[\left(\overline{Q}_{ij\,2n-1} + \overline{Q}_{ij\,2N-2n+2}\right)\left(z_{2n-1}^3 - z_{2n-2}^3\right)\right] + \sum_{k=2m+1}^{2N-2m}\overline{Q}_{ij\,k}\left(z_k^3 - z_{k-1}^3\right) + 2\overline{Q}_{rij}\left(z_{2m}^3 - z_{2m-1}^3\right)\right\}$$

(2.96)

where, for the external tapered layers,

$$h = \frac{t}{\cos\alpha}$$

$$z_{2n-1} = x\tan\alpha + t(1-N) + h(n-1)$$

$$z_{2n-2} = z_{2n-1} - h,\ 1 \le n \le m$$

$$\tan\alpha = \frac{t(N-R)\left(\sqrt{3t^2(N-R)^2 + L^2} - 2L\right)}{t^2(N-R)^2 - L^2}$$

For the internal horizontal layers,

$$z_k = t(k-N),\ 2m+1 < k \le 2N-2m$$

For the horizontal and tapered layers adjacent to the resin,

$$z_{2m} = t(2m-N)$$

$$z_{2m-1} = x\tan\alpha + t(1-N) + h(m-1)$$

2.3.3.2 Example Applications

In this section, we will present an example to show the bending stiffness coefficients of different taper models.

Example 2.3 Bending stiffness coefficient of tapered composite beam

A tapered composite beam is made up of NCT301 graphite-epoxy. Its mechanical properties are shown in Table 2.2.

The geometric properties of the beam are: length $L = 0.03048$ m ; individual ply thickness $t = 0.0001524$ m . There are thirty-two plies at the left end and sixteen plies at the right end. Sixteen layers are dropped. The configuration of both ends are $[(0/90)_8]_S$

and $[(0/90)_4]_S$ respectively.

There are sixteen layers that are dropped, so there are totally eight small domains. Tables 2.3 and 2.4 give the first two bending stiffness coefficients D_{11} of different taper models.

Table 2.3 D_{11} of the first domain for different taper models

Taper Model	1st domain
A	$684.692-28321.8x+311354x^2-194743x^3$
B	$732.371-28285.8x+310860x^2-194276x^3$
C	$784.346-37649.3x+583372x^2-194743x^3$
D	$794.875-9849.63x+100489x^2-193811x^3$
F	$784.364-37663.5x+587092x^2-520273x^3$
M	$784.346-37649.3x+583372x^2-194743x^3$

Table 2.4 D_{11} of the second domain for different taper models

Taper Model	2nd domain
A	$684.692-28321.8x+311354x^2-194743x^3$
B	$730.084-28285.8x+310860x^2-194276x^3$
C	$782.138-36903.9x+518158x^2-194743x^3$
D	$804.611-17038.7x+165505x^2-193811x^3$
F	$784.662-37897.8x+648585x^2-5900250x^3$
M	$784.662-37897.8x+648585x^2-5900250x^3$

As can be seen from the above table, the expressions of D_{11} of Model A are same in the first two domains and they should be the same throughout the whole beam. Within the first domain, Models C and M have the same D_{11}, because these two models have the same physical configurations within this domain. Furthermore, their D_{11} is very close to that of Model F. That is because the only difference is that in Model F, the dropped-off part is laminate while in Models C and M it is resin. Model D has the largest value of

D_{11}.

The coefficients throughout the whole beam are plotted in Figures 2.15 and 2.16.

In Figure 2.15, the line of Model A is a real continuous curve, because throughout the whole beam, D_{11} is always the same cubic function of x as given in tables 2.3 and 2.4. This is due to the fact that the dropped part is the big resin pocket and is isotropic. The lines of Models C, F and M seem to be also continuous curves but in fact, their curvatures differ from interval to interval, as revealed in tables 2.3 and 2.4. Moreover, these three lines seem overlapped but they are not (tables 2.3 and 2.4). They are very close because the dropped parts, resin or plies, are at the center of the beam. The effect caused by the dropped-off resin or laminate at the center of the beam is small compared with other parts. This effect is negligible.

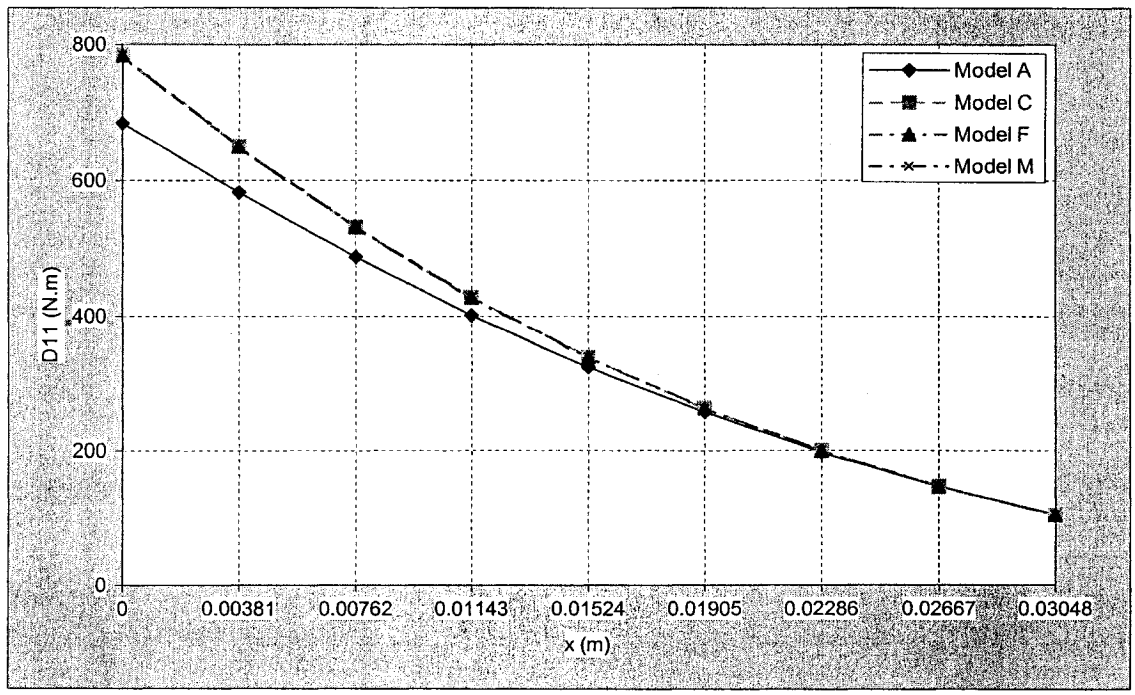

Figure 2.15 D_{11} of Models A, C, F, and M

In Figure 2.16, Models B and D give interesting discontinuous segments. That is because the plies are not dropped-off regularly but are cut at the sections suddenly, not like the other models. For model B, the discontinuities at sections 1, 3, 5 and 7 are smaller than that at sections 2, 4, and 6. This is because the dropped-off plies within domains 1, 3, 5, and 7 have 90° orientation while the dropped-off plies within domains 2, 4, and 6 have 0° orientation. The bending stiffness coefficient of 0° orientation ply is much larger than that of 90° orientation ply. For a 0° orientation ply, the major contribution to D_{11} is given by fiber while for a 90° orientation ply, the major contribution is given by resin. The segment of model D is a good contrast. The discontinuities decrease regularly, because all the dropped plies have 90° orientation.

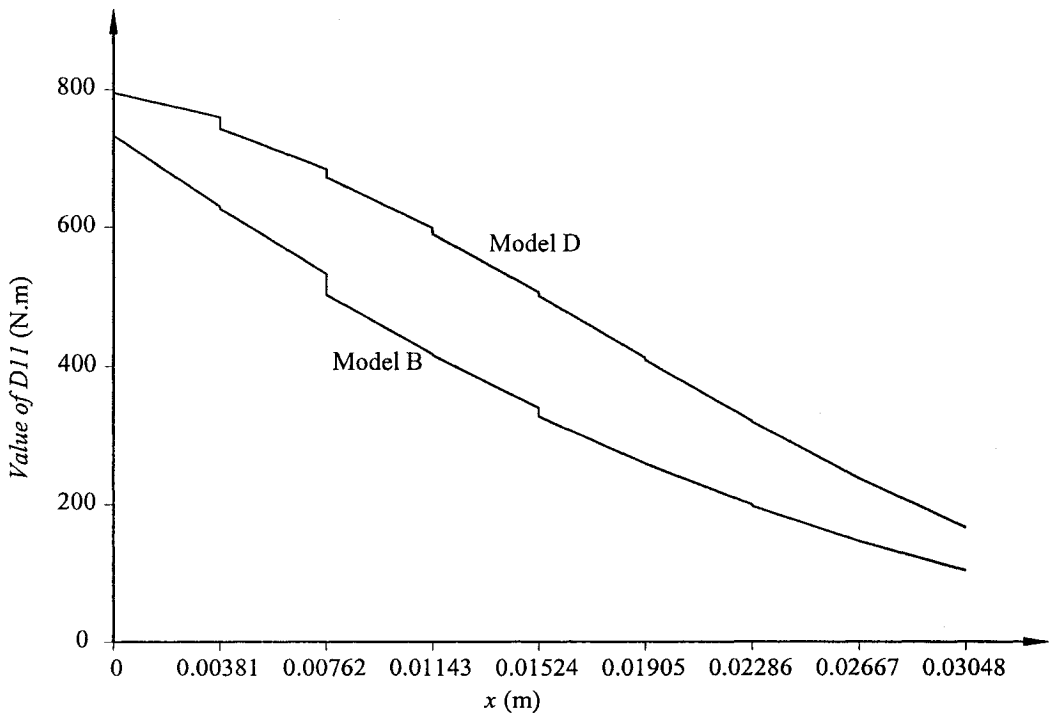

Figure 2.16 D_{11} of Models B and D

At $x = 0.00381\,\mathrm{m}$, the dropped-off plies of both models B and D have 90° orientation, but obviously the discontinuity of model D is larger than that of Model B. This is because the dropped-off ply of model D is near the top edge while that of model B is at the middle. The contribution of a ply near the edge is larger than that of the internal ones.

Moreover, the discontinuities of both Models B and D vanish near the left end of the beam because the dropped plies are very close to the mid-plane. Then they contribute a little to the bending stiffness.

2.4 Conclusion

In this chapter, we have derived the formulations for tapered laminates. The stiffness and compliance matrices differ from that of uniform beam. Each term of these matrices can be nonzero. Then we derived the A, B and D matrices of tapered plate and examples have been given for beams with different configurations. The elastic properties of different models differ from each other; some are continuous while the others are segments. These various properties affect the behavior of tapered composite beam. In the following chapters, we will study the free vibration of tapered composite beam.

Chapter 3

Free Vibration Analysis of Tapered Laminated Composite Beam

3.1 Introduction

Beams are widely used in civil, mechanical and aerospace structures. In the thesis, we limit our study to laminated composite beam. According to various length-to-height ratios of beams, we apply Classical Laminate Theory (CLT) or First-order Shear Deformation Theory (FSDT). The former accounts for bending moment effects on stresses and deformations. Transverse shear forces are recovered from equilibrium but their effect on beam deformations is neglected. Its fundamental assumption is that cross-sections remain plane and normal to the deformed longitudinal axis. The rotation occurs about a neutral axis that passes through the centroid of the cross-section. Meanwhile, the FSDT corrects the classical beam theory by including first-order shear deformation effects. In this theory, cross-sections remain plane and rotate about the same neutral axis as the Euler-Bernoulli model, but do not remain normal to the deformed longitudinal axis. The deviation from normality is produced by a transverse shear that is assumed to be constant over the cross-section.

These two theories are based on the assumptions of small deformations and linear

elastic isotropic material behavior. In addition, both models neglect changes in dimensions of the cross-sections as the beam deforms.

In this chapter, we will derive the formulations based on CLT and FSDT for vibration of tapered laminated beam, using both Ritz method and Hierarchical Finite Element Method (HFEM). Then some examples using Ritz method, conventional FEM and HFEM will be given. The exact solutions of these examples will be presented if available.

3.2 Formulation based on Classical Laminate Theory

3.2.1 Solution using Ritz method and based on CLT

In this section, we will derive the formulations for Ritz method based on the classical laminate theory and then give some examples, including uniform and tapered composite beams.

3.2.1.1 Formulation using Ritz method based on CLT

The Ritz method provides a convenient method for obtaining approximate solutions to boundary value problems. This approach is equally applicable to bending, buckling, and free vibration analysis. For the free vibration problem without external forces, the governing energy condition can be written as:

$$\Pi = U + T \tag{3.1}$$

where U is the strain energy and T is the kinetic energy.

The strain energy of an elastic solid written in Cartesian coordinates can be

explained as following:

$$U = \frac{1}{2}\int\int\int\left(\sigma_x\varepsilon_x + \sigma_y\varepsilon_y + \sigma_z\varepsilon_z + \tau_{yz}\gamma_{yz} + \tau_{xz}\gamma_{xz} + \tau_{xy}\gamma_{xy}\right)dxdydz \tag{3.2}$$

Taking into account the basic assumptions of laminated plate theory as discussed in Chapter 2, i.e., $\sigma_z = \tau_{yz} = \tau_{xz} = 0$, the right-hand side of Equation 3.2 has three terms left:

$$U = \frac{1}{2}\int\int\int\left(\sigma_x\varepsilon_x + \sigma_y\varepsilon_y + \tau_{xy}\gamma_{xy}\right)dxdydz \tag{3.3}$$

For pure bending of a beam, ϵ_y and γ_{xy} are ignored, only ϵ_x is nonzero. The displacements u, v and w from Equations 2.73 to 2.75 can be written as:

$$u(x,y,z) = -z\frac{\partial w(x)}{\partial x} \tag{3.4}$$

$$v(x,y,z) = 0$$

$$w(x,y,z) = w(x) \tag{3.5}$$

For one-dimensional problem, from Equations 3.4 and 3.5, the strain and stress are given by:

$$\epsilon_x = -z\frac{\partial^2 w}{\partial x^2} \tag{3.6}$$

$$\sigma_x = \overline{Q}_{11}\varepsilon_x = -\overline{Q}_{11}z\frac{\partial^2 w}{\partial x^2} \tag{3.7}$$

The strain energy can be further simplified to:

$$U = \frac{1}{2}\int\int\int\sigma_x\varepsilon_x dxdydz \tag{3.8}$$

Substituting Equations 3.6 and 3.7 into Equation 3.8 yields:

$$U = \frac{1}{2}\int\int\int\left(-\overline{Q}_{11}z\frac{\partial^2 w}{\partial x^2}\right)\left(-z\frac{\partial^2 w}{\partial x^2}\right)dxdydz$$

$$= \frac{1}{2}\int\int\int\overline{Q}_{11}z^2\left(\frac{\partial^2 w}{\partial x^2}\right)^2 dxdydz \tag{3.9}$$

$$= \frac{1}{2}\int_0^{l_e} bD_{11}\left(\frac{\partial^2 w}{\partial x^2}\right)^2 dx$$

The kinetic energy of an elastic body in terms of an xyz coordinate system is of the form [1]:

$$T = \frac{1}{2}\int\int\int\rho\left[\left(\frac{\partial u}{\partial t}\right)^2 + \left(\frac{\partial v}{\partial t}\right)^2 + \left(\frac{\partial w}{\partial t}\right)^2\right]dxdydz \tag{3.10}$$

where ρ is the density of the material at a point (x, y, z). In the case of pure bending based on the classical laminate theory, substituting Equations 3.4 and 3.5 into Equation 3.10, the kinetic energy can be written as:

$$T = \frac{1}{2}\int\int\int\rho\left[\left(-z\frac{\partial^2 w}{\partial x \partial t}\right)^2 + \left(\frac{\partial w}{\partial t}\right)^2\right]dxdydz \tag{3.11}$$

We have assumed that the rotary inertia terms are negligible, thus the first term in kinetic energy T can be ignored:

$$T = \frac{1}{2}\int_{-\frac{H}{2}}^{\frac{H}{2}}\int_0^{l_e}\rho b\left(\frac{\partial w}{\partial t}\right)^2 dxdz \tag{3.12}$$

where b is the constant width of the beam.

For free vibration, time can be removed from the above equation by considering harmonic displacement field of the form:

$$w(x,t) = W(x)e^{i\omega t} \tag{3.13}$$

where ω is the natural frequency of vibration and W is the magnitude of

vibration. Thus,

$$T = \frac{1}{2}\int_{-\frac{H}{2}}^{\frac{H}{2}}\int_0^{l_e} \rho b\left[\frac{\partial\left(We^{i\omega t}\right)}{\partial t}\right]^2 dxdz$$
$$= \frac{1}{2}\int_{-\frac{H}{2}}^{\frac{H}{2}}\int_0^{l_e} \rho b\left(i\omega We^{i\omega t}\right)^2 dxdz \qquad (3.14)$$
$$= -\frac{\omega^2}{2}\int_{-\frac{H}{2}}^{\frac{H}{2}}\int_0^{l_e} \rho b w^2 dxdz$$

For uniform composite beam, there is only one kind of material and its density is constant. But some other models, i.e. models A, B, C, D, and M, consist of two parts, i.e., laminate and resin as shown in Figure 3.1.

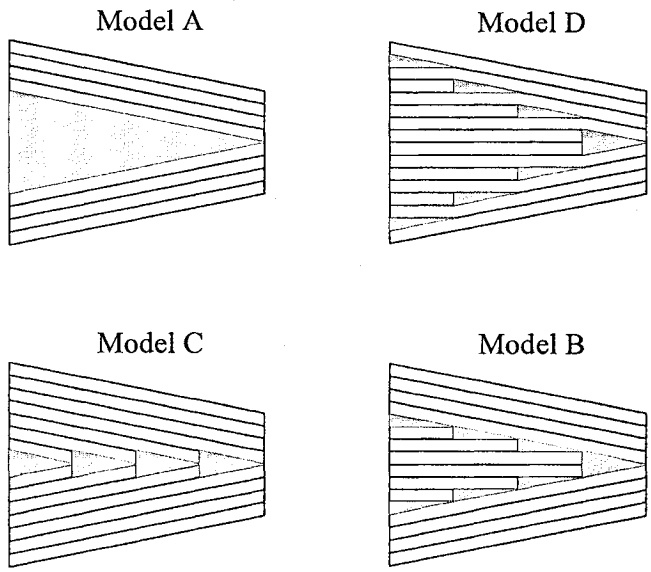

Figure 3.1 Tapered beam models, A, B, C, and D

Therefore, the kinetic energy is expressed by:

$$T = -\frac{\omega^2}{2}\int_0^{l_e} b\left(\rho_L H_L + \rho_r H_r\right) w^2 dx \qquad (3.15)$$

where

ρ_L --- Density of laminate (constant)

H_L --- Total height of laminate (can be discontinuous functions of x)

ρ_r --- Density of resin (constant)

H_r --- Total height of resin (can be discontinuous functions of x)

Note that, H_L and H_r can be linear functions of x and their expressions can vary from domain to domain.

Thus, for free vibration without external force, the stationary value is:

$$\Pi = U + T = \frac{1}{2}\int_0^{l_e} bD_{11}\left(\frac{\partial^2 w}{\partial x^2}\right)^2 dx - \frac{\omega^2}{2}\int_0^{l_e} b(\rho_L H_L + \rho_r H_r)w^2 dx \tag{3.16}$$

In Ritz method, a solution is sought in the form:

$$W(x) = \sum_{i=1}^{N} c_i \phi_i \tag{3.17}$$

where c_i is undetermined coefficient, and ϕ_i is the interpolation function satisfying the boundary conditions and is known.

Substituting Equation 3.17 into Equation 3.16 leads to a minimization problem relative to the undetermined coefficients. Then we can impose the stationary condition:

$$\frac{\partial \Pi}{\partial c_i} = 0 \tag{3.18}$$

For the formulation presented here, Π is always quadratic in the undetermined coefficients c_i. We can get a set of N linear simultaneous equations. Expressing these N equations in a matrix form, we have:

$$[[K] - \omega^2 [M]]\{c\} = 0 \tag{3.19}$$

For free vibration problem, Equation 3.19 leads to a classic eigenvalue problem. That is, the free vibration frequencies are chosen such that the determinants of the coefficients c_i vanish.

3.2.1.2 Example applications

In this section, we will apply Ritz method to a uniform laminated composite beam with different boundary conditions. Then, a tapered laminated composite beam with these boundary conditions is presented.

Example 3.1 vibration of a simply supported uniform composite beam using Ritz method

A uniform composite beam with both ends simply supported as shown in Figure 3.2 is made up of NCT301 graphite-epoxy. Its mechanical properties are shown in Table 2.2.

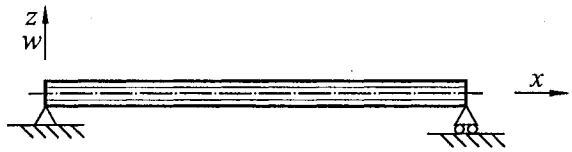

Figure 3.2 Simply supported uniform composite beam

The geometric properties of the beam are: length $L = 0.3048\,\mathrm{m}$; individual ply thickness $t = 0.0001524\,\mathrm{m}$. There are 32 plies in the laminate and the configuration of

the laminate is $[(0/90)_8]_S$. The laminate thickness of $H = 0.0048768\,\text{m}$ is obtained by multiplying the number of plies, 32 in this case, with the ply thickness, i.e. $0.0001524\,\text{m}$.

The exact solution is given by [2]

$$\omega_i = \frac{i^2\pi^2}{L^2}\sqrt{\frac{D_{11}}{\rho H}} \tag{3.20}$$

For this uniform composite beam, the bending stiffness coefficient is

$D_{11} = 817.127\,\text{N.m}$

Substituting the value of D_{11} into Equation 3.20 yields the natural frequencies of the beam. The first four exact natural frequencies are calculated as:

$$\omega_1 = \frac{\pi^2}{0.3048^2}\sqrt{\frac{817.127}{1660.8\times 0.0001524\times 32}} = 1067.06\,\text{rad/sec}$$

$\omega_2 = 4268.24\,\text{rad/sec}$

$\omega_3 = 9603.53\,\text{rad/sec}$

$\omega_4 = 17072.9\,\text{rad/sec}$

In this example, both polynomial and trigonometric interpolation functions are assumed for displacement W. Every polynomial or trigonometric term satisfies the simply supported boundary conditions.

At first, polynomial interpolation functions are given to W:

$$W = \sum_{i=1}^{N} c_i x^i (L - x) \tag{3.21}$$

Table 3.1 gives the calculated natural frequencies of this simply supported composite beam using the above polynomial interpolation functions:

Table 3.1 Natural frequencies of uniform composite beam described in Example 3.1 using polynomial interpolation functions

	1R*	2R	3R	4R	5R	Exact
ω_1	1184.35	1184.35	1067.38	1067.38	1067.06	1067.06
ω_2		5427.37	5427.37	4286.31	4286.31	4268.24
ω_3			14251.0	14251.0	9766.84	9603.53
ω_4				29842.3	29842.3	17072.9

*1R means W has one interpolation term.

As can be seen from Table 3.1, the natural frequencies converge to the exact solution rapidly.

Then, trigonometric interpolation functions are assumed for the displacement:

$$W = \sum_{i=1}^{N} c_i \sin \frac{i\pi x}{L} \tag{3.22}$$

Table 3.2 gives the calculated natural frequencies using the above trigonometric interpolation functions:

Table 3.2 Natural frequencies of uniform composite beam described in Example 3.1 using trigonometric interpolation functions

	1R	2R	3R	4R	5R	Exact
ω_1	1067.06	1067.06	1067.06	1067.06	1067.06	1067.06
ω_2		4268.24	4268.24	4268.24	4268.24	4268.24
ω_3			9603.53	9603.53	9603.53	9603.53
ω_4				17072.9	17072.9	17072.9

Table 3.2 shows perfect accuracy, even when W has only one interpolation term. The result gives the exact solution. This is because of the trigonometric function. The exact solution comes from solving the governing differential equation by assuming harmonic vibration:

$$w = c_i e^{i\omega t} \sin \frac{i\pi x}{L} \tag{3.23}$$

which is similar to what assumed for w in Ritz method.

Example 3.2 vibration of a fixed-fixed uniform composite beam using Ritz method

The same uniform composite beam in Example 3.1 with both ends fixed is shown in Figure 3.3.

Figure 3.3 Fixed-fixed uniform composite beam

The exact solution is given by [2]:

$$\omega_i = \frac{k_i^2}{L^2}\sqrt{\frac{D_{11}}{\rho H}} \tag{3.24}$$

The first four coefficients k_i are:

$k_1 = 4.7300407$, $k_2 = 7.8532046$, $k_3 = 10.995608$, $k_4 = 14.137166$.

In order to satisfy the boundary condition, we assume the displacement function as:

$$W = \sum_{i=1}^{N} c_i x^i (L-x)\sin\frac{\pi x}{L} \tag{3.25}$$

Table 3.3 gives the results.

Table 3.3 Natural frequencies of uniform composite beam described in Example 3.2

	1R	2R	3R	4R	5R	Exact
ω_1	2423.49	2423.49	2418.97	2418.97	2418.90	2418.90
ω_2		6689.91	6689.91	6668.34	6668.34	6667.80
ω_3			13403.9	13403.9	13080.1	13071.6
ω_4				23079.8	23079.9	21607.9

The convergence of the natural frequencies of this fixed-fixed composite beam is similar to that of the simply supported beam obtained by using polynomial interpolation functions (Table 3.1). The convergence is fast but not as perfect as that of the simply supported beam obtained by using trigonometric interpolation functions (Table 3.2.).

Example 3.3 vibration of a fixed-free uniform composite beam using Ritz method

The same uniform composite beam in Example 3.1 with one end fixed and another end free is shown in Figure 3.4.

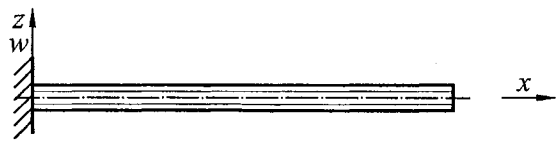

Figure 3.4 Fixed-free uniform composite beam

The exact solution is given by [2]:

$$\omega_i = \frac{k_i^2}{L^2}\sqrt{\frac{D_{11}}{\rho H}} \tag{3.26}$$

where,

$k_1 = 1.8751038,\ k_2 = 4.6940911,\ k_3 = 7.8547574,\ k_4 = 10.995541$

The displacement function is assumed as:

$$W = \sum_{i=1}^{N} c_i x^{i+1} \tag{3.27}$$

Table 3.4 gives the result.

Table 3.4 Natural frequencies of uniform composite beam described in Example 3.3

	1R	2R	3R	4R	5R	Exact
ω_1	483.508	381.944	380.251	380.137	380.136	380.136
ω_2		3763.17	2403.78	2395.61	2382.34	2382.27
ω_3			12773.3	6848.76	6837.21	6670.44
ω_4				30445.0	13895.0	13071.4

From the above three examples, we can see that Ritz method shows rapid convergence to the exact solutions. These results are used to compare the results from hierarchical finite element method. The following is the application of Ritz method to tapered composite beam.

Example 3.4 vibration of a simply supported tapered composite beam using Ritz method

A tapered composite beam made up of NCT301 graphite-epoxy has configuration of Model F. Both of its ends are simply supported as shown in Figure 3.5. Its mechanical properties are shown in Table 2.2.

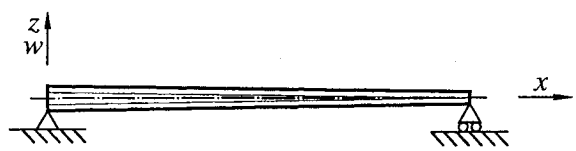

Figure 3.5 Simply supported tapered composite beam

The geometric properties of the beam are: length $L = 0.3048\,\text{m}$; individual ply thickness $t = 0.0001524\,\text{m}$. There are 32 plies at the left end and 30 plies at the right end. Two layers are dropped off. The configuration of both ends are $[(0/90)_8]_S$ and $[(0/90)_7/0]_S$ respectively. The height of each ply in z direction is $h = 0.00015240001905\,\text{m}$. It is almost as same as the thickness $t = 0.0001524\,\text{m}$, because the tapered angle is only $\alpha = 0.02865°$. The bending stiffness coefficient is a cubic function of x throughout the entire length:

$$D_{11} = 817.122 - 490.366x + 95.5097x^2 - 1.01515x^3$$

For this example, we also use both polynomial and trigonometric interpolation functions to calculate the frequencies. The interpolation functions are as same as Equations 3.21 and 3.22 respectively.

Table 3.5 gives the natural frequencies of the tapered composite beam using polynomial functions.

Table 3.5 Natural frequencies of tapered composite beam described in Example 3.4 using polynomial interpolation functions

	1R	2R	3R	4R	5R	10R
ω_1	1149.23	1147.61	1035.07	1034.86	1034.57	1034.57
ω_2		5268.50	5256.77	4157.93	4156.02	4138.85
ω_3			13837.4	13795.3	9476.08	9312.21
ω_4				28984.7	28873.8	16554.8

The results have little difference from that of the uniform beam case and the convergence is similar. That is reasonable because the tapered angle is so small. So far, we do not know the exact solution for this example. But from this table, it seems we can expect we have got a very good approximate solution. The same example will be

evaluated by finite element method.

Now trigonometric interpolation function is assumed for W, as given by Equation 3.22. Table 3.6 gives the natural frequencies.

Table 3.6 Natural frequencies of tapered composite beam described in Example 3.4 using trigonometric interpolation functions

	1R	2R	3R	4R	5R	10R
ω_1	1035.11	1034.57	1034.57	1034.57	1034.57	1034.57
ω_2		4141.38	4138.88	4138.87	4138.85	4138.85
ω_3			9318.52	9312.28	9312.28	9312.21
ω_4				16567.2	16555.0	16554.8

As can be seen the convergence is still very fast, but the results from low order displacement functions are not close to that from high order displacement function, unlike the case of the uniform composite beam. That is because the taper angle results in a cubic D_{11}. Few trigonometric terms can not accurately describe the real displacement. When more terms are used in the displacement function, more accurate values of frequencies are obtained in the vibration analysis.

Example 3.5 vibration of a fixed-fixed tapered composite beam using Ritz method

The same tapered composite beam of Example 3.4 is fixed at both ends as shown in Figure 3.6.

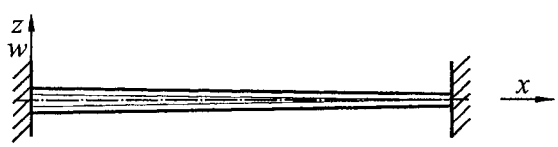

Figure 3.6 Fixed-fixed tapered composite beam

The displacement is assumed as same as Equation 3.25 according to the boundary condition: Table 3.7 gives similar convergence to that of the uniform composite beam case.

Table 3.7 Natural frequencies of tapered composite beam described in Example 3.5

	1R	2R	3R	4R	5R	10R
ω_1	2352.03	2350.12	2345.55	2345.55	2345.48	2345.48
ω_2		6492.74	6486.00	6465.99	6465.87	6465.36
ω_3			13010.5	12991.4	12684.1	12674.7
ω_4				22407.5	22360.1	20951.8

Example 3.6 vibration of a fixed-free tapered composite beam using Ritz method

The boundary condition is changed to fixed-free for the same composite beam in Example 3.4, as shown in Figure 3.7, and the displacement is assumed as same as Equation 3.27.

Figure 3.7 Fixed-free tapered composite beam

Table 3.8 Natural frequencies of tapered composite beam described in Example 3.6

	1R	2R	3R	4R	5R	10R
ω_1	474.298	384.175	383.279	383.118	383.116	383.116
ω_2		3576.78	2354.46	2351.89	2337.84	2337.67
ω_3			12030.9	6662.19	6661.60	6494.73
ω_4				28580.9	13497.7	12701.4

Because this beam is unidirectionally tapered, we can expect that changing the boundary condition to free-fixed should change the natural frequency. Then it is necessary to give a free-fixed boundary condition example.

Example 3.7 vibration of a free-fixed tapered composite beam using Ritz method

The boundary condition is changed to free-fixed as shown in Figure 3.8 for the same composite beam in Example 3.4, and the displacement is assumed as:

$$w = \sum_{i=1}^{N} c_i (L - x)^{i+1}$$

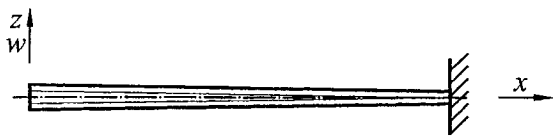

Figure 3.8 Free-fixed tapered composite beam

Table 3.9 Natural frequencies of tapered composite beam described in Example 3.7

	1R	2R	3R	4R	5R	10R
ω_1	464.205	357.165	354.543	354.483	354.483	354.483
ω_2		3725.11	2310.04	2293.80	2282.60	2282.56
ω_3			12752.6	6629.56	6594.42	6441.69
ω_4				30487.6	13474.2	12648.3

From the above examples, we can say that Ritz method has good convergence and converges to the exact solution for uniform beam. It even shows perfect accuracy for the simply supported uniform composite beam by using trigonometric interpolation functions. In addition, it seems also to converge to a very good approximate solution for tapered laminated beam. In the following, the hierarchical finite element method is used for the same examples. Then we can compare the results from both methods.

3.2.2 Solution using Hierarchical Finite Element Method and based on CLT

In this section, first we will derive the formulations for HFEM based on the classical laminate theory and then verify the same examples given in the previous section.

3.2.2.1 Formulation using HFEM based on CLT

In the previous section, we have already derived the stationary value (Equation 3.16) based on the classical laminate theory:

From Hamilton's principle, the governing equations of motion and the proper boundary conditions are determined from the variational equations [1]:

$$\delta\Pi = 0 \tag{3.28}$$

$$\delta\Pi = \int_0^{l_e} bD_{11}\frac{d^2w}{dx^2}\frac{d^2\delta w}{dx^2}dx - \omega^2\int_0^{l_e} b(\rho_L H_L + \rho_r H_r)w\delta w dx = 0 \tag{3.29}$$

$$\int_0^{l_e} D_{11}\frac{d^2w}{dx^2}\frac{d^2\delta w}{dx^2}dx - \omega^2\int_0^{l_e} (\rho_L H_L + \rho_r H_r)w\delta w dx = 0 \tag{3.30}$$

In the formulation of the finite element model using the conventional formulation, we assumed a cubic displacement function for *W*. In the hierarchical formulation, we modify the approximating function by adding trigonometric or polynomial functions [1]. In this thesis, we assume the displacement function as:

$$W = c_1 + c_2 x + c_3 x^2 + c_4 x^3 + \sum_{n=1}^{N} c_{n+4}\sin\frac{n\pi x}{l_e} \quad \text{n=1, 2, 3...} \tag{3.31}$$

It is imperative to mention here why we add some trigonometric terms into the displacement function. If the polynomial terms are used by themselves they will be sufficient to describe the displacement and the rotation of the beam cross-section within

the element. The additional trigonometric sine term allows for better description of the transverse displacement and the rotation of the beam cross-section within the element. Inter-element compatibility is achieved by matching the generalized co-ordinates at the element end nodes. All of the hierarchical terms should be zero at the coordinates of the two nodes of each element.

Equation 3.31 may be written as:

$$W = \left[1 \quad x \quad x^2 \quad x^3 \quad \sin\frac{\pi x}{l_e} \quad \sin\frac{2\pi x}{l_e} \quad \cdots \quad \sin\frac{n\pi x}{l_e} \right]_{1\times(n+4)} \begin{Bmatrix} c_1 \\ c_2 \\ c_3 \\ c_4 \\ c_5 \\ c_6 \\ \vdots \\ c_{n+4} \end{Bmatrix}_{(n+4)\times 1} = [K_w]\{c\} \tag{3.32}$$

The rotation is the once differential of transverse displacement:

$$\theta = \left[0 \quad 1 \quad 2x \quad 3x^2 \quad \frac{\pi}{l_e}\cos\frac{\pi x}{l_e} \quad \frac{2\pi}{l_e}\cos\frac{2\pi x}{l_e} \quad \cdots \quad \frac{n\pi}{l_e}\cos\frac{n\pi x}{l_e} \right]_{1\times(n+4)} \begin{Bmatrix} c_1 \\ c_2 \\ c_3 \\ c_4 \\ c_5 \\ c_6 \\ \vdots \\ c_{n+4} \end{Bmatrix}_{(n+4)\times 1}$$

$$= [K_\theta]\{c\} \tag{3.33}$$

In local coordinate system, the nodal displacements and rotations are:

$$\{u\}=\begin{Bmatrix} w_1 \\ \theta_1 \\ w_2 \\ \theta_2 \\ A_1 \\ A_2 \\ \vdots \\ A_n \end{Bmatrix}_{(n+4)\times 1} = \begin{bmatrix} 1 & 0 & 0 & 0 & 0 & 0 & & 0 \\ 0 & 1 & 0 & 0 & \frac{\pi}{l_e} & \frac{2\pi}{l_e} & & \frac{n\pi}{l_e} \\ 1 & l_e & l_e^2 & l_e^3 & 0 & 0 & & 0 \\ 0 & 1 & 2l_e & 3l_e^2 & -\frac{\pi}{l_e} & \frac{2\pi}{l_e} & & (-1)^n\frac{n\pi}{l_e} \\ 0 & 0 & 0 & 0 & 1 & 0 & & 0 \\ 0 & 0 & 0 & 0 & 0 & 1 & & 0 \\ & & & & & & \ddots & \\ 0 & 0 & 0 & 0 & 0 & 0 & 0 & 1 \end{bmatrix}_{(n+4)\times(n+4)} \begin{Bmatrix} c_1 \\ c_2 \\ c_3 \\ c_4 \\ c_5 \\ c_6 \\ \vdots \\ c_{n+4} \end{Bmatrix}_{(n+4)\times 1}$$

$$= [K_u]\{c\} \tag{3.34}$$

In finite element method, the transverse displacement is then expressed by interpolation functions and nodal displacements:

$$W = \begin{bmatrix} N_1^w & N_2^w & N_3^w & N_4^w & N_5^w & N_6^w & \cdots & N_{n+4}^w \end{bmatrix}_{1\times(n+4)} \begin{Bmatrix} w_1 \\ \theta_1 \\ w_2 \\ \theta_2 \\ A_1 \\ A_2 \\ \vdots \\ A_n \end{Bmatrix}_{(n+4)\times 1} = [N^w]\{u\} \tag{3.35}$$

Substituting Equations 3.32 and 3.34 into Equation 3.35 yields:

$$[N^w] = [K_w][K_u]^{-1} \tag{3.36}$$

The expanded interpolation functions are:

$$\begin{cases} N_1^w = 1-3\dfrac{x^2}{l_e^2}+2\dfrac{x^3}{l_e^3} \\ N_2^w = x-\dfrac{2x^2}{l_e}+\dfrac{x^3}{l_e^2} \\ N_3^w = 3\dfrac{x^2}{l_e^2}-2\dfrac{x^3}{l_e^3} \\ N_4^w = -\dfrac{x^2}{l_e}+\dfrac{x^3}{l_e^2} \\ N_5^w = -\dfrac{\pi x}{l_e}+\dfrac{\pi x^2}{l_e^2}+\sin\dfrac{\pi x}{l_e} \\ N_6^w = -\dfrac{2\pi x}{l_e}+3\dfrac{2\pi x^2}{l_e^2}-2\dfrac{2\pi x^3}{l_e^3}+\sin\dfrac{2\pi x}{l_e} \\ \quad\vdots \\ N_{n+4}^w = -\dfrac{n\pi x}{l_e}+\left[(-1)^n+2\right]\dfrac{n\pi x^2}{l_e^2}-\left[(-1)^n+1\right]\dfrac{n\pi x^3}{l_e^3}+\sin\dfrac{n\pi x}{l_e} \end{cases} \tag{3.37}$$

Using the notation:

$$\left[N^M\right]=\frac{d^2\left[N^w\right]}{dx^2} \tag{3.38}$$

Equation 3.19 can be written as:

$$\left[\int_0^{l_e} D_{11}\left[N^M\right]^T\left[N^M\right]dx-\omega^2\int_0^{l_e}\left(\rho_L H_L+\rho_r H_r\right)\left[N^w\right]^T\left[N^w\right]dx\right]\{u\}=0 \tag{3.39}$$

That is:

$$\left[[K]-\omega^2[M]\right]\{u\}=0 \tag{3.40}$$

where $[K]$ is the stiffness matrix and $[M]$ is the mass matrix.

$$[K]=\int_0^{l_e} D_{11}\left[N^M\right]^T\left[N^M\right]dx \tag{3.41}$$

$$[M]=\int_0^{l_e}\left(\rho_L H_L+\rho_r H_r\right)\left[N^w\right]^T\left[N^w\right]dx \tag{3.42}$$

Note that, each element could include several domains and each domain could have different D_{11}, H_L, and H_r. Therefore, $[K]$ and $[M]$ should be the sum of integrations in each domain.

As same as in Ritz method, solving the eigenvalue problem $\left|[K]-\omega^2[M]\right|=0$, we can get the natural frequencies.

3.2.2.2 Example applications

Now we can check Examples 3.1 to 3.7 using HFEM instead of Ritz method. First of all, we use HFEM without hierarchical term, in another word, conventional FEM to re-solve Example 3.1. The displacement function is written as:

$$W = c_1 + c_2 x + c_3 x^2 + c_4 x^3 \tag{3.43}$$

Then we use one hierarchical term.

$$W = c_1 + c_2 x + c_3 x^2 + c_4 x^3 + c_5 \sin\frac{\pi x}{l_e} \tag{3.44}$$

Also we use two hierarchical terms to get more accurate results and compare the result with that from the conventional FEM.

$$W = c_1 + c_2 x + c_3 x^2 + c_4 x^3 + c_5 \sin\frac{\pi x}{l_e} + c_6 \sin\frac{2\pi x}{l_e} \tag{3.45}$$

Tables 3.10 to 3.12 give the results for Example 3.1 obtained from the above three models respectively. The exact solution is from Equation 3.20.

Table 3.10 Natural frequencies of uniform composite beam described in Example 3.1 using conventional FEM based on CLT

	2E*	4E	6E	8E	10E	12E	Exact
ω_1	1074.78	1067.38	1067.11	1067.08	1067.07	1067.06	1067.06
ω_2		4299.11	4271.69	4269.54	4268.69	4268.47	4268.24
ω_3		10166.2	9641.44	9621.13	9608.66	9606.46	9603.53
ω_4			17274.8	17196.5	17101.2	17091.3	17072.9

*2E means two-elements model.

Table 3.11 Natural frequencies of uniform composite beam described in Example 3.1 using one-hierarchical-term model based on CLT

	2E1T*	4E1T	6E1T	8E1T	10E1T	12E1T	Exact
ω_1	1067.14	1067.06	1067.06	1067.06	1067.06	1067.06	1067.06
ω_2		4268.56	4268.27	4268.24	4268.24	4268.24	4268.24
ω_3		9610.58	9604.27	9603.68	9603.58	9603.55	9603.53
ω_4			17079.4	17074.3	17073.3	17073.1	17072.9

*2E1T means two-elements model, and w has one trigonometric hierarchical term.

Table 3.12 Natural frequencies of uniform composite beam described in Example 3.1 using two-hierarchical-terms model based on CLT

	2E2T	4E2T	6E2T	8E2T	10E2T	12E2T	Exact
ω_1	1067.07	1067.06	1067.06	1067.06	1067.06	1067.06	1067.06
ω_2		4268.27	4268.25	4268.24	4268.24	4268.24	4268.24
ω_3		9603.76	9603.61	9603.56	9603.55	9603.54	9603.53
ω_4			17073.3	17073.1	17073.0	17073.0	17072.9

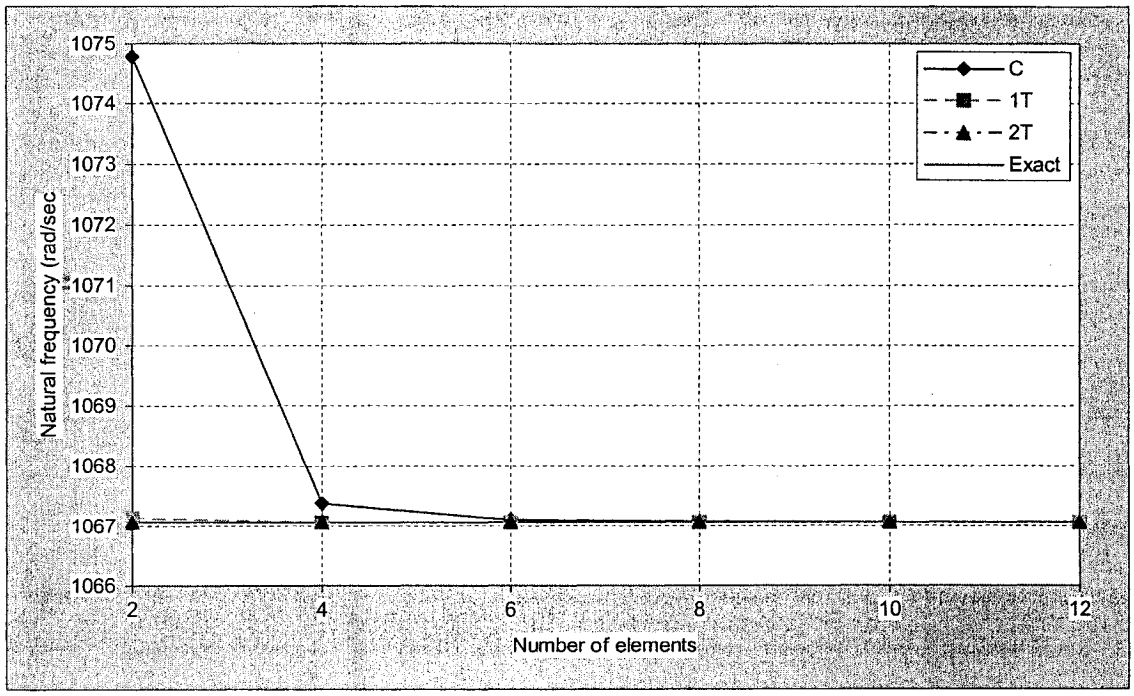

Figure 3.9 First mode frequency of simply supported uniform composite beam based on CLT

Figure 3.9 shows the comparison between conventional and hierarchical FEM

obtained from this example. Only the first natural frequency is plotted in this figure. We can observe from the tables that the other frequencies have similar convergence of ω_1.

For this simply supported uniform composite beam, both conventional FEM and HFEM show rapid convergence. At the same time, HFEM gives much more accurate results compared with those from conventional FEM, especially for the two-elements and four-elements models.

In above three examples, we fixed the number of hierarchical terms and increased the number of element from two to twelve, and the comparison shows the considerable improvement of hierarchical FEM. Next, for this same example, we will fix the number of elements but increase the number of hierarchical terms to observe the convergence.

Table 3.13 Natural frequencies of uniform composite beam described in Example 3.1 using two-elements model based on CLT

	2E0T	2E1T	2E2T	2E3T	2E4T	2E5T	2E6T	Exact
ω_1	1074.78	1067.14	1067.07	1067.06	1067.06	1067.06	1067.06	1067.06

Table 3.14 Natural frequencies of uniform composite beam described in Example 3.1 using three-elements model based on CLT

	3E0T	3E1T	3E2T	3E3T	3E4T	3E5T	3E6T	Exact
ω_1	1067.92	1067.07	1067.06	1067.06	1067.06	1067.06	1067.06	1067.06
ω_2	4318.69	4269.86	4268.32	4268.27	4268.24	4268.24	4268.24	4268.24

Table 3.15 Natural frequencies of uniform composite beam described in Example 3.1 using four-elements model based on CLT

	4E0T	4E1T	4E2T	4E3T	4E4T	4E5T	4E6T	Exact
ω_1	1067.38	1067.06	1067.06	1067.06	1067.06	1067.06	1067.06	1067.06
ω_2	4299.11	4268.56	4268.27	4268.24	4268.24	4268.24	4268.24	4268.24
ω_3	10166.2	9610.58	9603.76	9603.66	9603.55	9603.55	9603.54	9603.53

Table 3.16 Natural frequencies of uniform composite beam described in Example 3.1 using five-elements model based on CLT

	5E0T	5E1T	5E2T	5E3T	5E4T	5E5T	5E6T	Exact
ω_1	1067.17	1067.06	1067.06	1067.06	1067.06	1067.06	1067.06	1067.06
ω_2	4275.31	4268.33	4268.25	4268.24	4268.24	4268.24	4268.24	4268.24
ω_3	9679.80	9605.56	9603.67	9603.58	9603.54	9603.54	9603.53	9603.53
ω_4	17466.3	17090.9	17073.4	17073.3	17073.0	17073.0	17073.0	17072.9

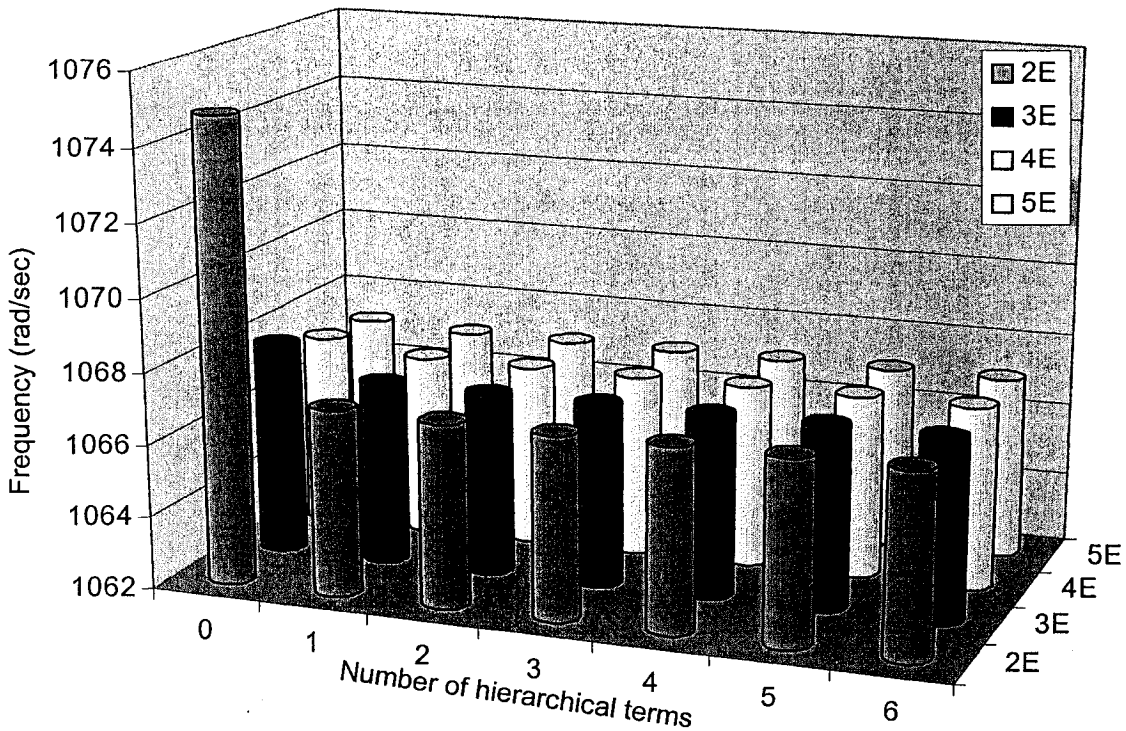

Figure 3.10 3-D plot of the first mode frequency

Figure 3.10 shows the first mode frequencies of two-elements to five-elements models. It is plotted using 3-D column with cylindrical shape. As can be seen the frequency converges fast by increasing the number of elements or the number of hierarchical terms. The two-elements conventional model shows more inaccuracy than the others.

For the sake of numerical observation, these frequencies are also plotted by four

lines as shown in figure 3.11.

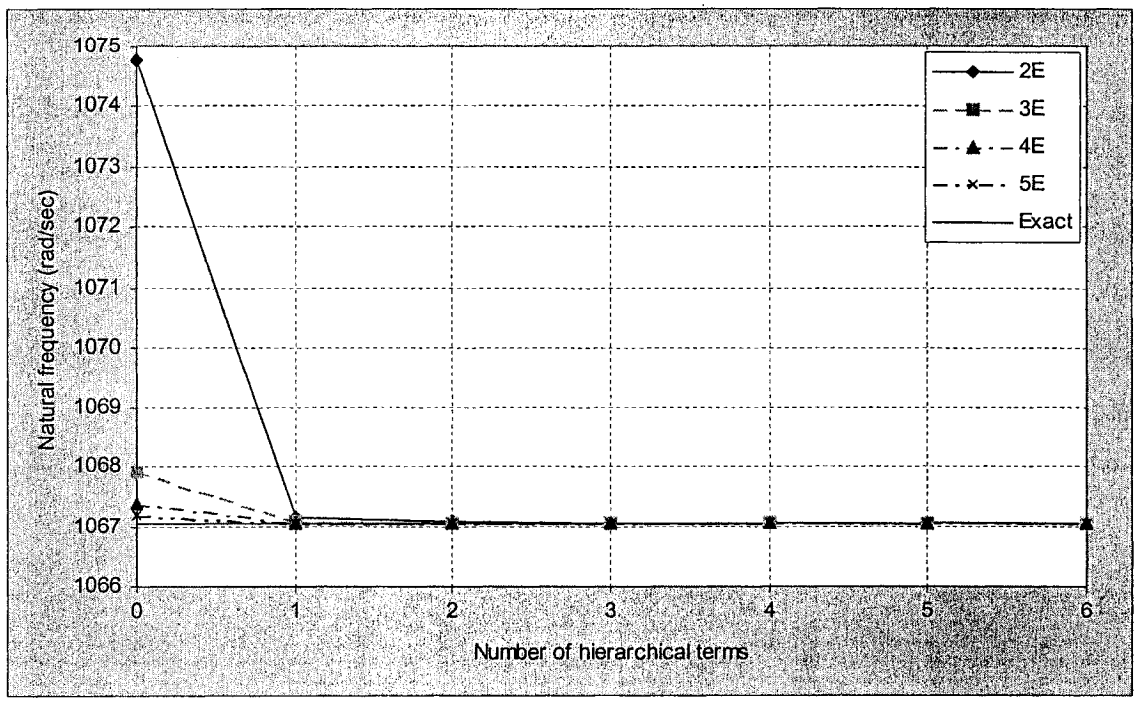

Figure 3.11 2-D plot of the first mode frequency

Obviously, the convergence by increasing number of hierarchical terms is faster then that by increasing number of elements. The two-elements two-hierarchical model gives almost the exact solution, while the conventional FEM shows more inaccuracy even though the number of elements reaches five. HFEM shows critical advantages of using fewer elements and obtaining better accuracy.

The same comparison is also done to the same beam but with different boundary conditions. Tables 3.17 to 3.19 and 3.20 to 3.22 give the first four modes' frequencies for fixed-fixed beam described in Example 3.2 and fixed-free beam described in Example 3.3 respectively. Figures 3.12 and 3.13 plot the first mode frequencies.

Table 3.17 Natural frequencies of uniform composite beam described in Example 3.2 using conventional FEM based on CLT

	2E	4E	6E	8E	10E	12E	Exact
ω_1	2458.11	2422.11	2419.55	2419.11	2418.99	2418.94	2418.90
ω_2		6729.48	6680.89	6672.01	6669.54	6668.64	6667.80
ω_3		13350.7	13165.2	13102.5	13084.5	13077.8	13071.6
ω_4			21985.6	21742.7	21665.0	21635.9	21607.9

Table 3.18 Natural frequencies of uniform composite beam described in Example 3.2 using one-hierarchical-term model based on CLT

	2E1T	4E1T	6E1T	8E1T	10E1T	12E1T	Exact
ω_1	2420.70	2418.93	2418.91	2418.90	2418.90	2418.90	2418.90
ω_2		6669.33	6667.95	6667.83	6667.81	6667.80	6667.80
ω_3		13102.5	13073.6	13072.0	13071.7	13071.6	13071.6
ω_4			21623.9	21610.8	21608.8	21608.3	21607.9

Table 3.19 Natural frequencies of uniform composite beam described in Example 3.2 using two-hierarchical-terms model based on CLT

	2E2T	4E2T	6E2T	8E2T	10E2T	12E2T	Exact
ω_1	2419.03	2418.91	2418.91	2418.90	2418.90	2418.90	2418.90
ω_2		6667.94	6667.83	6667.81	6667.81	6667.80	6667.80
ω_3		13072.4	13071.8	13071.6	13071.6	13071.6	13071.6
ω_4			21608.6	21608.2	21608.1	21608.0	21607.9

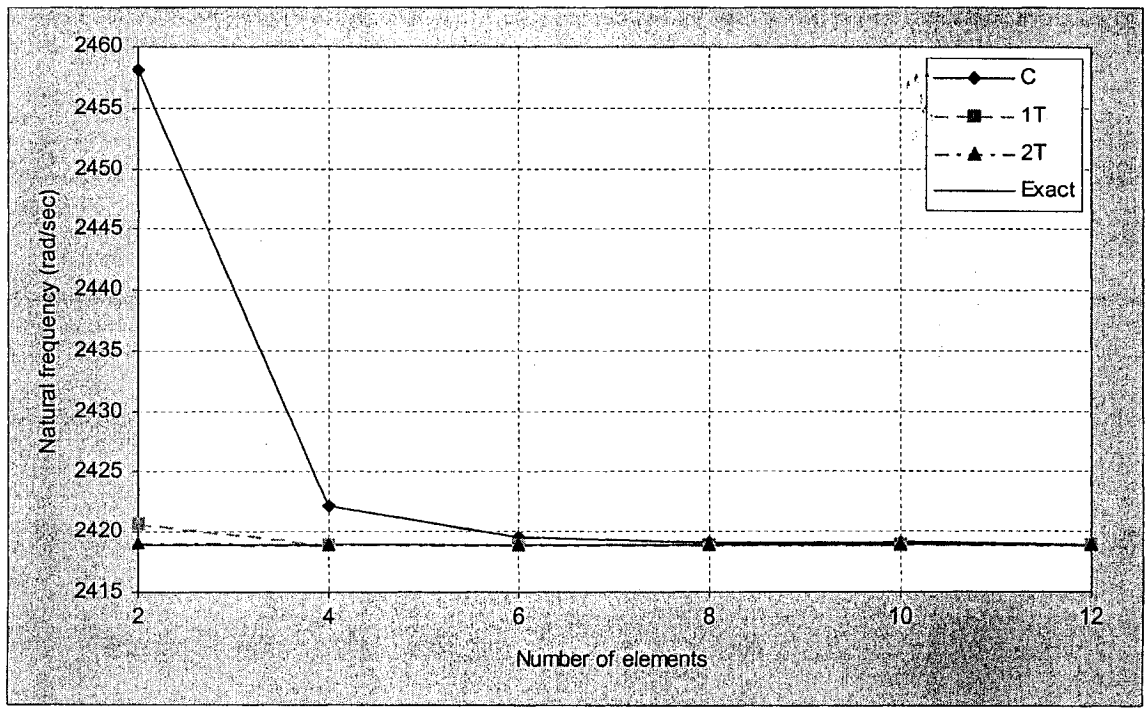

Figure 3.12 First mode frequency of fixed-fixed uniform composite beam based on CLT

Table 3.20 Natural frequencies of uniform composite beam described in Example 3.3 using conventional FEM based on CLT

	2E	4E	6E	8E	10E	12E	Exact
ω_1	380.320	380.149	380.139	380.137	380.137	380.137	380.136
ω_2		2385.05	2382.86	2382.46	2382.35	2382.31	2382.27
ω_3		6722.08	6682.64	6674.49	6672.14	6671.27	6670.44
ω_4			13155.6	13100.7	13083.9	13077.5	13071.4

Table 3.21 Natural frequencies of uniform composite beam described in Example 3.3 using one-hierarchical-term model based on CLT

	2E1T	4E1T	6E1T	8E1T	10E1T	12E1T	Exact
ω_1	380.139	380.137	380.136	380.136	380.136	380.136	380.136
ω_2		2382.33	2382.28	2382.28	2382.27	2382.27	2382.27
ω_3		6672.83	6670.67	6670.48	6670.45	6670.44	6670.44
ω_4			13074.3	13072.0	13071.6	13071.5	13071.4

Table 3.22 Natural frequencies of uniform composite beam described in Example 3.3 using two-hierarchical-terms model based on CLT

	2E2T	4E2T	6E2T	8E2T	10E2T	12E2T	Exact
ω_1	380.137	380.136	380.136	380.136	380.136	380.136	380.136
ω_2		2382.28	2382.28	2382.28	2382.27	2382.27	2382.27
ω_3		6670.57	6670.47	6670.45	6670.44	6670.44	6670.44
ω_4			13071.6	13071.5	13071.4	13071.4	13071.4

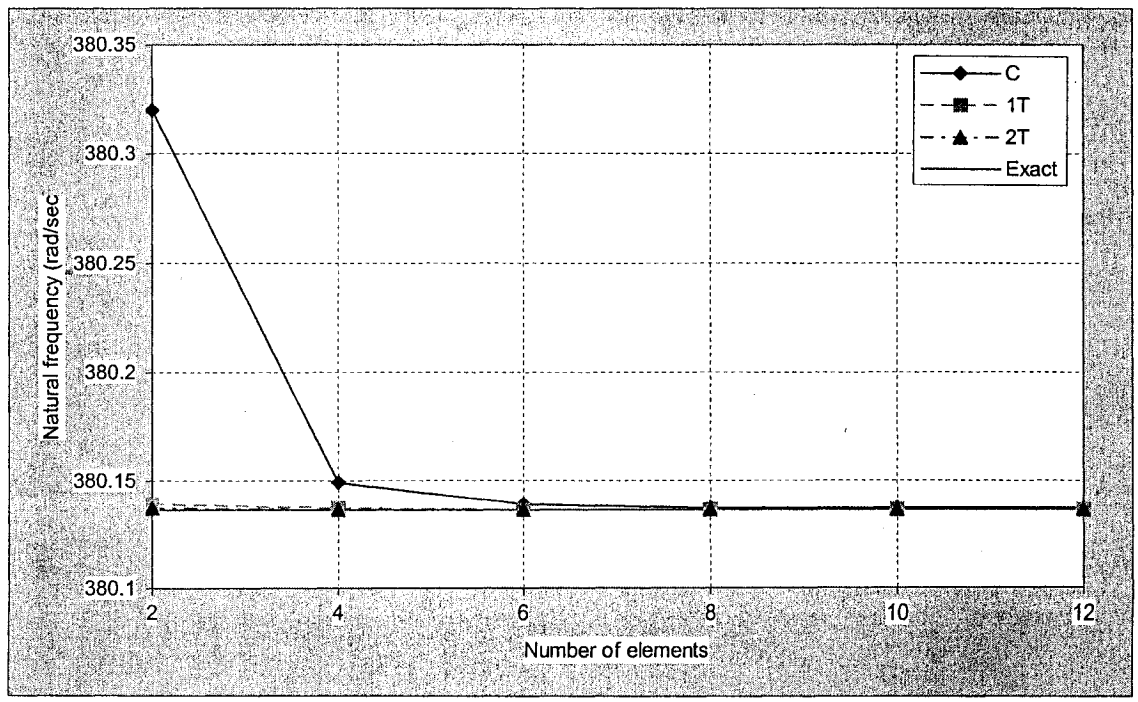

Figure 3.13 First mode frequency of fixed-free uniform composite beam based on CLT

As can be seen from these three examples, both conventional FEM and HFEM show rapid convergence for uniform composite beam with different boundary conditions. At the same time, HFEM gives much more accurate results compared with those from conventional FEM, especially for the two-elements and four-elements models. With two hierarchical terms, we can use just a two-elements model to obtain considerable accuracy for the first mode frequency.

The following is the calculation of natural frequency for the tapered composite beam given in Example 3.4, but using HFEM instead of Ritz method. This problem has also been solved in Amit's thesis [56]. Because the taper angle α is so small, Amit ignored the effect on the ply stiffness caused by the taper angle. Therefore, the stiffness matrix of ply has been given by Equation 2.14 instead of 2.69.

$$D_{11} = 817.127 - 490.370x + 95.5104x^2 - 1.01515x^3$$

The frequency without considering the effect on the ply stiffness caused by α is given in Table 3.23:

Table 3.23 Natural frequencies of tapered composite beam described in Example 3.4 using conventional FEM ignoring the effect of α

	2E	4E	8E	12E	16E	10R
ω_1	1038.73	1034.84	1034.59	1034.57	1034.57	1034.57
ω_2		4155.27	4139.94	4139.08	4138.93	4138.85
ω_3		9483.39	9324.25	9314.66	9313.01	9312.23
ω_4			16620.3	16568.3	16559.2	16554.9

In this thesis, we consider the effect of α and the bending stiffness coefficient is:

$$D_{11} = 817.122 - 490.366x + 95.5097x^2 - 1.01515x^3$$

The differences between these two D_{11} coefficients is very small, because α is only 0.02865°. In addition, for an Euler-Bernoulli beam, α can not be large because of the ratio of length-to-thickness.

The natural frequencies are almost same because of the close bending stiffness coefficient D_{11} values, as given in Tables 3.24 to 3.26:

Table 3.24 Natural frequencies of tapered composite beam described in Example 3.4 using conventional FEM based on CLT

	2E	4E	8E	12E	16E	10R
ω_1	1038.73	1034.84	1034.58	1034.57	1034.57	1034.57
ω_2		4155.26	4139.93	4139.06	4138.92	4138.85
ω_3		9483.36	9324.22	9314.63	9312.98	9312.21
ω_4			16620.3	16568.3	16559.1	16554.8

Table 3.25 Natural frequencies of tapered composite beam described in Example 3.4 using one-hierarchical-term model based on CLT

	2E1T	4E1T	8E1T	12E1T	16E1T	10R
ω_1	1034.65	1034.57	1034.57	1034.57	1034.57	1034.57
ω_2		4139.16	4138.86	4138.85	4138.85	4138.85
ω_3		9319.00	9312.36	9312.23	9312.21	9312.21
ω_4			16556.1	16555.0	16554.9	16554.8

Table 3.26 Natural frequencies of tapered composite beam described in Example 3.4 using two-hierarchical-terms model based on CLT

	2E2T	3E2T	4E2T	5E2T	6E2T	7E2T	8E2T	10R
ω_1	1034.58	1034.57	1034.57	1034.57	1034.57	1034.57	1034.57	1034.57
ω_2		4138.93	4138.88	4138.87	4138.86	4138.85	4138.85	4138.85
ω_3			9312.43	9312.34	9312.29	9312.26	9312.24	9312.21
ω_4				16555.3	16555.1	16555.0	16555.0	16554.8

As can be seen from the above tables, the natural frequencies from both conventional FEM and HFEM converge fast to those from Ritz method, but HFEM gives much more accurate results compared with those from conventional FEM using the same

number of elements.

Tables 3.27 to 3.29 give the first four modes' frequencies for the fixed-fixed tapered composite beam described in Example 3.5.

Table 3.27 Natural frequencies of tapered composite beam described in Example 3.5 using conventional FEM based on CLT

	2E	4E	8E	12E	16E	10R
ω_1	2384.66	2348.65	2345.68	2345.52	2345.49	2345.48
ω_2		6525.51	6469.47	6466.18	6465.62	6465.36
ω_3		12949.2	12704.8	12680.8	12676.6	12674.7
ω_4			21082.8	20979.0	20960.5	20951.8

Table 3.28 Natural frequencies of tapered composite beam described in Example 3.5 using one-hierarchical-term model based on CLT

	2E1T	4E1T	8E1T	12E1T	16E1T	10R
ω_1	2347.19	2345.51	2345.48	2345.48	2345.48	2345.48
ω_2		6466.84	6465.39	6465.37	6465.36	6465.36
ω_3		12704.4	12675.1	12674.7	12674.7	12674.7
ω_4			20954.6	20952.1	20951.9	20951.8

Table 3.29 Natural frequencies of tapered composite beam described in Example 3.5 using two-hierarchical-terms model based on CLT

	2E2T	3E2T	4E2T	5E2T	6E2T	7E2T	8E2T	10R
ω_1	2345.60	2345.51	2345.49	2345.49	2345.48	2345.48	2345.48	2345.48
ω_2		6465.73	6465.50	6465.43	6465.40	6465.38	6465.37	6465.36
ω_3			12675.4	12675.0	12674.9	12674.8	12674.7	12674.7
ω_4				20953.1	20952.5	20952.2	20952.1	20951.8

Tables 3.30 to 3.32 give the first four modes' frequencies for the fixed-free tapered composite beam described in Example 3.6.

Table 3.30 Natural frequencies of tapered composite beam described in Example 3.6

using conventional FEM based on CLT

	2E	4E	8E	12E	16E	10R
ω_1	383.276	383.128	383.117	383.116	383.116	383.116
ω_2		2340.26	2337.85	2337.71	2337.69	2337.67
ω_3		6543.03	6498.62	6495.53	6494.99	6494.73
ω_4			12729.5	12707.3	12703.3	12701.4

Table 3.31 Natural frequencies of tapered composite beam described in Example 3.6 using one-hierarchical-term model based on CLT

	2E1T	4E1T	8E1T	12E1T	16E1T	10R
ω_1	383.119	383.116	383.116	383.116	383.116	383.116
ω_2		2337.73	2337.68	2337.67	2337.67	2337.67
ω_3		6497.18	6494.78	6494.74	6494.73	6494.73
ω_4			12702.0	12701.5	12701.4	12701.4

Table 3.32 Natural frequencies of tapered composite beam described in Example 3.6 using two-hierarchical-terms model based on CLT

	2E2T	3E2T	4E2T	5E2T	6E2T	7E2T	8E2T	10R
ω_1	383.117	383.116	383.116	383.116	383.116	383.116	383.116	383.116
ω_2		2337.70	2337.68	2337.68	2337.68	2337.67	2337.67	2337.67
ω_3			6494.86	6494.79	6494.76	6494.75	6494.74	6494.73
ω_4				12701.7	12701.6	12701.5	12701.5	12701.4

Tables 3.33 to 3.35 give the first four modes' frequencies for the free-fixed tapered composite beam described in Example 3.7.

Table 3.33 Natural frequencies of tapered composite beam described in Example 3.7 using conventional FEM based on CLT

	2E	4E	8E	12E	16E	10R
ω_1	354.694	354.497	354.484	354.483	354.483	354.483
ω_2		2285.41	2282.76	2282.60	2282.58	2282.56
ω_3		6493.79	6445.69	6442.51	6441.95	6441.69
ω_4			12677.1	12654.3	12650.2	12648.3

Table 3.34 Natural frequencies of tapered composite beam described in Example 3.7 using one-hierarchical-term model based on CLT

	2E1T	4E1T	8E1T	12E1T	16E1T	10R
ω_1	354.484	354.483	354.483	354.483	354.483	354.483
ω_2		2282.61	2282.57	2282.57	2282.56	2282.56
ω_3		6443.90	6441.74	6441.70	6441.69	6441.69
ω_4			12648.8	12648.3	12648.3	12648.3

Table 3.35 Natural frequencies of tapered composite beam described in Example 3.7 using two-hierarchical-terms model based on CLT

	2E2T	3E2T	4E2T	5E2T	6E2T	7E2T	8E2T	10R
ω_1	354.484	354.483	354.483	354.483	354.483	354.483	354.483	354.483
ω_2		2282.59	2282.57	2282.57	2282.57	2282.57	2282.57	2282.56
ω_3			6441.82	6441.75	6441.73	6441.71	6441.70	6441.69
ω_4				12648.6	12648.5	12648.4	12648.3	12648.3

So far, Ritz method, conventional FEM and hierarchical FEM have been described and example problems have been solved to illustrate their applications, for both uniform and tapered composite Euler-Bernoulli beams. The HFEM shows much better accuracy than the conventional FEM. In the next section, we will apply Ritz method, conventional FEM and HFEM to uniform and tapered composite Timoshenko beams.

3.3 Formulation based on First-order Shear Deformation Theory

3.3.1 Solution using Ritz method and based on FSDT

In this section, we will derive the solution using Ritz method based on the first-order shear deformation theory and then give some examples, including uniform and tapered composite beams.

3.3.1.1 Formulation using Ritz method based on FSDT

The basic assumptions for the shear deformation theory remain the same as listed in chapter 2 for the classical laminate theory, with an exception being assumption 5 concerning the neglect of the interlaminar shear strain γ_{xz} and γ_{yz}. Thus for the first-order shear deformation theory, the displacements are assumed to be of the forms:

$$u(x,y,z,t) = u^o(x,y,t) + z\psi_x(x,y,t) \tag{3.46}$$

$$v(x,y,z,t) = v^o(x,y,t) + z\psi_y(x,y,t) \tag{3.47}$$

$$w(x,y,z,t) = w^o(x,y,t) \tag{3.48}$$

where ψ_x and ψ_y are the rotations about x and y axes respectively.

The curvatures become:

$$\kappa_x^o = \frac{\partial \psi_x}{\partial x} \tag{3.49}$$

$$\kappa_y^o = \frac{\partial \psi_y}{\partial y} \tag{3.50}$$

$$\kappa_{xy}^o = \frac{\partial \psi_x}{\partial y} + \frac{\partial \psi_y}{\partial x} \tag{3.51}$$

From the plane stress assumption, we have the same stress-strain relation and *ABD* matrices for FSDT as those for CLT (Equation 2.79 and 2.82 respectively), except that the curvatures are different.

Because now the shear deformation is not negligible, we express the interlaminar strains by:

$$\gamma_{yz} = \gamma_{yz}^o = \frac{\partial w^o}{\partial y} + \psi_y \tag{3.52}$$

$$\gamma_{xz} = \gamma_{xz}^{o} = \frac{\partial w^{o}}{\partial x} + \psi_x \tag{3.53}$$

In chapter 2, we have already derived the relationship between stress and strain for a ply in a tapered composite beam, and each term of stiffness matrix can be nonzero:

$$\begin{Bmatrix} \sigma_x \\ \sigma_y \\ \sigma_z \\ \tau_{yz} \\ \tau_{xz} \\ \tau_{xy} \end{Bmatrix} = \begin{bmatrix} \overline{C}_{11} & \overline{C}_{12} & \overline{C}_{13} & \overline{C}_{14} & \overline{C}_{15} & \overline{C}_{16} \\ & \overline{C}_{22} & \overline{C}_{23} & \overline{C}_{24} & \overline{C}_{25} & \overline{C}_{26} \\ & & \overline{C}_{33} & \overline{C}_{34} & \overline{C}_{35} & \overline{C}_{36} \\ & & & \overline{C}_{44} & \overline{C}_{45} & \overline{C}_{46} \\ & & & & \overline{C}_{55} & \overline{C}_{56} \\ sym & & & & & \overline{C}_{66} \end{bmatrix} \begin{Bmatrix} \varepsilon_x \\ \varepsilon_y \\ \varepsilon_z \\ \gamma_{yz} \\ \gamma_{xz} \\ \gamma_{xy} \end{Bmatrix} \tag{3.54}$$

The transverse shearing stresses can be isolated from the above six stresses:

$$\begin{Bmatrix} \tau_{yz} \\ \tau_{xz} \end{Bmatrix} = \begin{bmatrix} \overline{C}_{14} & \overline{C}_{24} & \overline{C}_{34} & \overline{C}_{44} & \overline{C}_{45} & \overline{C}_{46} \\ \overline{C}_{15} & \overline{C}_{25} & \overline{C}_{35} & \overline{C}_{45} & \overline{C}_{55} & \overline{C}_{56} \end{bmatrix} \begin{Bmatrix} \varepsilon_x \\ \varepsilon_y \\ \varepsilon_z \\ \gamma_{yz} \\ \gamma_{xz} \\ \gamma_{xy} \end{Bmatrix} \tag{3.55}$$

From the displacement $w(x,y,z,t) = w^{o}(x,y,t)$, we can get $\varepsilon_z = 0$. Thus there are five strains that have contributions to τ_{xz} and τ_{yz}. In this thesis, we assume that the contributions of ε_x, ε_y, and γ_{xy} are negligible. Therefore, the shearing stresses are:

$$\begin{Bmatrix} \tau_{yz} \\ \tau_{xz} \end{Bmatrix} = k \begin{bmatrix} \overline{C}_{44} & \overline{C}_{45} \\ \overline{C}_{45} & \overline{C}_{55} \end{bmatrix} \begin{Bmatrix} \gamma_{yz} \\ \gamma_{xz} \end{Bmatrix} \tag{3.56}$$

where k is the shear correction factor [2]. In this thesis, we choose $k = 5/6$.

The strain energy, Equation 3.2, reduces to five terms

$$
\begin{aligned}
U &= \frac{1}{2}\int\int\int\left(\sigma_x\varepsilon_x + \sigma_y\varepsilon_y + \tau_{xy}\gamma_{xy} + \tau_{yz}\gamma_{yz} + \tau_{xz}\gamma_{xz}\right)dxdydz \\
&= \frac{1}{2}\int\int\int\begin{bmatrix}\left(\overline{Q}_{11}\varepsilon_x + \overline{Q}_{12}\varepsilon_y + \overline{Q}_{16}\gamma_{xy}\right)\varepsilon_x \\ +\left(\overline{Q}_{12}\varepsilon_x + \overline{Q}_{22}\varepsilon_y + \overline{Q}_{26}\gamma_{xy}\right)\varepsilon_y \\ +\left(\overline{Q}_{16}\varepsilon_x + \overline{Q}_{26}\varepsilon_y + \overline{Q}_{66}\gamma_{xy}\right)\gamma_{xy} \\ +k\left(\overline{C}_{44}\gamma_{yz} + \overline{C}_{45}\gamma_{xz}\right)\gamma_{yz} \\ +k\left(\overline{C}_{45}\gamma_{yz} + \overline{C}_{55}\gamma_{xz}\right)\gamma_{xz}\end{bmatrix}dxdydz \\
&= \frac{1}{2}\int\int\int\begin{bmatrix}\overline{Q}_{11}\varepsilon_x^2 \\ +2\overline{Q}_{21}\varepsilon_x\varepsilon_y + \overline{Q}_{22}\varepsilon_y^2 \\ +2\overline{Q}_{61}\varepsilon_x\gamma_{xy} + 2\overline{Q}_{62}\varepsilon_y\gamma_{xy} + \overline{Q}_{66}\gamma_{xy}^2 \\ +k\overline{C}_{44}\gamma_{yz}^2 \\ 2k\overline{C}_{45}\gamma_{yz}\gamma_{xz} + k\overline{C}_{55}\gamma_{xz}^2\end{bmatrix}dxdydz
\end{aligned}
\tag{3.57}
$$

We begin our study with one-dimensional case. For this case, due to the first-order shear deformation, we have only two strains for a composite beam:

$$\varepsilon_x = z\frac{\partial\psi}{\partial x} \tag{3.58}$$

$$\gamma_{xz} = \psi + \frac{\partial w}{\partial x} \tag{3.59}$$

where ψ and w are functions of x and time t. Therefore, the strain energy reduces to two terms:

$$
\begin{aligned}
U &= \frac{1}{2}\int\int\int\left(\overline{Q}_{11}\varepsilon_x^2 + k\overline{C}_{55}\gamma_{xz}^2\right)dxdydz \\
&= \frac{1}{2}\int\int\int\left[\overline{Q}_{11}z^2\left(\frac{\partial\psi}{\partial x}\right)^2 + k\overline{C}_{55}\left(\psi + \frac{\partial w}{\partial x}\right)^2\right]dxdydz \\
&= \frac{1}{2}\int\int b\left[\overline{Q}_{11}z^2\left(\frac{\partial\psi}{\partial x}\right)^2 + k\overline{C}_{55}\left(\psi + \frac{\partial w}{\partial x}\right)^2\right]dxdz \\
&= \frac{1}{2}\int_0^{\ell_e} b\left[D_{11}\left(\frac{\partial\psi}{\partial x}\right)^2 + kA_{55}\left(\psi + \frac{\partial w}{\partial x}\right)^2\right]dx
\end{aligned}
\tag{3.60}
$$

Following the same procedure used for the classical laminate theory, we have the

kinetic energy:

$$T = \frac{1}{2}\iiint \rho\left[\left(\frac{\partial u}{\partial t}\right)^2 + \left(\frac{\partial v}{\partial t}\right)^2 + \left(\frac{\partial w}{\partial t}\right)^2\right]dxdydz$$
$$= \frac{1}{2}\iiint \rho\left[z^2\left(\frac{\partial \psi}{\partial t}\right)^2 + \left(\frac{\partial w}{\partial t}\right)^2\right]dxdydz \tag{3.61}$$
$$= \frac{1}{2}\int_{-\frac{H}{2}}^{\frac{H}{2}}\int_0^{l_e} \rho b\left[z^2\left(\frac{\partial \psi}{\partial t}\right)^2 + \left(\frac{\partial w}{\partial t}\right)^2\right]dxdz$$

Harmonic displacement functions are also assumed for w and ψ:

$$w(x,t) = W(x)e^{i\omega t} \tag{3.62}$$

$$\psi(x,t) = \Psi(x)e^{i\omega t} \tag{3.63}$$

Then, similar to Equation 3.14,

$$T = -\frac{\omega^2}{2}\int_{-\frac{H}{2}}^{\frac{H}{2}}\int_0^{l_e} \rho b\left(z^2\psi^2 + w^2\right)dxdz \tag{3.64}$$

We have assumed that the rotary inertia is negligible, that means the first term in kinetic energy can be ignored:

$$T = -\frac{\omega^2}{2}\int_{-\frac{H}{2}}^{\frac{H}{2}}\int_0^{l_e} \rho b w^2 dxdz = -\frac{\omega^2}{2}\int_0^{l_e} b\left(\rho_L H_L + \rho_r H_r\right)w^2 dx \tag{3.65}$$

It has the same expression as that based on the classical laminate theory.

The stationary value for a composite beam based on FSDT becomes:

$$\Pi = U + T = \frac{1}{2}\int_0^{l_e} b\left[D_{11}\left(\frac{\partial \psi}{\partial x}\right)^2 + kA_{55}\left(\psi + \frac{\partial w}{\partial x}\right)^2\right]dx - \frac{\omega^2}{2}\int_0^{l_e} b\left(\rho_L H_L + \rho_r H_r\right)w^2 dx \tag{3.66}$$

In Ritz method, we assume that $W = \sum_{i=1}^{N} c_i\phi_i$ and $\Psi = \sum_{i=1}^{N} e_i\varphi_i$ according to different boundary conditions and substitute them into Equation 3.66. Then we can impose the stationary condition:

$$\frac{\partial \Pi}{\partial c_i} = 0 \text{ and } \frac{\partial \Pi}{\partial e_i} = 0 \tag{3.67}$$

We can get a matrix equation:

$$\left[[K] - \omega^2 [M]\right]\{c\} = 0 \tag{3.68}$$

Again, solving the eigenvalue problem $\left|[K] - \omega^2 [M]\right| = 0$, we can get the free vibration frequencies. The procedures are as same as those for the classical laminate theory.

3.3.1.2 Example applications

Example 3.8 vibration of simply supported uniform beams using Ritz method based on FSDT

The beam and boundary condition are as same as those in Example 3.1. The length-to-height ratio is 62.5. It is a typical Euler-Bernoulli beam but we apply the first-order shear deformation theory. The exact solution is from reference [2]:

$$\omega = \frac{m^2\pi^2}{L}\sqrt{\frac{D_{11}kA_{55}}{\left(D_{11}m^2\pi^2 + L^2 kA_{55}\right)\rho H}} \tag{3.69}$$

where the material properties of the beam in this example are

$A_{55} = 18726912 \text{ Nm}^{-1}$

$D_{11} = 817.127 \text{ N.m}$

The exact solutions of this example are

$\omega_1 = 1064.10$

$\omega_2 = 4221.53$

$\omega_3 = 9371.81$

$\omega_4 = 16360.4$

Then trigonometric interpolation functions are assumed for this simply supported boundary condition:

$$W = \sum_{i=1}^{N} c_i \sin\frac{i\pi x}{L},\ \Psi = \sum_{i=1}^{N} e_i \cos\frac{i\pi x}{L} \tag{3.70}$$

Table 3.36 gives the calculated natural frequency using the above trigonometric interpolation functions:

Table 3.36 Natural frequencies of long uniform composite beam described in Example 3.8 using Ritz method based on FSDT

	1R	2R	3R	4R	5R	Exact	Bernoulli
ω_1	1064.10	1064.10	1064.10	1064.10	1064.10	1064.10	1067.06
ω_2		4221.53	4221.53	4221.53	4221.53	4221.53	4268.24
ω_3			9371.81	9371.81	9371.81	9371.81	9603.53
ω_4				16360.4	16360.4	16360.4	17072.9

The above table shows perfect accuracy although W and Ψ have only one interpolation term each. The result matches the exact solution. This is because of the assumed trigonometric function. The exact solution comes from solving the governing differential equation by assuming harmonic vibration [1]:

$$w = c_i e^{i\omega t} \sin\frac{i\pi x}{L},\ \psi = e_i e^{i\omega t} \cos\frac{i\pi x}{L} \tag{3.71}$$

They are as same as what we assumed in Ritz method.

Meanwhile, the frequencies based on FSDT are very close to those based on classical laminate theory. That is what we expected, because the length-to-height ratio is so large.

For the same beam, we just shorten the length to $L = 0.03048\,\text{m}$. The length-to-

height ratio is 6.25. It is a typical Timoshenko Beam. The frequencies based on FSDT should differ from that based on the classical laminate theory.

Table 3.37 Natural frequencies of short uniform composite beam described in Example 3.8 using Ritz method based on FSDT

	1R	2R	3R	4R	5R	Exact	Bernoulli
ω_1	85535.8	85535.8	85535.8	85535.8	85535.8	85535.8	106706
ω_2		237674	237674	237674	237674	237674	426824
ω_3			391857	391857	391857	391857	960353
ω_4				542611	542611	542611	1707295

As can be seen, the frequencies match the exact solutions and are smaller than those based on classical laminate theory. That is what we have expected. So far, all the results show good accuracy for uniform beam. The next step is to verify the natural frequencies of tapered composite beams based on FSDT.

Example 3.9 vibration of simply supported tapered beams using Ritz method based on FSDT

The tapered beam and boundary condition are as same as those in Example 3.4. The length-to-height ratio is 62.5. It is a typical Euler-Bernoulli beam but here we apply the first-order shear deformation theory. The transverse shear stiffness of this tapered composite beam is a function of x and the bending stiffness is as same as that based on CLT.

$$A_{55} = 18726912 - 3200000x$$

$$D_{11} = 817.122 - 490.366x + 95.5097x^2 - 1.01515x^3$$

Table 3.38 Natural frequencies of long tapered composite beam described in Example 3.9 using Ritz method based on FSDT

	1R	2R	3R	4R	5R	Bernoulli
ω_1	1032.42	1031.89	1031.89	1031.89	1031.89	1034.57
ω_2		4098.90	4096.48	4096.47	4096.45	4138.85
ω_3			9107.43	9101.65	9101.65	9312.21
ω_4				15916.9	15906.2	16554.8

As can be seen from Table 3.38, the convergence of the natural frequencies is similar to that of the frequencies based on the classical laminate theory for the same beam.

Again for the same beam, we just shorten the length to $L = 0.03048\,\text{m}$. The length-to-height ratio is 6.25. The material properties become:

$$A_{55} = 18735567 - 32001364x$$

$$D_{11} = 816.591 - 4900.49x + 9544.85x^2 - 1015.16x^3$$

Table 3.39 Natural frequencies of short tapered composite beam described in Example 3.9 using Ritz method based on FSDT

	1R	2R	3R	4R	5R	Bernoulli
ω_1	83928.8	83899.7	83899.7	83899.5	83899.5	103422
ω_2		235854	235810	235810	235809	413748
ω_3			390752	390714	390714	930912
ω_4				542297	542267	1654936

From the above examples we can say that based on FSDT, Ritz method also has ideal convergence and seems to converge to the exact solution for tapered composite beam. The following formulation is using hierarchical finite element method to re-solve the same example problems and compare the results from both methods.

3.3.2 Solution using Hierarchical Finite Element Method and based on FSDT

3.3.2.1 Formulation using HFEM based on FSDT

In Hierarchical finite element method, we assume the displacement and rotation functions as:

$$W = c_1 + c_3 x + \sum_{n=2}^{N} c_{n+3} \sin\frac{n\pi x}{2l_e}$$

$$= \begin{bmatrix} 1 & x & \sin\frac{\pi x}{l_e} & \sin\frac{2\pi x}{l_e} & \cdots & \sin\frac{n\pi x}{2l_e} \end{bmatrix}_{1\times\left(\frac{n}{2}+2\right)} \begin{Bmatrix} c_1 \\ c_3 \\ c_5 \\ c_7 \\ \vdots \\ c_{n+3} \end{Bmatrix}_{\left(\frac{n}{2}+2\right)\times 1}$$

$$= \begin{bmatrix} 1 & 0 & x & 0 & \sin\frac{\pi x}{l_e} & 0 & \sin\frac{2\pi x}{l_e} & 0 & \cdots & \sin\frac{n\pi x}{2l_e} & 0 \end{bmatrix}_{1\times(n+4)} \begin{Bmatrix} c_1 \\ c_2 \\ c_3 \\ c_4 \\ c_5 \\ c_6 \\ c_7 \\ c_8 \\ \vdots \\ c_{n+3} \\ c_{n+4} \end{Bmatrix}_{(n+4)\times 1} \tag{3.72}$$

$$= [K^w]\{c\}$$

$$\Psi = c_2 + c_4 x + \sum_{n=2}^{N} c_{n+4} \sin\frac{n\pi x}{2l_e}$$

$$== \begin{bmatrix} 1 & x & \sin\frac{\pi x}{l_e} & \sin\frac{2\pi x}{l_e} & \cdots & \sin\frac{n\pi x}{2l_e} \end{bmatrix}_{1\times\left(\frac{n}{2}+2\right)} \begin{Bmatrix} c_2 \\ c_4 \\ c_6 \\ c_8 \\ \vdots \\ c_{n+4} \end{Bmatrix}_{\left(\frac{n}{2}+2\right)\times 1}$$

$$= \begin{bmatrix} 0 & 1 & 0 & x & 0 & \sin\frac{\pi x}{l_e} & 0 & \sin\frac{2\pi x}{l_e} & \cdots & 0 & \sin\frac{n\pi x}{2l_e} \end{bmatrix}_{1\times\left(\frac{n}{2}+2\right)} \begin{Bmatrix} c_1 \\ c_2 \\ c_3 \\ c_4 \\ c_5 \\ c_6 \\ c_7 \\ c_8 \\ \vdots \\ c_{n+3} \\ c_{n+4} \end{Bmatrix}_{(n+4)\times 1} \tag{3.73}$$

$$= \left[K^{\psi}\right]\{c\}$$

where, n=2, 4, 6, 8…

In local coordinate system, the nodal displacements and rotations are:

$$\{u\} = \begin{Bmatrix} w_1 \\ \psi_1 \\ w_2 \\ \psi_2 \\ A_1 \\ A_2 \\ A_3 \\ A_4 \\ \vdots \\ A_{n-1} \\ A_n \end{Bmatrix}_{(n+4)\times 1} = \begin{bmatrix} 1 & 0 & 0 & 0 & 0 & 0 & 0 & 0 & 0 & 0 \\ 0 & 1 & 0 & 0 & 0 & 0 & 0 & 0 & 0 & 0 \\ 1 & 0 & l_e & 0 & 0 & 0 & 0 & 0 & 0 & 0 \\ 0 & 1 & 0 & l_e & 0 & 0 & 0 & 0 & 0 & 0 \\ 0 & 0 & 0 & 0 & 1 & 0 & 0 & 0 & 0 & 0 \\ 0 & 0 & 0 & 0 & 0 & 1 & 0 & 0 & 0 & 0 \\ 0 & 0 & 0 & 0 & 0 & 0 & 1 & 0 & 0 & 0 \\ 0 & 0 & 0 & 0 & 0 & 0 & 0 & 1 & 0 & 0 \\ & & & & & & & & \ddots & \\ 0 & 0 & 0 & 0 & 0 & 0 & 0 & 0 & 1 & 0 \\ 0 & 0 & 0 & 0 & 0 & 0 & 0 & 0 & 0 & 1 \end{bmatrix}_{(n+4)\times(n+4)} \begin{Bmatrix} c_1 \\ c_2 \\ c_3 \\ c_4 \\ c_5 \\ c_6 \\ c_7 \\ c_8 \\ \vdots \\ c_{n+3} \\ c_{n+4} \end{Bmatrix}_{(n+4)\times 1}$$
$$= [K^u]\{c\} \tag{3.74}$$

The displacement and rotation can also be expressed as:

$$W = \begin{bmatrix} N_1^w & N_2^w & N_3^w & N_4^w & N_5^w & N_6^w & N_7^w & N_8^w & \cdots & N_{n+3}^w & N_{n+4}^w \end{bmatrix}_{1\times(n+4)} \begin{Bmatrix} w_1 \\ \psi_1 \\ w_2 \\ \psi_2 \\ A_1 \\ A_2 \\ A_3 \\ A_4 \\ \vdots \\ A_{n-1} \\ A_n \end{Bmatrix}_{(n+4)\times 1}$$
$$= [N^w]\{u\} \tag{3.75}$$

Similarly,

$$\Psi = [N^w]\{u\} \tag{3.76}$$

Substituting Equations 3.72 and 3.74 into Equation 3.75 yields:

$$[N^w]\{u\} = [N^w]\,[K^u]\{c\} = [K^w]\{c\} \tag{3.77}$$

Then, the interpolation functions for displacement can be expressed by

$$\left[N^{w}\right]=\left[K^{w}\right]\left[K^{u}\right]^{-1} \tag{3.78}$$

The expanded interpolation functions are:

$$\begin{cases} N_1^w = 1-\dfrac{x}{l_e} \\ N_2^w = 0 \\ N_3^w = \dfrac{x}{l_e} \\ N_4^w = 0 \\ N_5^w = \sin\dfrac{\pi x}{l_e} \\ N_6^w = 0 \\ N_7^w = \sin\dfrac{2\pi x}{l_e} \\ N_8^w = 0 \\ \quad\vdots \\ N_{n+3}^w = \sin\dfrac{n\pi x}{2l_e} \\ N_{n+4}^w = 0 \end{cases} \tag{3.79}$$

Similarly, the interpolation functions for rotation can be expressed by

$$\left[N^{\psi}\right]=\left[K^{\psi}\right]\left[K^{u}\right]^{-1} \tag{3.80}$$

$$\begin{cases} N_1^{\psi} = 0 \\ N_2^{\psi} = 1 - \dfrac{x}{l_e} \\ N_3^{\psi} = 0 \\ N_4^{\psi} = \dfrac{x}{l_e} \\ N_5^{\psi} = 0 \\ N_6^{\psi} = \sin\dfrac{\pi x}{l_e} \\ N_7^{\psi} = 0 \\ N_8^{\psi} = \sin\dfrac{2\pi x}{l_e} \\ \quad \vdots \\ N_{n+3}^{\psi} = 0 \\ N_{n+4}^{\psi} = \sin\dfrac{n\pi x}{2l_e} \end{cases} \tag{3.81}$$

Here we use the following three notations:

$$\left[N^{dw}\right] = \frac{d\left[N^{w}\right]}{dx} \tag{3.82}$$

$$\left[N^{d\psi}\right] = \frac{d\left[N^{\psi}\right]}{dx} \tag{3.83}$$

$$\left[N^{\psi dw}\right] = \left[N^{\psi}\right] + \left[N^{dw}\right] \tag{3.84}$$

Finally, we can get the governing equation for HFEM based on FSDT from the stationary condition (Equation 3.66) by variational method:

$$\int_0^{l_e}\left[D_{11}\left[N^{d\psi}\right]^T\left[N^{d\psi}\right] + kA_{55}\left[N^{\psi dw}\right]^T\left[N^{\psi dw}\right]\right]dx\{u\} - \omega^2\int_0^{l_e}(\rho_L H_L + \rho_r H_r)\left[N^{w}\right]^T\left[N^{w}\right]dx\{u\} = 0 \tag{3.85}$$

The stiffness and mass matrices are:

$$[K] = \int_0^{l_e}\left[D_{11}\left[N^{d\psi}\right]^T\left[N^{d\psi}\right] + kA_{55}\left[N^{\psi dw}\right]^T\left[N^{\psi dw}\right]\right]dx \tag{3.86}$$

$$[M]=\int_0^{l_e}(\rho_L H_L+\rho_r H_r)[N^w]^T[N^w]dx \tag{3.87}$$

Equation 3.85 can be written as:

$$[[K]-\omega^2[M]]\{u\}=0 \tag{3.88}$$

As same as in Ritz method, solving the eigenvalue equation $|[K]-\omega^2[M]|=0$, we can get the natural frequencies.

Now we can check Examples 3.8 to 3.9 using HFEM based on FSDT.

3.3.2.2 Example applications

Example 3.10 vibration of a simply supported uniform beam using HFEM based on FSDT

The uniform beam and boundary condition are as same as in Example 3.1. The length-to-height ratio is 62.5. It is a typical Euler-Bernoulli beam but we apply the first-order shear deformation theory and use conventional FEM and HFEM.

Table 3.40 Natural frequencies of long uniform composite beam described in Example 3.10 using conventional FEM based on FSDT

	2E	4E	8E	16E	32E	64E	128E	Exact
ω_1	7967.00	3583.19	1960.98	1340.82	1139.25	1083.36	1068.95	1064.10
ω_2		16387.3	8078.49	5370.03	4530.40	4300.46	4241.38	4221.53
ω_3		42368.9	19043.5	12106.8	10096.5	9556.30	9418.15	9371.81
ω_4			35876.6	21579.2	17718.5	16704.5	16446.7	16360.4

Table 3.41 Natural frequencies of long uniform composite beam described in Example 3.10 using two-hierarchical-terms model based on FSDT

	2E2T*	4E2T	6E2T	8E2T	10E2T	12E2T	Exact
ω_1	1440.01	1152.37	1101.28	1084.18	1076.60	1072.61	1064.10
ω_2		4811.81	4442.43	4330.92	4285.34	4262.97	4221.53
ω_3		11567.2	10145.3	9728.98	9568.26	9493.39	9371.81
ω_4			18425.5	17277.1	16844.2	16648.8	16360.4

*2E2T means two-elements model, w and ψ have one interpolation term each

Table 3.42 Natural frequencies of long uniform composite beam described in Example 3.10 using four-hierarchical-terms model based on FSDT

	2E4T	4E4T	6E4T	8E4T	10E4T	12E4T	Exact
ω_1	1131.96	1100.98	1086.67	1078.69	1074.13	1071.35	1064.10
ω_2		4342.51	4302.63	4276.79	4260.53	4250.17	4221.53
ω_3		9601.77	9526.73	9485.40	9455.49	9434.80	9371.81
ω_4			16591.7	16539.4	16499.4	16468.5	16360.4

From Tables 3.40 to 3.42, we can say that when we apply FSDT to an Euler-Bernoulli beam, the results from FEM are more inaccurate than those from Ritz method especially when few-elements model is used. For the conventional FEM, the natural frequencies can not reach the exact solutions even when we use one hundred and twenty-eight elements. Compared with Tables 3.36, 3.41 and 3.42 show that HFEM for an Euler-Bernoulli beam based on FSDT does not have acceptable accuracy when two-elements model is used. At the same time, HFEM shows rapid convergence if we increase the hierarchical terms.

For the same beam, we just shorten the length to $L = 0.03048\,\mathrm{m}$. The length-to-height ratio is 6.25. It is a typical Timoshenko Beam. The following tables give the natural frequencies of this short beam.

Table 3.43 Natural frequencies of short uniform composite beam described in Example 3.10 using conventional FEM based on FSDT

	2E	4E	8E	16E	32E	64E	128E	Exact
ω_1	117272	93215.5	87434.1	86009.0	85654.0	85565.4	85543.2	85535.8
ω_2		281781	248546	240370	238347	237842	237716	237674
ω_3		501916	423264	399636	393794	392341	391978	391857
ω_4			610687	559657	546851	543670	542876	542611

Table 3.44 Natural frequencies of short uniform composite beam described in Example 3.10 using two-hierarchical-terms model based on FSDT

	2E2T	4E2T	6E2T	8E2T	10E2T	12E2T	Exact
ω_1	86967.8	85714.9	85598.5	85567.7	85555.2	85548.9	85535.8
ω_2		239651	238236	237922	237812	237762	237674
ω_3		401048	394333	392863	392377	392170	391857
ω_4			550232	545619	544103	543473	542611

Table 3.45 Natural frequencies of short uniform composite beam described in Example 3.10 using four-hierarchical-terms model based on FSDT

	2E4T	4E4T	6E4T	8E4T	10E4T	12E4T	Exact
ω_1	85819.3	85633.8	85582.1	85562.4	85553.0	85547.8	85535.8
ω_2		238094	237906	237815	237768	237740	237674
ω_3		392672	392400	392217	392106	392038	391857
ω_4			543526	543283	543103	542979	542611

The first mode frequency is plotted in figure 3.14 to compare the convergences between conventional FEM and HFEM.

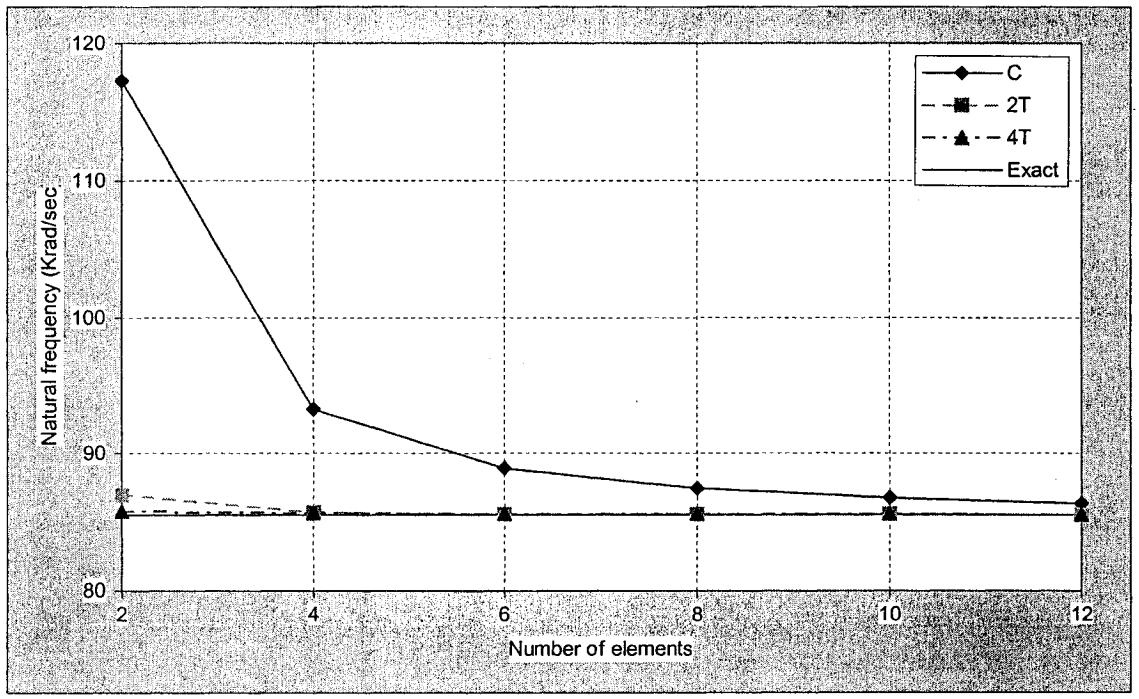

Figure 3.14 First mode frequency of simply supported uniform composite beam based on FSDT

Form this figure, we can see that the top curve shows a typical slow convergence of conventional FEM for FSDT. Furthermore, this curve is always above the exact solution and it seems that it can not reach the exact solution. That is because of the shear lock. On the other hand, HFEM has much better accuracy than the conventional FEM, the two lower curves almost reach the exact solution.

Furthermore, the accuracy from both conventional and hierarchical FEM is much better than that shown in tables 3.40 to 3.42. This is because if we apply FSDT to an Euler-Bernoulli beam, we need many-elements model to reach acceptable results.

In order to see how the hierarchical method affects the accuracy, we can increase both the number of elements and the number of trigonometric terms. Moreover, we can see if HFEM can fix the problem of shear lock.

Table 3.46 Natural frequencies of short uniform composite beam described in Example 3.10 using two-elements model based on FSDT

	2E2T	2E4T	2E6T	2E8T	2E10T	2E12T	Exact
ω_1	86967.8	85819.3	85653.6	85587.6	85566.1	85553.4	85535.8

Table 3.47 Natural frequencies of short uniform composite beam described in Example 3.10 using four-elements model based on FSDT

	4E2T	4E4T	4E6T	4E8T	4E10T	4E12T	Exact
ω_1	85714.9	85633.8	85556.8	85551.9	85541.9	85541.0	85535.8
ω_2	239651	238094	237839	237749	237717	237699	237674
ω_3	401048	392672	392462	392028	392002	391919	391857

Table 3.48 Natural frequencies of short uniform composite beam described in Example 3.10 using six-elements model based on FSDT

	6E2T	6E4T	6E6T	6E8T	6E10T	6E12T	Exact
ω_1	85598.5	85582.1	85544.3	85543.3	85538.4	85538.2	85535.8
ω_2	238236	237906	237733	237713	237691	237687	237674
ω_3	394333	392400	392065	391954	391911	391889	391857
ω_4	550232	543526	543157	542792	542745	542675	542611

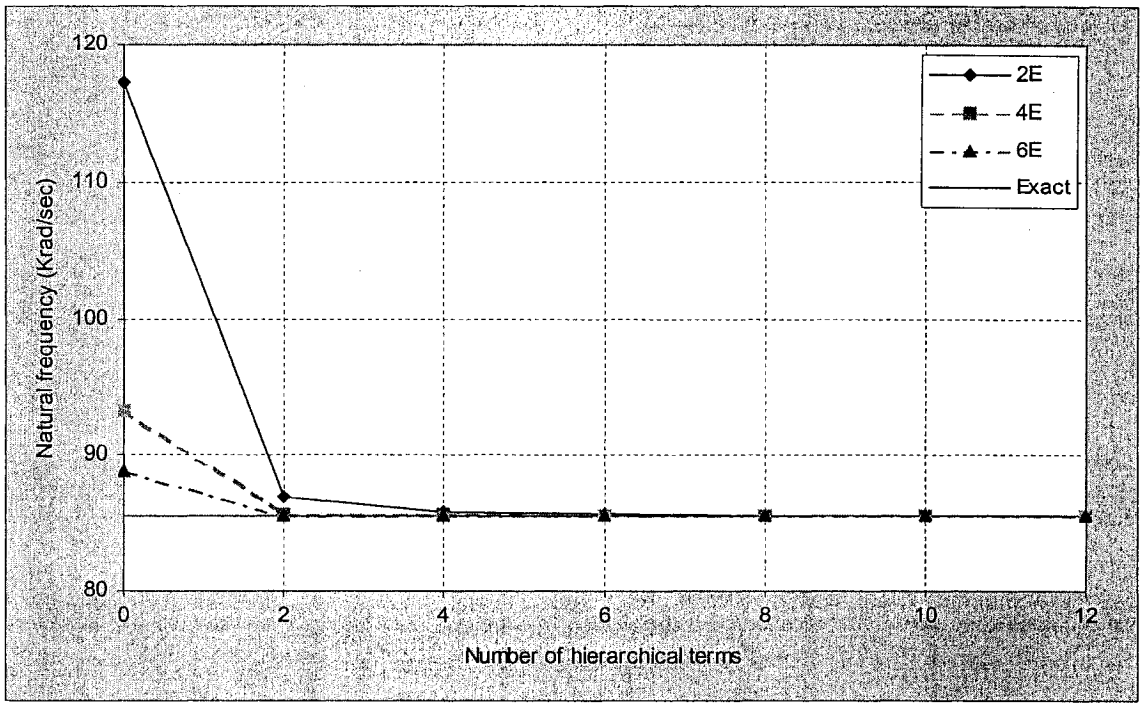

Figure 3.15 First mode frequency vs. number of hierarchical terms of simply supported uniform composite beam based on FSDT

The first mode frequency in tables 3.46 to 3.48 is plotted in Figure 3.15.

From the above figure, we can see that increasing the number of hierarchical terms helps the convergence considerably, especially at the beginning. Two-elements model gives good solution with using four hierarchical terms. Increasing the number of elements and the number of hierarchical terms lets the frequency reach almost the exact solution rapidly.

Since HFEM gives accurate solution for uniform laminated beam, we can apply it to the tapered Timoshenko beam to see if it can also converge to the solution that we got from Ritz method.

Example 3.11 vibration of a simply supported tapered composite beam using HFEM based on FSDT

The tapered beam and boundary condition are as same as those in Example 3.4. The length-to-height ratio is 6.25. It is a typical Timoshenko beam and we apply FSDT.

Table 3.49 Natural frequencies of tapered composite beam described in Example 3.11 using conventional FEM based on FSDT

	2E	4E	8E	16E	32E	64E	128E	10R
ω_1	116302	91741.7	85836	84379.7	84016.9	83926.3	83903.6	83899.4
ω_2		280795	246886	238555	236494	235980	235852	235809
ω_3		502711	422591	398607	392679	391204	390836	390714
ω_4			611142	559505	546554	543337	542534	542267

Table 3.50 Natural frequencies of tapered composite beam described in Example 3.11 using two-hierarchical-terms model based on FSDT

	2E2T	4E2T	6E2T	8E2T	10E2T	12E2T	10R
ω_1	85359.9	84079.4	83960.2	83928.6	83915.9	83909.4	83899.4
ω_2		237827	236382	236062	235950	235898	235809
ω_3		400060	393230	391735	391242	391031	390714
ω_4			549986	545312	543777	543139	542267

Table 3.51 Natural frequencies of tapered composite beam described in Example 3.11 using four-hierarchical-terms model based on FSDT

	2E4T	4E4T	6E4T	8E4T	10E4T	12E4T	10R
ω_1	84185.0	83996.1	83943.4	83923.3	83913.6	83908.3	83899.4
ω_2		236236	236045	235952	235904	235876	235809
ω_3		391539	391264	391079	390966	390897	390714
ω_4			543191	542946	542764	542638	542267

The first mode frequency is plotted in figure 3.16.

As can be seen that just like that in the uniform beam case, HFEM based on FSDT also gives better convergence than the conventional FEM for a tapered composite beam. The frequency seems to converge to the solution from Ritz method. At the same time, by only increasing the number of elements but using few hierarchical terms, result from HFEM does not converge rapidly to that from Ritz method.

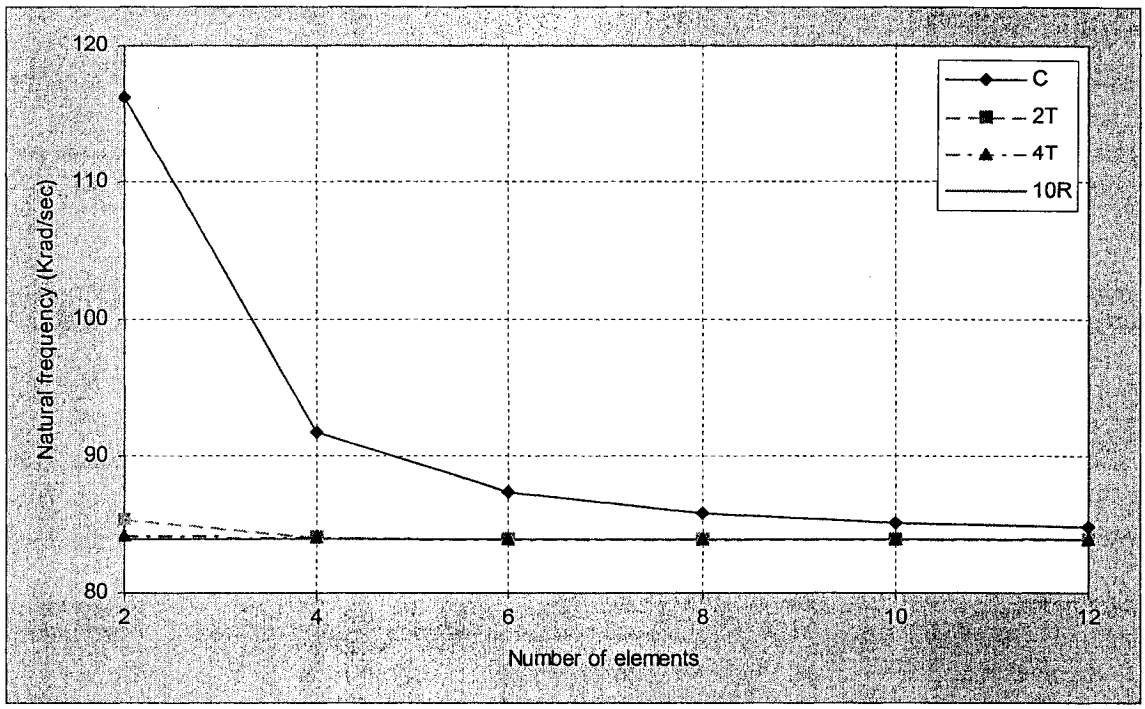

Figure 3.16 First mode frequency of simply supported tapered composite beam based on FSDT

Next, we are going to increase both the number of elements and the number of hierarchical terms to see if the solution can approach the solution from Ritz method. Because the six-elements model with hierarchical terms costs very long time, only two, three, four and five-elements models are used in this section.

Table 3.52 Natural frequencies of tapered composite beam described in Example 3.11 using two-elements model based on FSDT

	2E2T	2E4T	2E6T	2E8T	2E10T	2E12T	10R
ω_1	85359.9	84185.0	84016.6	83949.0	83927.1	83914.0	83899.4

Table 3.53 Natural frequencies of tapered composite beam described in Example 3.11 using three-elements model based on FSDT

	3E2T	3E4T	3E6T	3E8T	3E10T	3E12T	10R
ω_1	84313.7	84059.2	83938.8	83923.5	83907.9	83905.0	83899.4
ω_2	240959	236385	236168	235924	235897	235850	235809

Table 3.54 Natural frequencies of tapered composite beam described in Example 3.11 using four-elements model based on FSDT

	4E2T	4E4T	4E6T	4E8T	4E10T	4E12T	10R
ω_1	84079.4	83996.1	83917.5	83912.5	83902.3	83901.3	83899.4
ω_2	237827	236236	235977	235886	235853	235835	235809
ω_3	400060	391539	391328	390887	390861	390776	390714

Table 3.55 Natural frequencies of tapered composite beam described in Example 3.11 using five-elements model based on FSDT

	5E2T	5E4T	5E6T	5E8T	5E10T	5E12T	10R
ω_1	83997.4	83962.7	83909.0	83906.9	83899.9	83899.5	83899.4
ω_2	236805	236123	235903	235863	235835	235827	235809
ω_3	395255	391391	391056	390841	390799	390757	390714
ω_4	555975	543346	543148	542501	542476	542352	542267

The first mode frequency is plotted in figure 3.17.

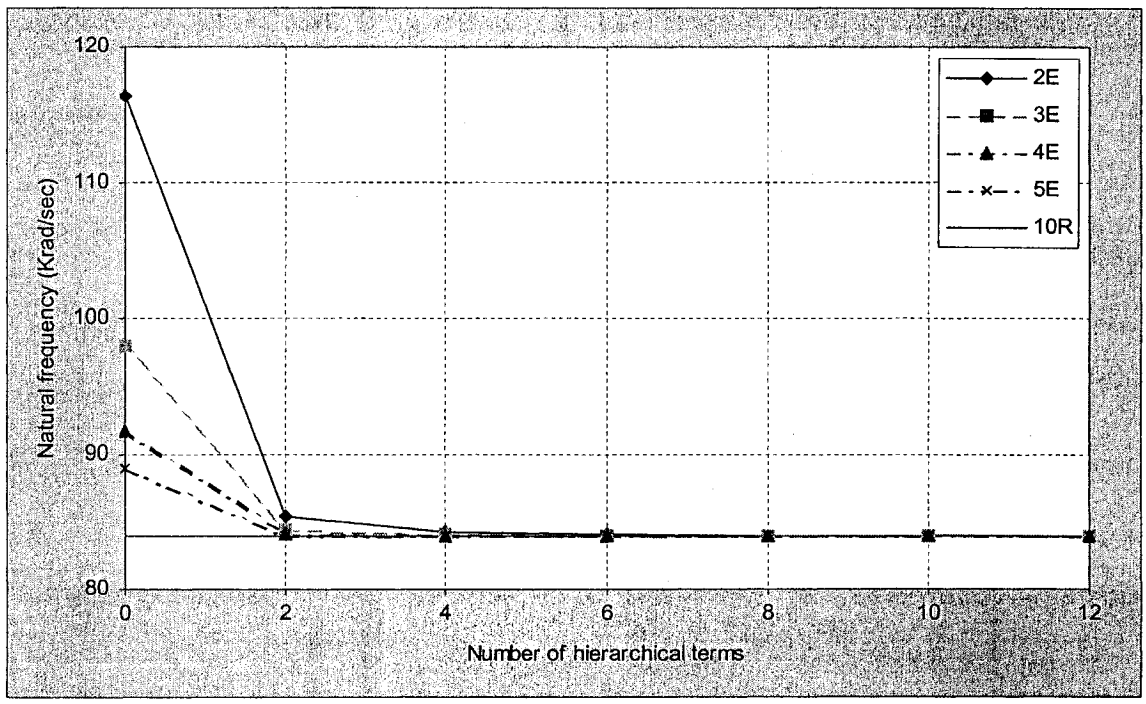

Figure 3.17 First mode frequency vs. number of hierarchical terms of simply supported tapered composite beam based on FSDT

As can be seen from both the tables and Figure 3.17, the natural frequency

converges to the result from Ritz method. By only increasing the number of elements, the frequency converges slowly. The frequency from the five-elements model without hierarchical term is inaccurate. At the same time, as soon as two hierarchical terms are given to the displacement and rotation functions (one term for each), the result is very close to that from Ritz method although we use the two-elements model. When we increase the number of hierarchical terms to four, the difference between the results from HFEM and Ritz method is almost invisible. The most important aspect is that when we use twelve hierarchical terms along with the five-elements model, the first mode frequency is same as that from Ritz method. The shear lock problem disappears.

3.4 Conclusions and discussions

So far, the conventional and the hierarchical FEM based on CLT and FSDT have been described and example problems have been solved to illustrate their applications, for both uniform and tapered composite beams. Based on both CLT and FSDT, the HFEM displays superior results as compared to the conventional FEM. We have seen how the results of the formulations compare with each other and within themselves from the tables and figures.

As can be seen, convergence to the exact solutions in the lowest two modes is much faster than in the third or fourth mode in the cases of both conventional FEM and hierarchical FEM. This is due to the fact that the higher is the mode the more complex is the mode shape. Therefore, the higher the mode is, the more number of hierarchical terms are needed to describe accurately this mode.

In order to get very accurate solution, direct integration is applied to Ritz method.

From the above examples, we can see that for different boundary conditions, ten interpolation terms give acceptable solution. Furthermore, Ritz method for simply supported boundary condition converges faster than the others. That is because the trigonometric interpolation function ($\sin x$) describes the harmonic vibration more accurately than the others. On the other hand, FEM seems to converge at the same speed for all the four kinds of boundary conditions. For HFEM, numerical integration is applied to save time because the integral is too complicated. The number of Gauss points used is from ten to twenty depending on the case to guarantee the accuracy.

Moreover, HFEM has much better accuracy compared with the conventional FEM. The shear lock problem prevents the conventional FEM to reach the exact solution. The solution from HFEM can almost reach the exact solution and the solution from Ritz method.

Due to the varying thickness of the beams, the transverse shear stiffness coefficient A_{55} and the bending stiffness coefficient D_{11} become linear and cubic functions respectively. This results in a fully populated stiffness and mass matrices and increases the computational effort required to obtain a solution. Nonetheless, the efficiency and accuracy of the solution for the tapered beams are forthcoming.

To sum up, in this chapter the Hierarchical Finite Element Method has been presented and its formulation has been applied to the free vibration analysis of both uniform and tapered Euler-Bernoulli and Timoshenko beams. To start with, Ritz method is presented and its derivation is detailed to stress the conceptual changes for tapered composite beam. All examples are solved by Ritz method, conventional FEM and HFEM so that besides the comparison that can be made with regard to the HFEM and Ritz

results, another comparison also can be made between conventional and hierarchical FEM. The detailed formulation of the HFEM is also given to stress the major aspects of the method.

The trigonometric form of HFEM is found to give highly accurate results, viz. frequencies in free vibration, with substantially less number of elements and system degrees of freedom. The effect of adding internal degrees of freedom enhances the performance of the element and hence a single more efficient element can do the work of many conventional elements combined. Also, the number of system degrees of freedom can be varied without changing the mesh of elements. Results can be achieved to any desired degree of accuracy by simply increasing the number of hierarchical terms in each element. In this chapter, example problems are given for both Euler-Bernoulli and Timoshenko models. The HFEM formulation gives much better results than the conventional formulation. In the next chapter, we will apply HFEM to tapered Euler-Bernoulli and Timoshenko beams with axial force.

Chapter 4

Free Vibration Analysis of Tapered Laminated Composite Beams subjected to Axial Force

4.1 Introduction

In the previous chapter, we have derived the formulations of vibration analysis of a tapered composite beam, based on both CLT and FSDT. At the end of each section, examples have been given. The results obtained using Ritz method, conventional FEM and HFEM match very well. When there is axial force acting at the ends of the beam, it affects the vibration frequencies. In this chapter, we will derive the formulations of vibration analysis of a tapered composite beam subjected to axial force, based on both CLT and FSDT. Ritz method and HFEM will also be applied to this problem and example problems will be given. In addition, all the compressing axial forces applied at the ends of beams in the examples will be much smaller than their corresponding buckling loads.

4.2 Formulation based on Classical Laminate Theory

4.2.1 Solution using Ritz method and based on CLT

In this section, we will derive the formulations using Ritz method based on the classical laminate theory for a tapered composite beam subjected to axial force and then give some examples, including uniform and tapered composite Euler-Bernoulli beams.

4.2.1.1 Formulation using Ritz method based on CLT

In Chapter 3, we have already derived the strain energy U of a tapered laminated beam (Equation 3.9). In the case where transverse deformation is taken into account, the actions exerted upon the laminate result from in-plane loads [1]. The potential energy of the in-plane loads N_x, N_{xy}, and N_y owed to a deflection w is

$$V = \frac{1}{2}\int\int\left[N_x\left(\frac{\partial w}{\partial x}\right)^2 + 2N_{xy}\frac{\partial w}{\partial x}\frac{\partial w}{\partial y} + N_y\left(\frac{\partial w}{\partial y}\right)^2\right]dxdy \tag{4.1}$$

In this section, we limit our discussion to a beam and there is only N_x acting on it. Thus the potential energy can be reduced to:

$$V = \frac{1}{2}\int\int N_x\left(\frac{\partial w}{\partial x}\right)^2 dxdy = \frac{1}{2}\int_0^{l_e} bN_x\left(\frac{\partial w}{\partial x}\right)^2 dx \tag{4.2}$$

In addition, the kinetic energy T is as same as that for a beam subjected to pure bending without axial force (Equation 3.15).

Therefore, the stationary value for the vibration analysis of a tapered laminated beam subjected to axial force includes three components [1]:

$$\Pi = U - V + T \tag{4.3}$$

Substituting Equations 3.9, 3.15 and 4.2 into Equation 4.3 yields:

$$\Pi = \frac{1}{2}\int_0^{l_e} bD_{11}\left(\frac{\partial^2 w}{\partial x^2}\right)^2 dx - \frac{1}{2}\int_0^{l_e} bN_x\left(\frac{\partial w}{\partial x}\right)^2 dx - \frac{\omega^2}{2}\int_0^{l_e} b(\rho_L H_L + \rho_r H_r)w^2 dx \qquad (4.4)$$

In order to use Ritz method, we assume the same interpolation functions for the displacement W that were used in Chapter 3 (Equation 3.17). Then we can substitute Equation 3.17 into Equation 4.4 and impose the stationary condition (Equation 3.18). Again we can get a set of N equations. Expressing this set of equations by a matrix equation yields Equation 3.19. Here, the $[M]$ matrix is as same as that we obtained in Section 3.2.1.1, but the $[K]$ matrix is different. Here, N_x is embedded in $[K]$ matrix because:

$$U - V = \frac{1}{2}\int_0^{l_e} bD_{11}\left(\frac{\partial^2 w}{\partial x^2}\right)^2 dx - \frac{1}{2}\int_0^{l_e} bN_x\left(\frac{\partial w}{\partial x}\right)^2 dx \qquad (4.5)$$

Solving this eigenvalue problem $|[K] - \omega^2[M]| = 0$, we can get the free vibration frequencies for beam subjected to axial force.

4.2.1.2 Example applications

In this section, we will apply Ritz method to a uniform laminated composite beam subjected to axial force. Furthermore, a tapered laminated composite beam is presented.

Example 4.1 vibration of a simply supported uniform composite beam subjected to axial force using Ritz method based on CLT

A uniform composite beam with both ends simply supported as shown in Figure 4.1 is made up of NCT301 graphite-epoxy. Its mechanical properties are shown in Table 2.2.

The geometric properties of the beam are: length $L = 0.3048\,\text{m}$; individual ply thickness $t = 0.0001524\,\text{m}$. There are 32 plies in the laminate and the configuration of the laminate is $[(0/90)_8]_S$. The laminate thickness of $H = 0.0048768\,\text{m}$ is obtained by multiplying the number of plies, 32 in this case with the ply thickness, i.e. $0.0001524\,\text{m}$. The length-to-height ratio is 62.5. It is subjected to axial force $N_x = 10\,\text{KN}$.

From Reference [1], we have the expression of buckling load:

$$N_{cr} = \frac{\pi^2}{L^2} D_{11} \tag{4.6}$$

For the beam given by Example 4.1, the bending stiffness coefficient is

$D_{11} = 817.127\ \text{N.m}$

Therefore, its first mode buckling load is $N_{cr} = 86.808\,\text{KN}$. The axial force applied on this beam $N_x = 10\,\text{KN}$ is much smaller than N_{cr}.

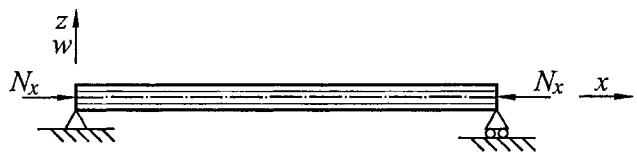

Figure 4.1 Simply supported uniform composite beam subjected to axial force

The exact solution is given by [2]:

$$\omega_m = \frac{m\pi}{L}\sqrt{\frac{1}{\rho H}\left(\frac{m^2\pi^2}{L^2}\frac{D}{A} - N_x\right)} \tag{4.7}$$

For symmetrical laminate, the above equation can be simplified to:

$$\omega_m = \frac{m\pi}{L}\sqrt{\frac{1}{\rho H}\left(\frac{D_{11}m^2\pi^2}{L^2} - N_x\right)} \tag{4.8}$$

Substituting the value of D_{11} into Equation 4.7, we can get the natural frequencies of the beam shown in Figure 4.1:

$\omega_1 = 1003.72$ rad/sec

$\omega_2 = 4206.33$ rad/sec

$\omega_3 = 9541.87$ rad/sec

$\omega_4 = 17011.4$ rad/sec

Then same trigonometric interpolation functions as those in Equation 3.22 are assumed for the displacement W. Table 4.1 gives the natural frequencies by using trigonometric interpolation functions:

Table 4.1 Natural frequencies of uniform composite beam described in Example 4.1 using trigonometric interpolation functions

	1R	2R	3R	4R	5R	Exact
ω_1	1003.72	1003.72	1003.72	1003.72	1003.72	1003.72
ω_2		4206.33	4206.33	4206.33	4206.33	4206.33
ω_3		9541.87	9541.87	9541.87	9541.87	9541.87
ω_4			17011.4	17011.4	17011.4	17011.4

As can be seen the Ritz method gives perfect results for this example, even when W has only one interpolation term. This is as same as that for the uniform composite beam without axial force discussed in Chapter 3.

Example 4.2 vibration of a simply supported tapered beam using Ritz method based on CLT

A tapered composite beam made up of NCT301 graphite-epoxy has configuration of model F. Both of its ends are simply supported as shown in Figure 4.2. Its mechanical properties are shown in Table 2.2.

The geometric properties of the beam are: length $L = 0.3048\,\text{m}$; individual ply thickness $t = 0.0001524\,\text{m}$. There are 32 plies at the left end and 30 plies at the right end. Two layers are dropped. The configuration of both ends are $[(0/90)_8]_S$ and $[(0/90)_7/0]_S$ respectively. The height of each ply in z direction is $h = 0.00015240001905\,\text{m}$. It is almost as same as the thickness $t = 0.0001524\,\text{m}$, because the tapered angle is only $\alpha = 0.02865°$. This beam is subjected to axial force $N_x = 10\,\text{KN}$. This axial force should be much less than the first mode buckling load of this tapered beam, because the first mode buckling load of the similar uniform beam in Example 4.1 is $N_{cr} = 86.808\,\text{KN}$.

The bending stiffness coefficient of this beam is

$$D_{11} = 817.122 - 490.366x + 95.5097x^2 - 1.01515x^3$$

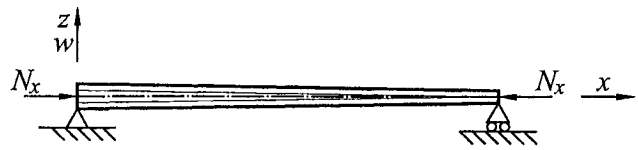

Figure 4.2 Simply supported tapered composite beam subjected to axial force

The same trigonometric interpolation function as in Example 4.1 is assumed for the displacement W. Table 4.2 gives the results.

Table 4.2 Natural frequencies of tapered composite beam described in Example 4.2 using trigonometric interpolation functions

	1R	2R	3R	4R	5R	10R
ω_1	967.496	966.896	966.896	966.892	966.892	966.891
ω_2		4075.46	4072.87	4072.86	4072.84	4072.84
ω_3			9252.92	9246.56	9246.55	9246.48
ω_4				16501.7	16489.4	16489.2

As can be seen the convergence is still very fast, but the results from low order displacement functions do not exactly match the solution obtained using ten interpolation terms, not like that in the case of uniform beam. That is because the tapered angle results in a cubic D_{11}. Few trigonometric terms can not accurately describe the displacement. The more trigonometric terms we use, the more accurate result we have.

The next step is to use HFEM to re-solve the same problems.

4.2.2 Solution using Hierarchical Finite Element Method and based on CLT

4.2.2.1 Formulation using HFEM based on CLT

In the above section, we have already derived the stationary value based on classical laminate theory for a composite beam subjected to axial force (Equation 4.4).

Imposing the stationary condition:

$$\delta\Pi = \delta U - \delta V + \delta T = 0 \tag{4.9}$$

We can obtain the governing equation for this problem:

$$\int_0^{l^e}\left[D_{11}\left[N^M\right]^T\left[N^M\right] - N_x\left[N^{dw}\right]^T\left[N^{dw}\right]\right]dx\{u\} - \omega^2\int_0^{l^e}\left(\rho_L H_L + \rho_r H_r\right)\left[N^w\right]^T\left[N^w\right]dx\{u\} = 0 \tag{4.10}$$

where the interpolation functions N^w, N^M and N^{dw} have the same forms as those we defined in Chapter 3 for HFEM based on CLT.

Equation 4.9 can be expressed by:

$$\left[[K]-\omega^2[M]\right]\{u\}=0 \tag{4.11}$$

where,

$$[K]=\int_0^{l_e}\left[D_{11}[N^M]^T[N^M]-N_x[N^{dw}]^T[N^{dw}]\right]dx \tag{4.12}$$

$$[M]=\int_0^{l_e}(\rho_L H_L+\rho_r H_r)[N^w]^T[N^w]dx \tag{4.13}$$

As same as that in Ritz method, solving the eigenvalue equation $\left[[K]-\omega^2[M]\right]=0$, we can get the natural frequencies.

Now we can re-solve Example 4.1 using HFEM.

4.2.2.2 Example applications

Example 4.3 vibration of a simply supported uniform composite beam subjected to axial force using HFEM based on CLT

This problem is same as Example 4.1 but we use HFEM instead of Ritz method.

Table 4.3 Natural frequencies of uniform composite beam described in Example 4.3 using conventional FEM based on CLT

	2E	4E	6E	8E	10E	12E	Exact
ω_1	1008.17	1004.01	1003.78	1003.74	1003.73	1003.72	1003.72
ω_2		4223.40	4209.83	4207.45	4206.79	4206.55	4206.33
ω_3		9718.28	9580.00	9554.30	9547.04	9544.38	9541.87
ω_4			17213.8	17079.0	17039.8	17025.2	17011.4

Table 4.4 Natural frequencies of uniform composite beam described in Example 4.3 using one-hierarchical-term model based on CLT

	2E1T	4E1T	6E1T	8E1T	10E1T	12E1T	Exact
ω_1	1003.80	1003.72	1003.72	1003.72	1003.72	1003.72	1003.72
ω_2		4206.66	4206.36	4206.33	4206.33	4206.33	4206.33
ω_3		9548.96	9542.61	9542.03	9541.92	9541.89	9541.87
ω_4			17017.9	17012.7	17011.8	17011.5	17011.4

Table 4.5 Natural frequencies of uniform composite beam described in Example 4.3 using two-hierarchical-terms model based on CLT

	2E2T	4E2T	6E2T	8E2T	10E2T	12E2T	Exact
ω_1	1003.73	1003.72	1003.72	1003.72	1003.72	1003.72	1003.72
ω_2		4206.36	4206.34	4206.33	4206.33	4206.33	4206.33
ω_3		9542.11	9541.96	9541.91	9541.89	9541.88	9541.87
ω_4			17011.7	17011.5	17011.4	17011.4	17011.4

Figure 4.3 shows the comparison between the results obtained using conventional FEM and hierarchical FEM for this example. Only the first natural frequency is plotted in this figure. We can observe from Tables 4.3 to 4.5 that the other frequencies have similar convergence.

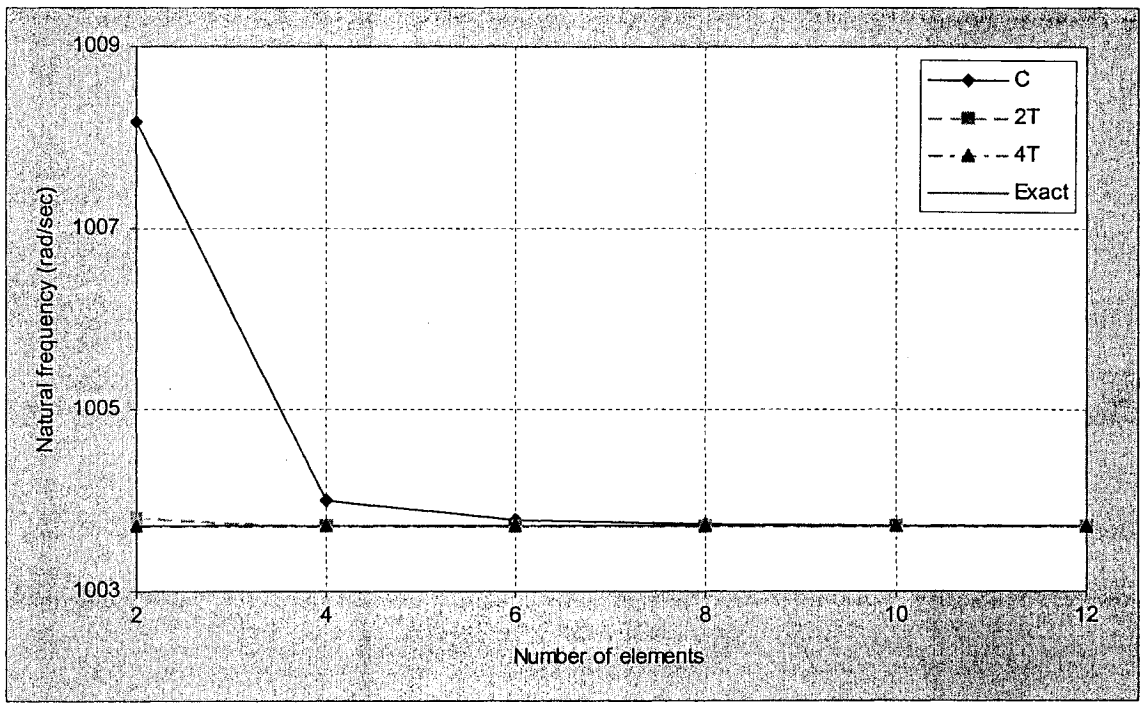

Figure 4.3 First mode frequency of simply supported uniform composite beam subjected to axial force based on CLT

For this simply supported uniform composite beam subjected to axial force, both conventional FEM and HFEM show rapid convergence. At the same time, HFEM gives

much more accurate results compared with those from conventional FEM, especially for the two-elements and four-elements models. This is as same as that for the uniform composite beam without axial force given in Chapter 3.

Then we can use HFEM to re-solve Example 4.2, the tapered composite beam subjected to axial force.

Example 4.4 vibration of a simply supported tapered beam subjected to axial force using HFEM based on CLT

This problem is same as Example 4.2 but we use HFEM instead of Ritz method. Tables 4.6 to 4.8 are the natural frequencies obtained using conventional FEM model, one-hierarchical-term model and two-hierarchical-term model respectively.

Table 4.6 Natural frequencies of tapered composite beam described in Example 4.4 using conventional FEM based on CLT

	2E	4E	6E	8E	10E	12E	10R
ω_1	971.322	967.183	966.949	966.910	966.899	966.895	966.891
ω_2		4089.49	4076.25	4073.93	4073.29	4073.06	4072.84
ω_3		9418.65	9283.56	9258.57	9251.50	9248.92	9246.48
ω_4			16686.0	16554.9	16516.8	16502.7	16489.2

Table 4.7 Natural frequencies of tapered composite beam described in Example 4.4 using one-hierarchical-term model based on CLT

	2E1T	4E1T	6E1T	8E1T	10E1T	12E1T	10R
ω_1	966.974	966.893	966.891	966.891	966.891	966.891	966.891
ω_2		4073.16	4072.87	4072.85	4072.84	4072.84	4072.84
ω_3		9253.31	9247.20	9246.63	9246.53	9246.50	9246.48
ω_4			16495.5	16490.5	16489.6	16489.3	16489.2

Table 4.8 Natural frequencies of tapered composite beam described in Example 4.4 using two-hierarchical-terms model based on CLT

	2E2T	4E2T	6E2T	8E2T	10E2T	12E2T	10R
ω_1	966.901	966.892	966.891	966.891	966.891	966.891	966.891
ω_2		4072.87	4072.85	4072.84	4072.84	4072.84	4072.84
ω_3		9246.71	9246.56	9246.51	9246.50	9246.49	9246.48
ω_4			16489.5	16489.4	16489.3	16489.2	16489.2

The first mode frequency is plotted in Figure 4.4.

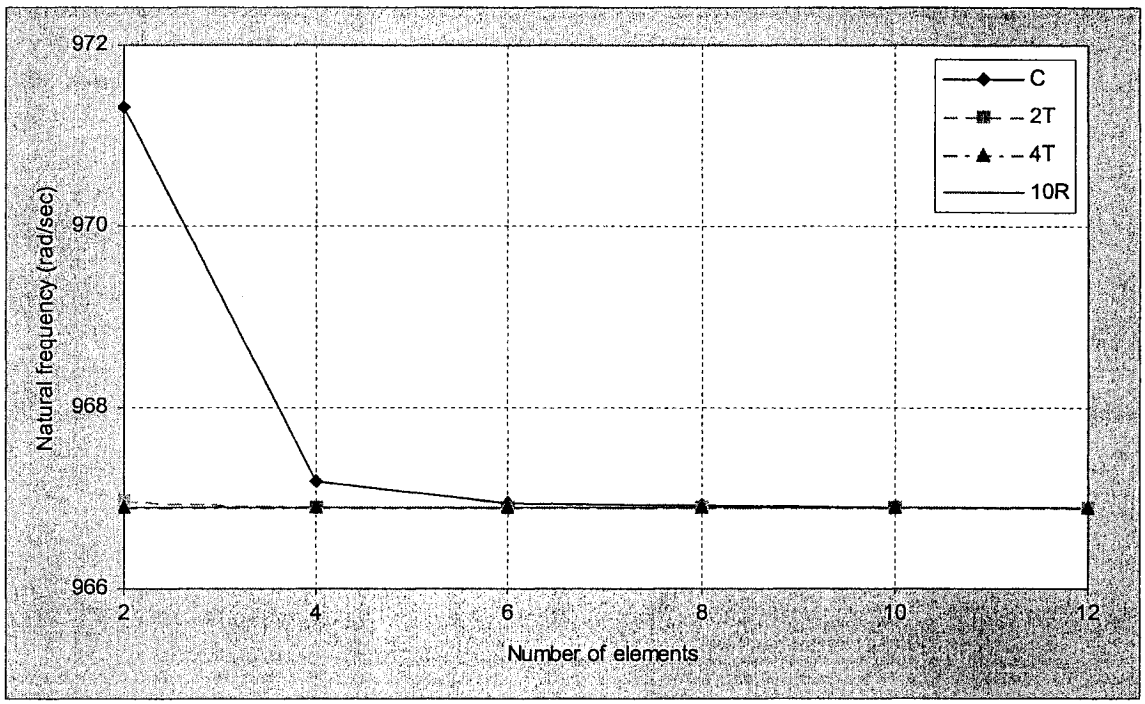

Figure 4.4 First mode frequency of simply supported tapered composite beam subjected to axial force based on CLT

As can be seen all the three curves converge to the exact solution. For conventional FEM, six-elements model gives acceptable accuracy. At the same time, HFEM shows critical advantages of using fewer elements and obtaining better accuracy. This is because the hierarchical formulations consider the internal degrees of freedom. Hence, the resulting expressions involving higher derivatives of the displacement field

are accurate. These are similar to those in the cases without axial force.

In the above three examples, we fixed the number of hierarchical terms and increased the number of elements from two to twelve, and the comparison shows the considerable improvement of hierarchical FEM. We can also fix the number of elements but increase the number of hierarchical terms to observe the convergence. Tbles 4.9 to 4.12 are results for Example 4.4.

Table 4.9 Natural frequencies of tapered composite beam described in Example 4.4 using HFEM with two-elements model based on CLT

	2E0T	2E1T	2E2T	2E3T	2E4T	2E5T	2E6T	10R
ω_1	971.322	966.974	966.901	966.893	966.892	966.891	966.891	966.891

Table 4.10 Natural frequencies of tapered composite beam described in Example 4.4 using HFEM with three-elements model based on CLT

	3E0T	3E1T	3E2T	3E3T	3E4T	3E5T	3E6T	10R
ω_1	967.800	966.900	966.894	966.891	966.891	966.891	966.891	966.891
ω_2	4122.81	4074.42	4072.92	4072.87	4072.84	4072.84	4072.84	4072.84

Table 4.11 Natural frequencies of tapered composite beam described in Example 4.4 using HFEM with four-elements model based on CLT

	4E0T	4E1T	4E2T	4E3T	4E4T	4E5T	4E6T	10R
ω_1	967.183	966.893	966.892	966.891	966.891	966.891	966.891	966.891
ω_2	4089.49	4073.16	4072.87	4072.85	4072.84	4072.84	4072.84	4072.84
ω_3	9418.65	9253.31	9246.71	9246.61	9246.50	9246.50	9246.49	9246.48

Table 4.12 Natural frequencies of tapered composite beam described in Example 4.4 using HFEM with five-elements model based on CLT

	5E0T	5E1T	5E2T	5E3T	5E4T	5E5T	5E6T	10R
ω_1	967.011	966.892	966.892	966.891	966.891	966.891	966.891	966.891
ω_2	4079.83	4072.93	4072.85	4072.84	4072.84	4072.84	4072.84	4072.84
ω_3	9321.11	9248.46	9246.62	9246.53	9246.48	9246.48	9246.48	9246.48
ω_4	16874.0	16506.5	16489.7	16489.5	16489.2	16489.2	16489.2	16489.2

Figure 4.5 plots the first mode frequency of two-elements to five-elements

models. As can be seen the frequency converges fast by increasing number of elements or the number of hierarchical terms. At the same time, the two-elements conventional model shows much more inaccuracy than the others. As soon as we use one hierarchical term, the first mode frequency becomes very close to that from Ritz method, even for the two-elements model.

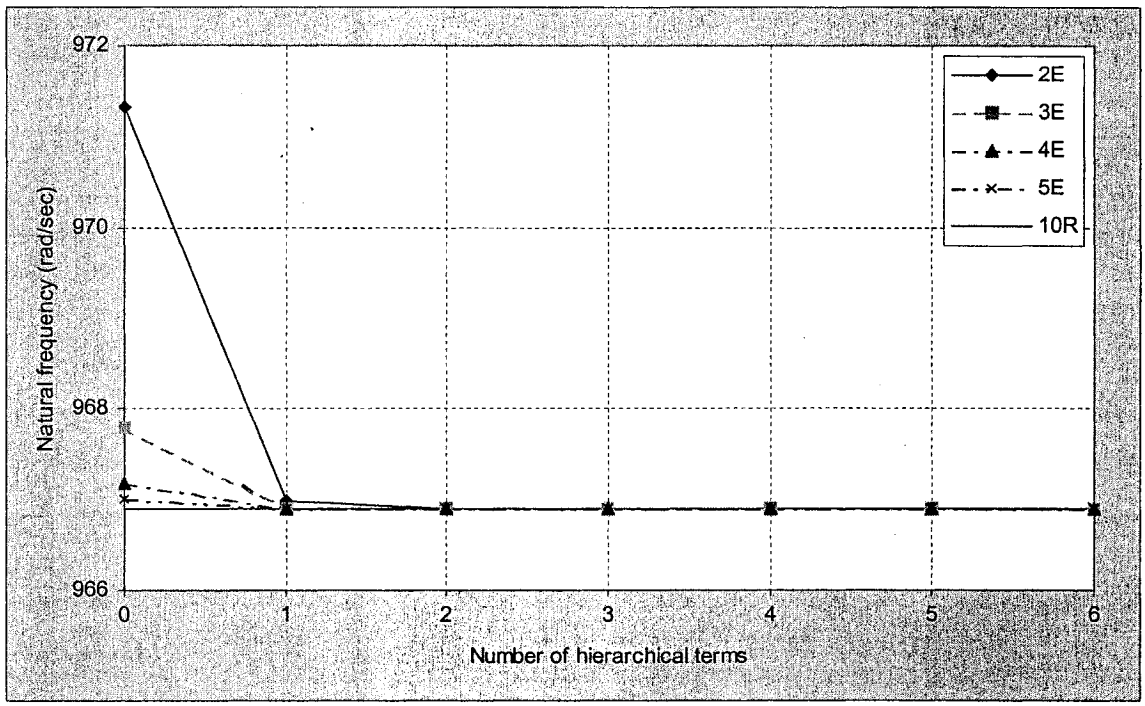

Figure 4.5 First mode frequency vs. number of hierarchical terms plot of simply supported tapered composite beam subjected to axial force based on CLT

So far, the conventional and the hierarchical finite element methods based on CLT have been described and example problems have been solved to illustrate their applications, for both uniform and tapered composite beams. In this section, only simply supported boundary condition is presented. The others will show up in Chapter 5. Similar to that in the case without axial force, given in Chapter 3, the HFEM displays superior results as compared to the conventional FEM. In the next section, we will apply HFEM to

a tapered Timoshenko beam subjected to axial force based on FSDT.

4.3 Formulation based on First-order Shear Deformation Theory

4.3.1 Solution using Ritz method and based on FSDT

In this section, we will derive the solution using Ritz method based on the first-order shear deformation theory and then give some example problems, including uniform and tapered composite beams subjected to axial force.

4.3.1.1 Formulation using Ritz method based on FSDT

In Chapter 3, we have already obtained the strain energy U (Equation 3.60) and kinetic energy T (Equation 3.65) of a tapered composite beam based on FSDT. In the case where transverse deformation is taken into account the actions exerted upon the laminate result from in-plane loads. The potential energy of the in-plane load N_x owed to a deflection W is as same as that based on the classical laminate theory, as given by Equation 4.2.

The stationary value for the vibration analysis of a tapered laminated beam subjected to axial force based on FSDT has the same form as in the case of classical laminate theory:

$$\Pi = U - V + T \tag{4.14}$$

Substituting Equations 3.60, 3.65, and 4.2 into Equation 4.13 yields:

$$\Pi = \frac{1}{2}\int_0^{l_e} b\left[D_{11}\left(\frac{\partial \psi}{\partial x}\right)^2 + kA_{55}\left(\psi + \frac{\partial w}{\partial x}\right)^2\right]dx - \frac{1}{2}\int_0^{l_e} bN_x\left(\frac{\partial w}{\partial x}\right)^2 dx - \frac{\omega^2}{2}\int_0^{l_e} b(\rho_L H_L + \rho_r H_r)w^2 dx \tag{4.15}$$

Assuming $W = \sum_{i=1}^{N} c_i \phi_i$ and $\Psi = \sum_{i=1}^{N} e_i \varphi_i$ according to different boundary conditions and imposing the stationary condition, Equation 3.67, we can obtain a matrix equation having the same form as Equation 3.68. Again, solving the eigenvalue problem $\left|[K] - \omega^2 [M]\right| = 0$, we can obtain the free vibration frequency.

The next step is to give some example problems, including a uniform laminated beam subjected to axial force. In order to have exact solutions to compare, we need to solve the differential equation for the vibration analysis of a uniform laminated beam subjected to axial force.

We have two differential equations for a uniform laminated beam subjected to axial force based on FSDT [2]:

$$\begin{aligned} kA_{55}\left(\frac{\partial \psi}{\partial x} + \frac{\partial^2 w}{\partial x^2}\right) - N_x \frac{\partial^2 w}{\partial x^2} &= \rho H \frac{\partial^2 w}{\partial t^2} \\ D_{11}\frac{\partial^2 \psi}{\partial x^2} - kA_{55}\left(\psi + \frac{\partial w}{\partial x}\right) &= I_{xy}\frac{\partial^2 \psi}{\partial t^2} \end{aligned} \tag{4.16}$$

Ignoring the rotary inertia moment yields:

$$\begin{aligned} kA_{55}\left(\frac{\partial \psi}{\partial x} + \frac{\partial^2 w}{\partial x^2}\right) - N_x \frac{\partial^2 w}{\partial x^2} &= \rho H \frac{\partial^2 w}{\partial t^2} \\ D_{11}\frac{\partial^2 \psi}{\partial x^2} - kA_{55}\left(\psi + \frac{\partial w}{\partial x}\right) &= 0 \end{aligned} \tag{4.17}$$

First of all, we consider a simply supported beam and assume the displacement and rotation functions as:

$$\psi = B_m e^{i\omega t}\cos\frac{m\pi x}{L}$$
$$w = C_m e^{i\omega t}\sin\frac{m\pi x}{L} \tag{4.18}$$

Substituting Equation 4.17 into Equation 4.16 gives

$$kA_{55}\frac{m\pi}{L}B_m + \left[(kA_{55} - N_x)\frac{m^2\pi^2}{L^2} - \rho H\omega^2\right]C_m = 0$$
$$\left(D_{11}\frac{m^2\pi^2}{L^2} + kA_{55}\right)B_m + kA_{55}\frac{m\pi}{L}C_m = 0 \tag{4.19}$$

Then we can condense out B_m,

$$\left\{\left(D_{11}\frac{m^2\pi^2}{L^2} + kA_{55}\right)\left[(kA_{55} - N_x)\frac{m^2\pi^2}{L^2} - \rho H\omega^2\right] - k^2A_{55}^2\frac{m^2\pi^2}{L^2}\right\}C_m = 0 \tag{4.20}$$

Because the coefficients are nonzero ($C_m \neq 0$), the other part of the left side of Equation 4.19 must be zero. Thus

$$\left(D_{11}m^2\pi^2 + L^2kA_{55}\right)\left(kA_{55} - N_x\right)m^2\pi^2 - L^2k^2A_{55}^2m^2\pi^2 = \left(D_{11}m^2\pi^2 + L^2kA_{55}\right)L^2\rho H\omega^2 \tag{4.21}$$

Then the natural frequency of a uniform laminated beam with axial force based on FSDT is of the form:

$$\omega = \frac{m\pi}{L}\sqrt{\frac{\left(D_{11}m^2\pi^2 + L^2kA_{55}\right)\left(kA_{55} - N_x\right) - L^2k^2A_{55}^2}{\left(D_{11}m^2\pi^2 + L^2kA_{55}\right)\rho H}} \tag{4.22}$$

4.3.1.2 Example Applications

In this section, we will apply Ritz method to a uniform laminated composite beam subjected to axial force. Furthermore, a tapered laminated composite beam subjected to axial force will be presented.

Example 4.5 vibration of a simply supported uniform composite beam subjected to axial force using Ritz method based on FSDT

This problem is similar to Example 4.1 except that the length $L = 0.03048\,\text{m}$ and the axial force $N_x = 100\,\text{KN}$. Its length-to-height ratio is 6.25.

From Reference [1], we have the expression of buckling load based on FSDT:

$$N_{cr} = \frac{kA_{55}D_{11}\pi^2}{D_{11}\pi^2 + kA_{55}L^2} \tag{4.23}$$

where the material properties of the beam in this example are

$A_{55} = 18726912\ \text{Nm}^{-1}$

$D_{11} = 817.127\ \text{N.m}$

Therefore, its first mode buckling load is $N_{cr} = 5578\,\text{KN}$. The axial force applied on this beam $N_x = 100\,\text{KN}$ is much smaller than N_{cr}.

The exact solution is given by Equation 4.21:

$\omega_1 = 84765.6\ \text{rad/sec}$

$\omega_2 = 236568\ \text{rad/sec}$

$\omega_3 = 390348\ \text{rad/sec}$

$\omega_4 = 540674\ \text{rad/sec}$

Then trigonometric interpolation functions are assumed for the displacement W and rotation Ψ as given by Equation 3.70. Table 4.13 gives the results.

Table 4.13 Natural frequencies of uniform composite beam described in Example 4.5 using Ritz method based on FSDT

	1R	2R	3R	4R	5R	Exact
ω_1	84765.6	84765.6	84765.6	84765.6	84765.6	84765.6
ω_2		236568	236568	236568	236568	236568
ω_3			390348	390348	390348	390348
ω_4				540674	540674	540674

It can be seen the Ritz method gives perfect solution for this problem, even when W and Ψ have only one interpolation term each. This is as same as that for the uniform composite beam without axial force discussed in Chapter 3 and that for the uniform composite beam with axial force based on CLT in Section 4.2.1.2.

Example 4.6 vibration of a simply supported tapered beam subjected to axial force using Ritz method based on FSDT

A tapered composite beam made up of NCT301 graphite-epoxy has configuration of model F. Both of its ends are simply supported as shown in Figure 4.2. Its mechanical properties are given in Table 2.2.

The geometric properties of the beam are: length $L = 0.03048\,\text{m}$; individual ply thickness $t = 0.0001524\,\text{m}$. There are 32 plies at the left end and 30 plies at the right end. Two layers are dropped. The configuration of both ends are $[(0/90)_8]_S$ and $[(0/90)_7/0]_S$ respectively. The height of each ply in z direction is $h = 0.000152401905\,\text{m}$. It is almost as same as the thickness $t = 0.0001524\,\text{m}$, because the tapered angle is only $\alpha = 0.2865^\circ$. This beam is subjected to axial force $N_x = 100\,\text{KN}$. This axial force should be much less than the first mode buckling load of this tapered beam, because the first mode buckling load of the similar uniform beam in Example 4.5 is $N_{cr} = 5578\,\text{KN}$

The bending stiffness coefficient is

$$D_{11} = 816.591 - 4900.51x + 9544.85x^2 - 1015.17x^3$$

Table 4.14 gives the first four natural frequencies.

Table 4.14 Natural frequencies of tapered composite beam described in Example 4.6 using Ritz method based on FSDT

	1R	2R	3R	4R	5R	10R	Uniform
ω_1	83118.3	83088.6	83088.6	83088.4	83088.4	83088.4	84765.6
ω_2		234703	234658	234658	234658	234657	236568
ω_3			389190	389151	389151	389151	390348
ω_4				540296	540266	540265	540674

As can be seen the convergence is still very fast, but the results from low order displacement functions do not match the solution obtained using ten interpolation terms. That is because the taper angle results in a cubic D_{11}. Few trigonometric terms can not accurately describe the displacement. The consequence is the inaccurate result.

The next step is to use HFEM to re-solve the same problems and compare the results from both methods.

4.3.2 Solution using Hierarchical Finite Element Method and based on FSDT

4.3.2.1 Formulation using HFEM based on FSDT

In the previous section, we have derived the stationary value (Equation 4.14) for a tapered composite beam with axial force based on FSDT. Then, imposing the stationary condition (Equation 4.8), we can obtain the governing equation:

$$\begin{aligned} &\int_0^{l_e} \left[D_{11} \left[N^{d\psi}\right]^T \left[N^{d\psi}\right] - N_x \left[N^{dw}\right]^T \left[N^{dw}\right] + kA_{55} \left[N^{\psi dw}\right]^T \left[N^{\psi dw}\right] \right] dx \{u\} \\ &- \omega^2 \int_0^{l_e} (\rho_L H_L + \rho_r H_r) \left[N^w\right]^T \left[N^w\right] dx \{u\} = 0 \end{aligned} \tag{4.24}$$

where the interpolation functions N^w, $N^{d\psi}$, $N^{\psi dw}$ and N^{dw} have the same forms as those we defined in Chapter 3 for HFEM based on FSDT.

Equation 4.22 can be written as:

$$\left[[K]-\omega^2[M]\right]\{u\}=0 \tag{4.25}$$

where,

$$[K]=\int_0^{l_e}\left[D_{11}\left[N^{d\psi}\right]^T\left[N^{d\psi}\right]-N_x\left[N^{dw}\right]^T\left[N^{dw}\right]+kA_{55}\left[N^{\psi dw}\right]^T\left[N^{\psi dw}\right]\right]dx \tag{4.26}$$

$$[M]=\int_0^{l_e}\left(\rho_L H_L+\rho_r H_r\right)\left[N^w\right]^T\left[N^w\right]dx \tag{4.27}$$

It is also an eigenvalue problem.

Now we can re-solve Examples 4.5 and 4.6 using HFEM instead of Ritz method.

4.3.2.2 Example applications

Example 4.7 vibration of a simply supported uniform beam subjected to axial force using HFEM based on FSDT

In this problem, the uniform composite beam and boundary condition are as same as those in Example 4.5 but we apply HFEM instead of Ritz method. Tables 4.15 to 4.17 are the natural frequencies obtained using conventional FEM model, two-hierarchical-terms model and four-hierarchical-terms model respectively.

Table 4.15 Natural frequencies of uniform composite beam described in Example 4.7 using conventional FEM based on FSDT

	2E	4E	6E	8E	10E	12E	Exact
ω_1	116590	92472.1	88163.0	86671.0	85983.4	85610.7	84765.6
ω_2		280646	256018	247433	243495	241368	236568
ω_3		500235	445925	421700	410349	404199	390348
ω_4			654297	608594	584399	571009	540674

Table 4.16 Natural frequencies of uniform composite beam described in Example 4.7 using two-hierarchical-terms model based on FSDT

	2E2T	4E2T	6E2T	8E2T	10E2T	12E2T	Exact
ω_1	86203.5	84945.4	84828.6	84797.6	84785.1	84778.7	84765.6
ω_2		238544	237129	236816	236706	236656	236568
ω_3		399525	392820	391352	390867	390660	390348
ω_4			548278	543675	542163	541534	540674

Table 4.17 Natural frequencies of uniform composite beam described in Example 4.7 using four-hierarchical-terms model based on FSDT

	2E4T	4E4T	6E4T	8E4T	10E4T	12E4T	Exact
ω_1	85050.1	84863.9	84812.1	84792.3	84782.9	84777.7	84765.6
ω_2		236987	236799	236709	236661	236634	236568
ω_3		391161	390890	390708	390597	390528	390348
ω_4			541587	541344	541164	541041	540674

The first mode frequency is plotted in Figure 4.6.

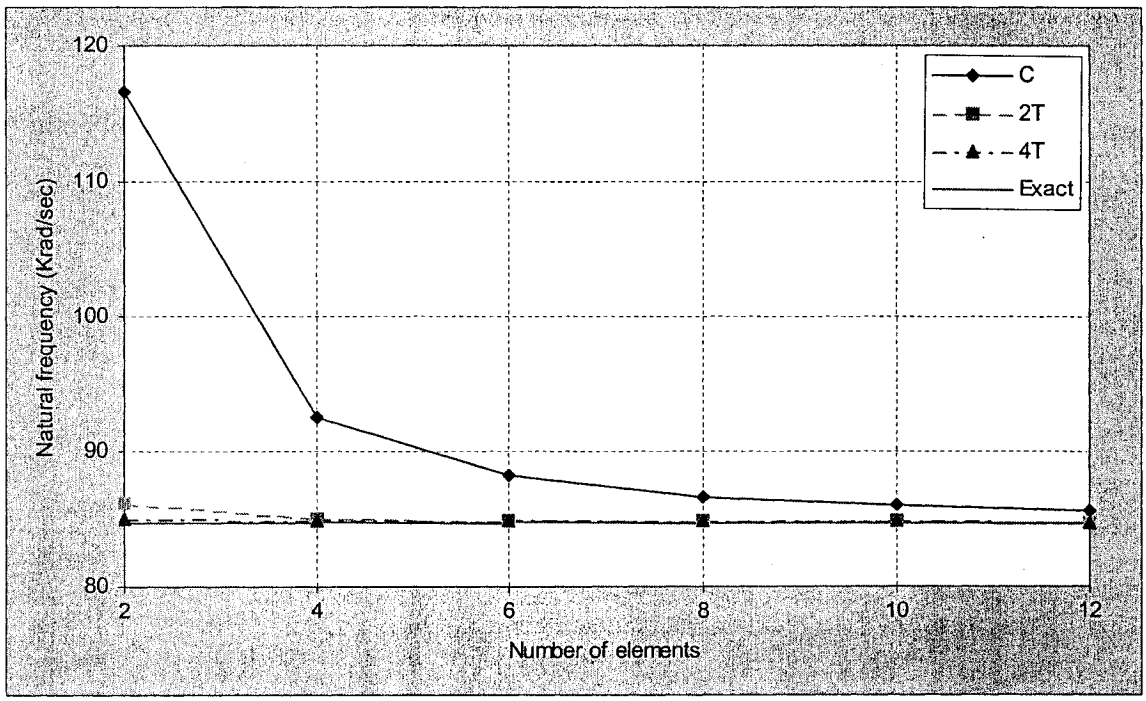

Figure 4.6 First mode frequency of simply supported uniform composite beam with axial force based on FSDT

Figure 4.6 is very similar to Figure 3.14 showing the first mode frequency of simply supported composite beam without axial force based on FSDT. The top curve shows a typical slow convergence of conventional FEM based on FSDT. Furthermore, this curve is always above the exact solution. Shear lock also happens to beam subjected to axial force. On the other hand, HFEM has much better accuracy than the conventional FEM, and the two lower curves almost reach the exact solution.

Example 4.8 vibration of a simply supported tapered beam subjected to axial force using HFEM based on FSDT

In this problem, the composite beam and boundary condition are as same as those in Example 4.6 but we apply HFEM here instead of Ritz method.

Table 4.18 Natural frequencies of tapered composite beam described in Example 4.8 using conventional FEM based on FSDT

	2E	4E	6E	8E	10E	12E	10R
ω_1	115592	90961.6	86558.3	85033.2	84330.2	83949.1	83088.4
ω_2		279619	254481	245729	241715	239548	234657
ω_3		500979	445586	420973	409448	403206	389151
ω_4			655311	608982	584493	570946	540265

Table 4.19 Natural frequencies of tapered composite beam described in Example 4.8 using two-hierarchical-terms model based on FSDT

	2E2T	4E2T	6E2T	8E2T	10E2T	12E2T	10R
ω_1	84555.6	83269.2	83149.4	83117.7	83104.8	83098.4	83088.4
ω_2		236675	235230	234910	234798	234747	234657
ω_3		398484	391663	390171	389678	389468	389151
ω_4			547967	543304	541772	541135	540265

Table 4.20 Natural frequencies of tapered composite beam described in Example 4.8 using four-hierarchical-terms model based on FSDT

	2E4T	4E4T	6E4T	8E4T	10E4T	12E4T	10R
ω_1	83375.1	83185.4	83132.5	83112.3	83102.6	83097.3	83088.4
ω_2		235084	234893	234801	234753	234725	234657
ω_3		389975	389700	389515	389403	389333	389151
ω_4			541187	540943	540761	540636	540265

The first mode frequency is plotted in Figure 4.7.

Just like that in the uniform beam case, HFEM based on FSDT gives better convergence than the conventional FEM, and it seems to converge to the solution from Ritz method. Next, we are going to increase both the number of elements and the number of hierarchical terms to see if the solution can rapidly approach the solution from Ritz method. Tables 4.21 to 4.24 give the results.

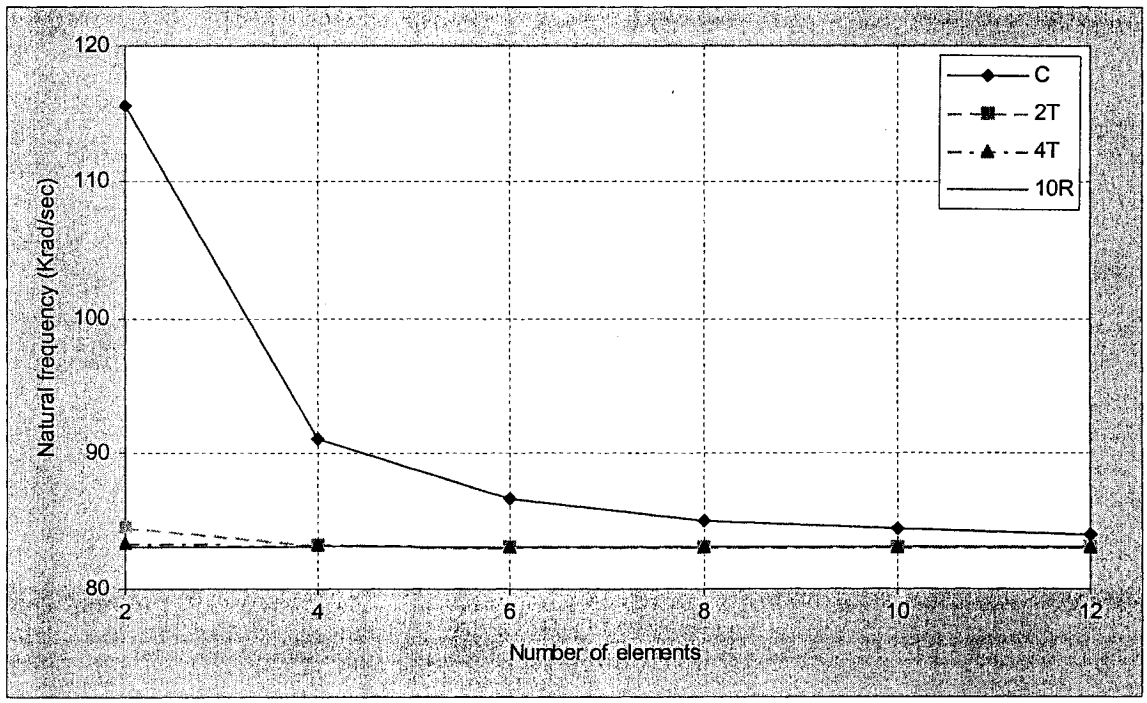

Figure 4.7 First mode frequency of simply supported tapered composite beam with axial force based on FSDT

Table 4.21 Natural frequencies of tapered composite beam described in Example 4.8 using HFEM with two-elements model based on FSDT

	2E0T	2E2T	2E4T	2E6T	2E8T	2E10T	2E12T	10R
ω_1	115592	84555.6	83375.1	83206.1	83138.1	83116.1	83103.0	83088.4

Table 4.22 Natural frequencies of tapered composite beam described in Example 4.8 using HFEM with three-elements model based on FSDT

	3E0T	3E2T	3E4T	3E6T	3E8T	3E10T	3E12T	10R
ω_1	97231.8	83504.6	83248.8	83127.9	83112.6	83096.9	83093.9	83088.4
ω_2	311857	239806	235233	235016	234772	234745	234698	234657

Table 4.23 Natural frequencies of tapered composite beam described in Example 4.8 using HFEM with four-elements model based on FSDT

	4E0T	4E2T	4E4T	4E6T	4E8T	4E10T	4E12T	10R
ω_1	90961.6	83269.2	83185.4	83106.5	83101.4	83091.2	83090.2	83088.4
ω_2	279619	236675	235084	234825	234734	234701	234683	234657
ω_3	500979	398484	389975	389764	389324	389297	389213	389151

Table 4.24 Natural frequencies of tapered composite beam described in Example 4.8 using HFEM with five-elements model based on FSDT

	5E0T	5E2T	5E4T	5E6T	5E8T	5E10T	5E12T	10R
ω_1	88100.6	83186.8	83151.9	83097.9	83095.8	83088.8	83088.4	83088.4
ω_2	263350	235653	234971	234751	234711	234683	234675	234657
ω_3	468797	393685	389826	389492	389278	389236	389194	389151
ω_4	680720	553945	541342	541145	540499	540474	540350	540265

The first mode frequency is plotted in Figure 4.8.

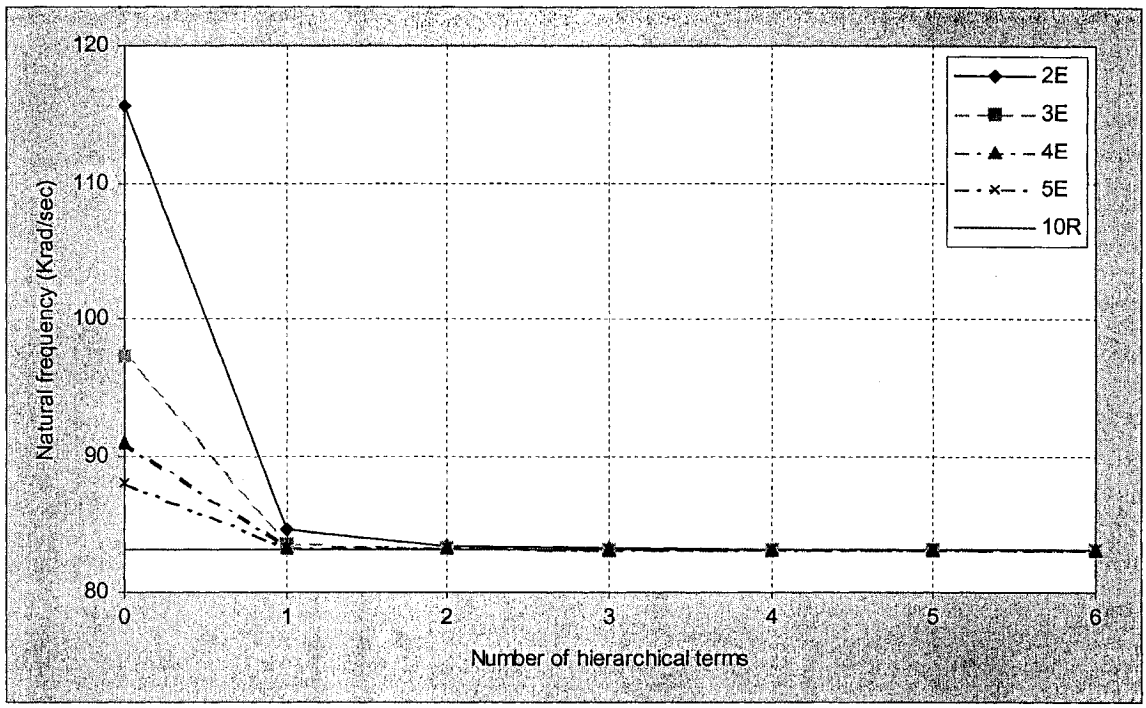

Figure 4.8 First mode frequency vs. number of hierarchical terms plot of simply supported tapered composite beam with axial force based on FSDT

Figure 4.8 is very similar to Figure 3.17 plotting the first mode frequency of simply supported tapered composite beam without axial force. Comparing the results for Examples 3.11 and 4.8, we can see that the axial force affects the value of natural frequencies but does not change the convergence of HFEM.

4.4 Conclusions and discussions

So far, the hierarchical FEM developed and applied to composite beams without axial force in the previous chapter have been applied in this chapter to beams subjected to axial force. These composite beams subjected to axial force have been modeled using CLT and FSDT. Results for both the Euler-Bernoulli and Timoshenko beams have been presented. The vibration analysis of uniform composite beams subjected to axial force is also performed and compared with the conventional formulation and the exact solution.

The application of HFEM is further extended to the thickness-tapered composite beams with axial force based on both CLT and FSDT.

Application of the hierarchical finite element method to composite beams subjected to axial force, as in the case of beams without axial force, yields the same advantages of numerical efficiency and faster convergence. Less number of elements are required to model and obtain precise answers for the vibration analysis of composite beams with or without axial force. The system degrees of freedom are also substantially less. The graphs in this chapter have given us a comparison of the convergence of natural frequencies obtained using HFEM and the conventional formulation to their exact solutions. There is a substantial reduction in the number of elements required to obtain results that are almost the same as exact solutions. Also, much less number of system degrees of freedom are required. For the Euler-Bernoulli beam, Figure 4.5 gives us the convergence to the solution from Ritz method with increase in the number of trigonometric terms. The non-dimensional frequencies for different modes are plotted versus the number of trigonometric terms for the simply supported beam. For the Timoshenko beam, Figure 4.10 illustrates the convergence of the two finite element methods and shows that HFEM gives better results.

The results obtained for the vibration analysis of tapered composite beams subjected to axial force show that the accuracy obtained is the same as that for beams without axial force. The inherent features and advantages of the HFEM as pointed out for the case of beams without axial force hold good for beams subjected to axial force too. In addition, the dynamic analysis performed for the uniform and tapered composite beams gives accurate results using minimum number of elements. The trigonometric HFEM is

applied to the example problems since it has been the best method for uniform beams.

Chapter 5

Parametric study on tapered composite beams

5.1 Introduction

In Chapter 2 we have already derived the formulations of elastic behavior for composite beam with different taper models. In Chapter 3, Ritz method and hierarchical finite element method have been applied for uniform-thickness, mid-plane tapered and internally-tapered composite beams based on both classical laminate theory and first-order shear deformation theory. Furthermore, in Chapter 4, these methods and theories have been applied to tapered composite beams subjected to axial force.

The examples described in Chapters 2, 3 and 4 were designed so as to focus our study on the effects of different types of tapered sections on vibration response. Major considerations in designing a tapered composite beam are ply orientations, taper angle and type of the tapered section. Six types of tapered sections were introduced as models A, B, C, D, F and M as shown in Figure 5.1.

The tapered beams are analyzed considering different types of internally tapered sections. Variations in the boundary conditions, stacking sequences and taper angles are considered for all cases. In general, there are two ways of changing the taper angle: (a)

change the length of tapered section while keeping the thickness of the thick and thin sections as constants. b) change the number of drop-off plies (i.e., change the thicknesses of thick and thin sections).

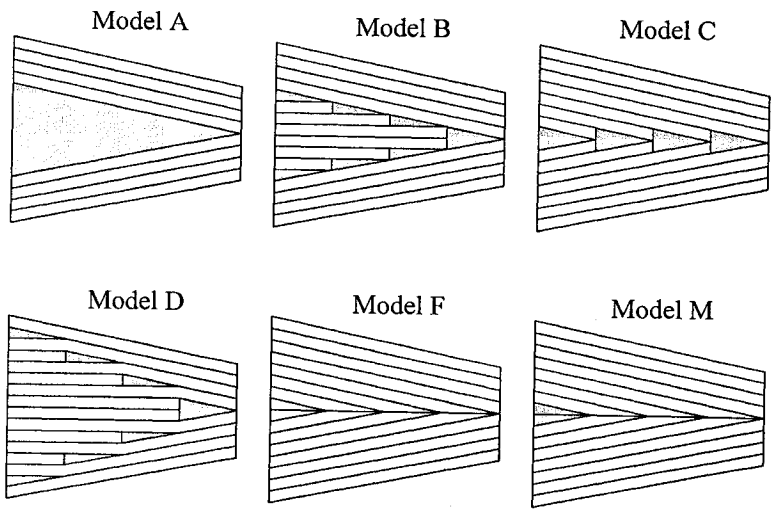

Figure 5.1 *Taper models A, B, C, D, F and M*

In this chapter, the parametric study is conducted on the tapered beams shown in Figure 5.1. The material chosen is NCT301 graphite-epoxy. The properties of the material are listed in Table 2.2. The specifications of composite (ply orientations) and geometric properties (number of plies, taper angle, and length) are detailed in individual problems. In all cases the laminate is symmetric. All problems are solved using Ritz method and HFEM based on FSDT. The results are summarized in tables and where applicable, in plots. The results are compared and interpreted right after each problem.

5.2 Parametric study on the free vibration of tapered composite beams

In this section, Ritz method will be applied to different composite beams with

various boundary conditions besides HFEM. The interpolation functions for Ritz method based on FSDT for the following four boundary conditions are given in table 5.1.

Table 5.1 Interpolation functions for different boundary conditions for Ritz method based on FSDT

	w	ψ
Simply supported	$\sum_{i=1}^{N} c_i \sin\frac{i\pi x}{L}$	$\sum_{i=1}^{N} e_i \cos\frac{i\pi x}{L}$
Fixed-fixed	$\sum_{i=1}^{N} c_i \sin\frac{i\pi x}{L}$	$\sum_{i=1}^{N} e_i \sin\frac{i\pi x}{L}$
Fixed-free	$\sum_{i=1}^{N} c_i \sin\frac{i\pi x}{2L}$	$\sum_{i=1}^{N} e_i \sin\frac{i\pi x}{2L}$
Free-fixed	$\sum_{i=1}^{N} c_i \cos\frac{i\pi x}{2L}$	$\sum_{i=1}^{N} e_i \cos\frac{i\pi x}{2L}$

5.2.1 Effect of boundary conditions

A tapered composite beam made up of NCT301 graphite-epoxy has configuration of model F. Its mechanical properties are listed in Table 2.2.

The geometric properties of the beam are: length $L = 0.0366\,\text{m}$; individual ply thickness $t = 0.0001524\,\text{m}$. There are 48 plies at the left end and 24 plies at the right end. 24 layers are dropped. The configuration of both ends are $[(0/90)_{12}]_S$ and $[(0/90)_6]_S$ respectively. The height of each ply in z direction is $h = 0.00015259\,\text{m}$. It is almost as same as the thickness $t = 0.0001524\,\text{m}$, because the tapered angle is only $\alpha = 2.8641^\circ$. The total height at the left end is $H = 0.00732435\,\text{m}$ and the length-to-height ratio is 5.0.

The transverse shear stiffness coefficient and bending stiffness coefficient are

$$A_{55} = (29.3854 - 321.150x)\times 10^6$$

$$D_{11} = 2527.03 - 101856x + 1344731x^2 - 1014731x^3$$

Table 5.2 gives the results from both Ritz method and HFEM. For Ritz method, we use ten interpolation terms and for HFEM, a twelve-elements and four-hierarchical-terms model is used. Figure 5.2 is the graphical form of Table 5.2.

Table 5.2 The lowest four natural frequencies of tapered beam described in Section 5.2.1

		Simply-supported	Fixed-fixed	Fixed-free	Free-fixed
ω_1	12E4T	64924.3	100530	35858.8	17055.1
	10R	64922.5	100513	35856.8	17051.7
ω_2	12E4T	192926	208815	123605	104922
	10R	192867	208750	123584	104900
ω_3	12E4T	324783	332908	247300	245013
	10R	324681	332755	247218	245021
ω_4	12E4T	454631	458820	376835	377416
	10R	454314	458620	376319	390264

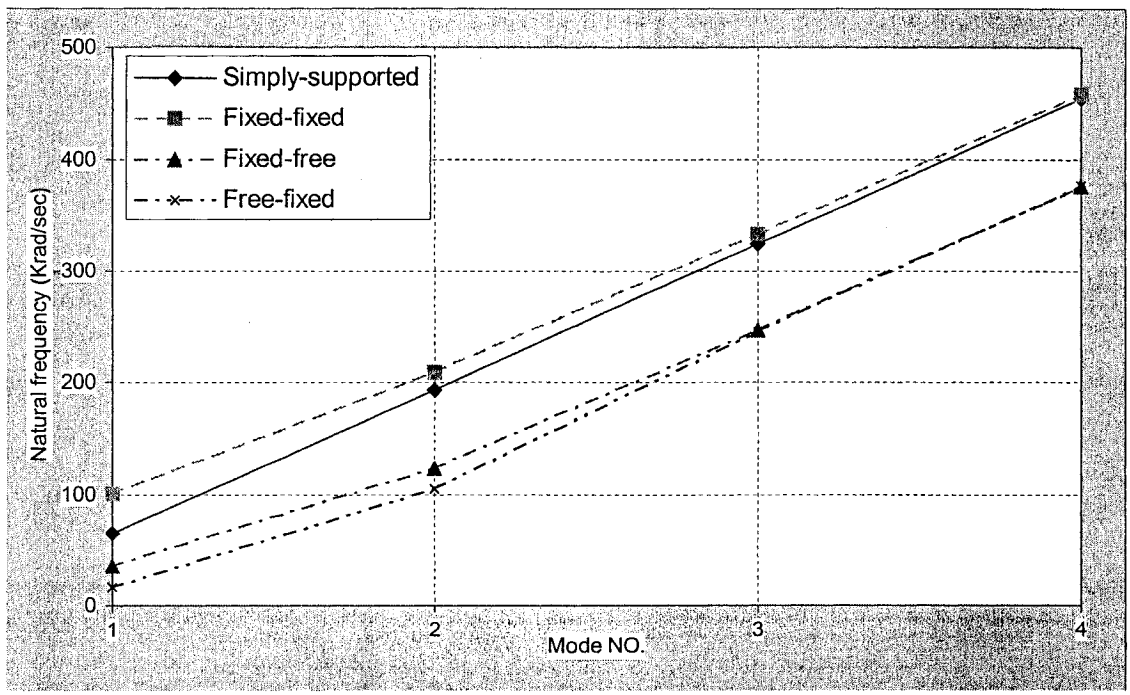

Figure 5.2 Effect of boundary condition on natural frequencies of the beam described in Section 5.2.1

Observation from Table 5.2 and Figure 5.2 shows that changing the boundary

condition results in a considerable variation in the natural frequencies. For this specific beam, the natural frequencies for the fixed-fixed support are the highest, the second rank is for the simply supported case, the third rank is for the fixed-free case and the lowest values are for free-fixed support. Zabihollah got the same conclusion in his thesis [10] although his example problem differs from the one presented here.

5.2.2 Effect of laminate configuration

The problem described in Section 5.2.1 is considered to investigate the effectof laminate configuration on the natural frequencies. The same material and geometric properties are used. The laminate configurations considered are: (i) LC1 that has $[(0/90)_{12}]_S$ configuration at thick section and $[(0/90)_6]_S$ configuration at thin section; (ii) LC2 that has $[(\pm 45)_{12}]_S$ configuration at thick section and $[(\pm 45)_6]_S$ configuration at thin section; (iii) LC3 that has $[0_4/(\pm 45)_8(-45)_4]_S$ configuration at thick section and $[0_4/(\pm 45)_4]_S$ configuration at thin section. The lowest four natural frequencies are determined for different boundary conditions and for the laminate configurations LC1, LC2 and LC3. In Section 5.2.1, we have already obtained the natural frequencies of the beam with configuration LC1 as given in Table 5.2. Tables 5.3 and 5.4 give the values of the lowest four natural frequencies of the beam with configurations LC2 and LC3 respectively.

Table 5.3 The natural frequencies of tapered beam with LC2 configuration corresponding to different boundary conditions

		Simply-supported	Fixed-fixed	Fixed-free	Free-fixed
ω_1	12E4T	51681.9	89035.4	28367.4	12851.6
	10R	51656.9	89011.4	28364.3	12847.4
ω_2	12E4T	167898	191916	106866	88684.9
	10R	167829	191837	106841	88650.3
ω_3	12E4T	297389	311424	221790	218702
	10R	297255	311258	221696	218402
ω_4	12E4T	427490	435601	348167	350030
	10R	427146	436164	348102	366290

Table 5.4 The natural frequencies of tapered beam with LC3 configuration corresponding to different boundary conditions

		Simply-supported	Fixed-fixed	Fixed-free	Free-fixed
ω_1	12E4T	69160.4	103874	37324.8	19042.7
	10R	69158.7	103858	37335.8	19039.7
ω_2	12E4T	200240	214366	128245	110331
	10R	200182	214303	128261	110308
ω_3	12E4T	333514	340505	255562	252870
	10R	333412	340315	255556	252456
ω_4	12E4T	464397	467831	386692	386357
	10R	464079	466975	386621	385994

Figures 5.3, 5.4, 5.5 and 5.6 show the effect of laminate configuration for simply supported, fixed-fixed, fixed-free and free-fixed boundary conditions respectively. The resource data are from Tables 5.2, 5.3 and 5.4.

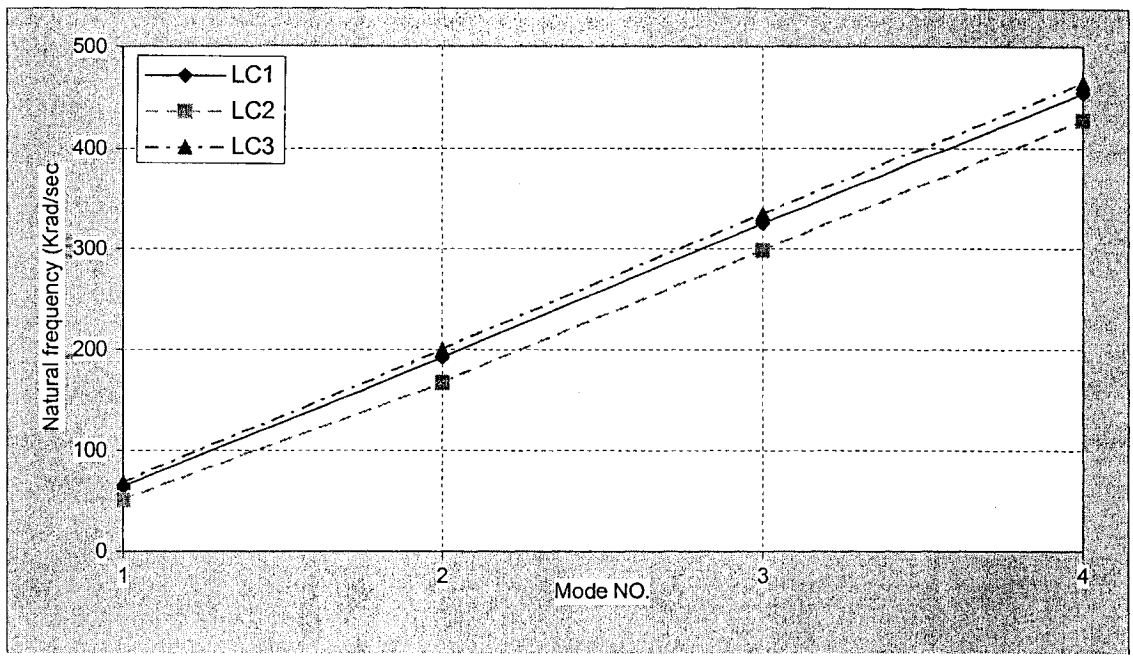

Figure 5.3 Natural frequencies of laminate configurations LC1, LC2 and LC3 with simply-supported boundary condition

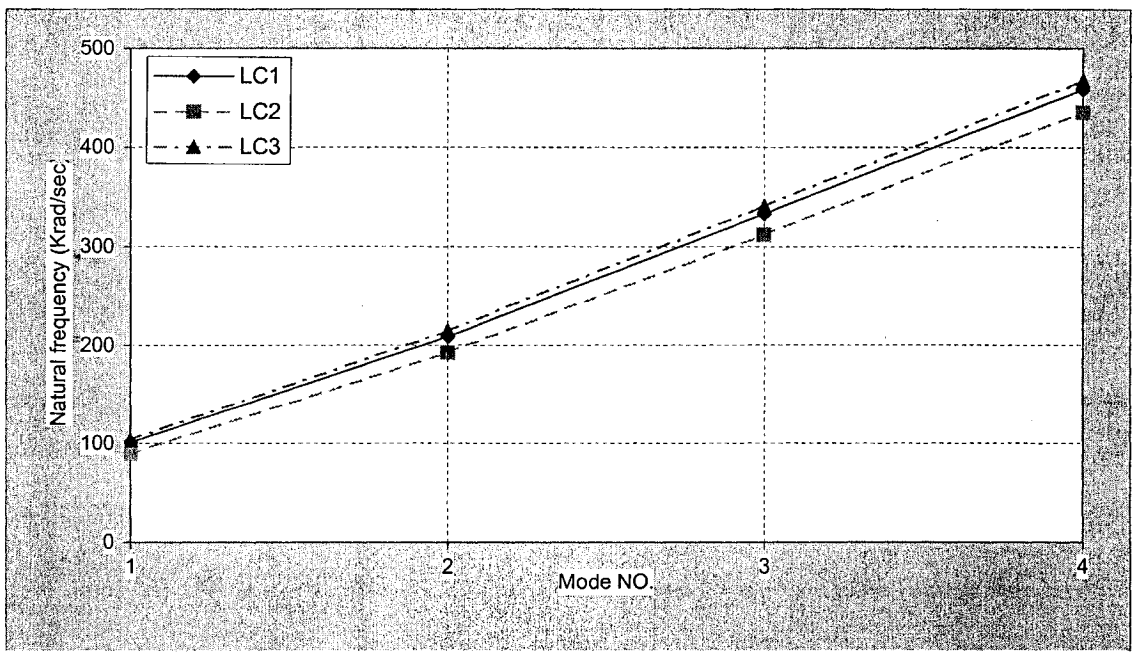

Figure 5.4 Natural frequencies of laminate configurations LC1, LC2 and LC3 with fixed-fixed boundary condition

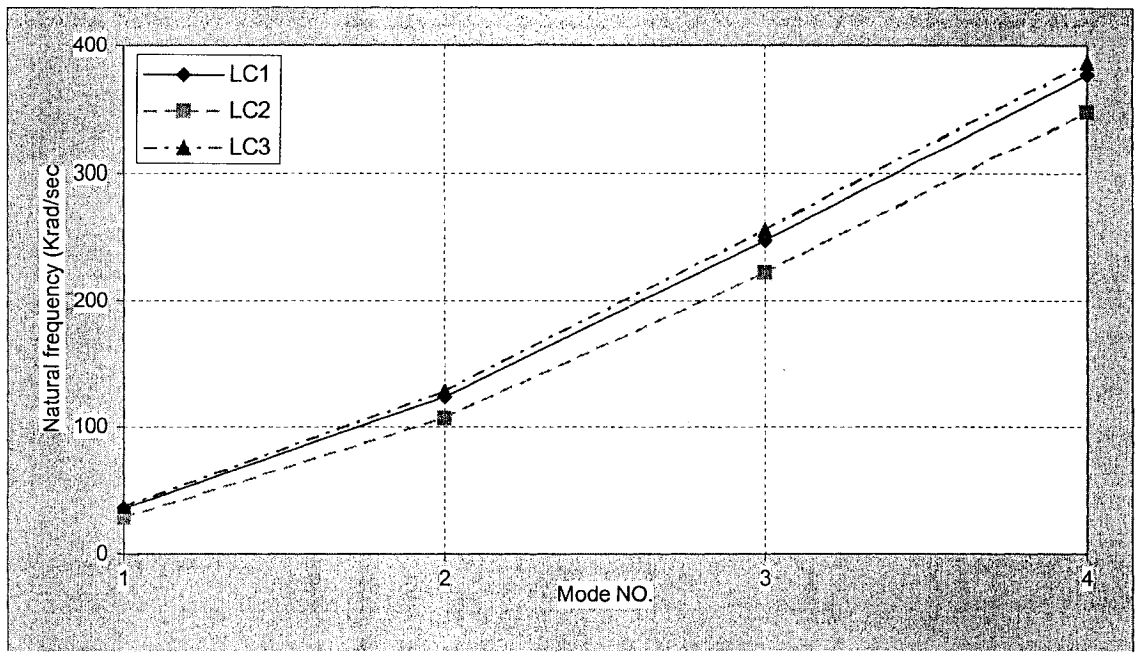

Figure 5.5 Natural frequencies of laminate configurations LC1, LC2 and LC3 with fixed-free boundary condition

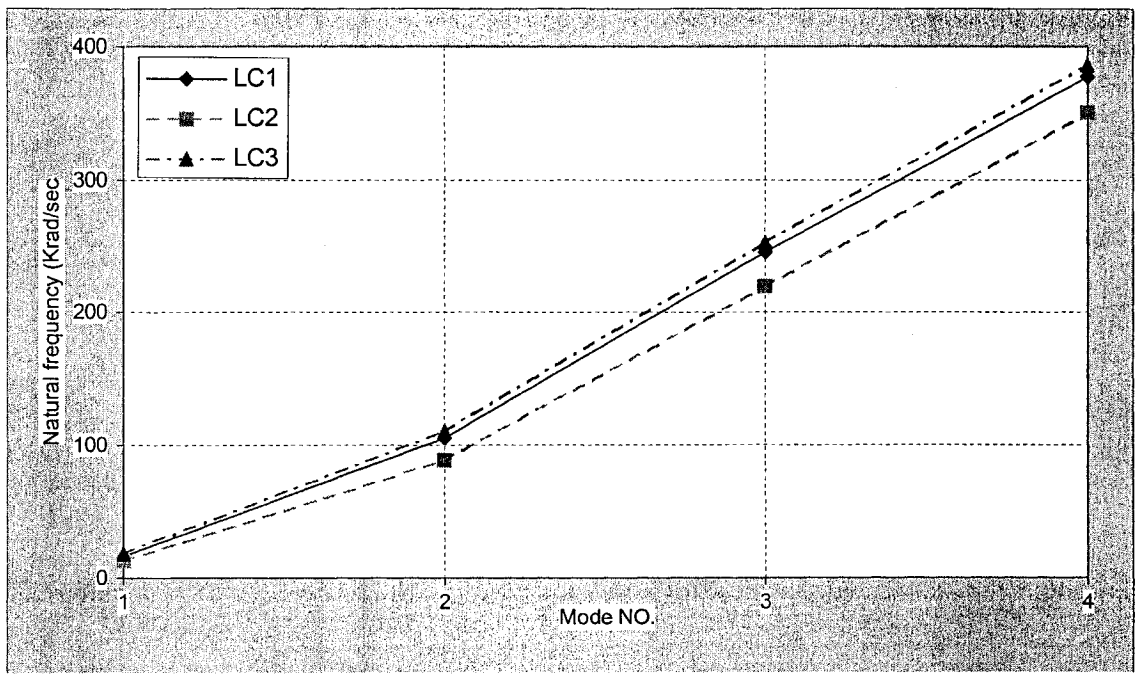

Figure 5.6 Natural frequencies of laminate configurations LC1, LC2 and LC3 with free-fixed boundary condition

As can be seen for all the four types of boundary conditions, the natural

frequencies for LC3 laminate configuration are the highest and the lowest values are claimed by LC2 laminate configuration. The changes in natural frequencies for different configurations are due to change in stiffness matrix for each configuration. Recalling Equation 3.86, one can see that stiffness matrix directly depends on the values of D_{11} and A_{55} if the geometry properties are same. Therefore, it is necessary to consider the change of ply orientation. Again tapered beam in Section 5.2.1 is considered here. The changes in the fundamental frequency corresponding to different ply orientation angles for the laminate with $[\pm\theta]$ ply group are shown in Table 5.5 and Figure 5.7.

Table 5.5 The fundamental natural frequency of tapered beam with $[\pm\theta]$ ply group corresponding to different boundary conditions

	0°	10°	20°	30°	40°	50°	60°	70°	80°	90°
1*	79885.8	78366	73860.8	66569.6	56996	46320.8	36802.1	31057.3	29351.9	29254.5
2*	115440	114150	110281	103802	94621	82926.3	70575.8	61945.7	59095.2	58862.7
3*	44717.4	43823	41178.9	36925.9	31401.1	25332.2	20006.2	16830.2	15894.5	15842.5
4*	21670.5	21151.7	19642.8	17294.4	14385.1	11359.3	8831.64	7373.2	6951.55	6929.57

*1—Simply supported; *2—Fixed-fixed; *3—Fixed-free; *4—Free-fixed

Obviously, the fundamental frequency drops very slowly for ply orientation angles close to 0° and 90°. In Figure 5.7, we can see that the largest slope of the curves is around 45°. Because the geometry properties do not change, the only factor to cause this is the change of material properties - D_{11} and A_{55}. This is similar to that in the uniform composite beam case. Meanwhile, the natural frequency of the beam with 0° plies is much larger than the beam with 90° plies. That is because the elastic modulus E_1 is much larger than E_2 and E_3, etc. Therefore, the bending stiffness coefficient of 0° ply is much larger than that of the 90° ply. Consequently, the more 0° plies a beam contains,

the higher natural frequency it has.

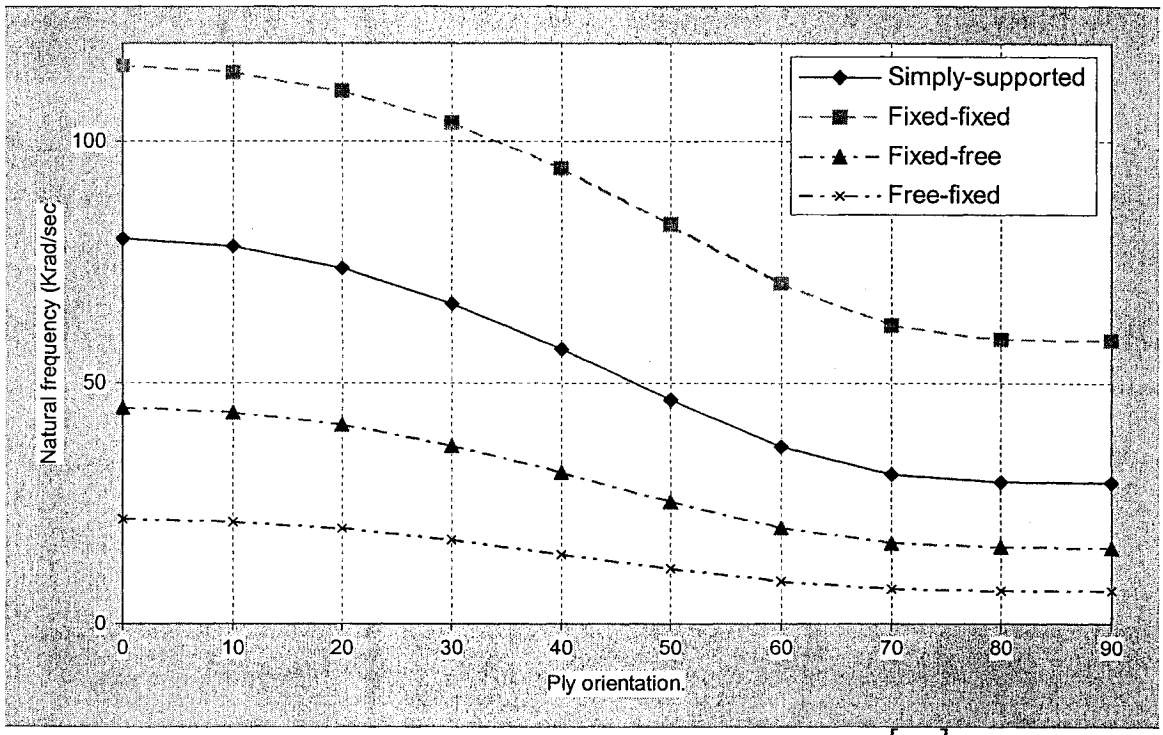

Figure 5.7 Fundamental frequencies of tapered beams with $[\pm\theta]$ ply group

5.2.3 Effect of the taper angle

To study the effect of taper angle on the natural frequencies, the tapered beam described in Section 5.2.1 is considered. Taper angles have been increased from 0° (uniform) to 5.0165° to investigate the effect of taper angle on natural frequencies. The ply configuration at the left section remains same, and the various tapered angles are obtained by fixing the length of the beam and decreasing the number of plies at the right section, from 48 to 40, 32, 22, 14 and 6.

Table 5.6 and Figure 5.8 show the effect of taper angle on the natural frequencies of tapered beam with simply supported boundary condition.

Table 5.6 Effect of taper angle on the natural frequencies of simply supported tapered beam

Number of plies at the right section	Taper angle α °	ω_1	ω_2	ω_3	ω_4
48	0	80688.5	209433	336215	460213
40	0.9543	76734.4	205427	333663	458932
32	1.9090	71578.8	200292	330140	456940
22	3.1030	62974.7	190584	322902	453515
14	4.0592	53710.6	178123	311362	444913
6	5.0165	40899.1	157422	287327	421606

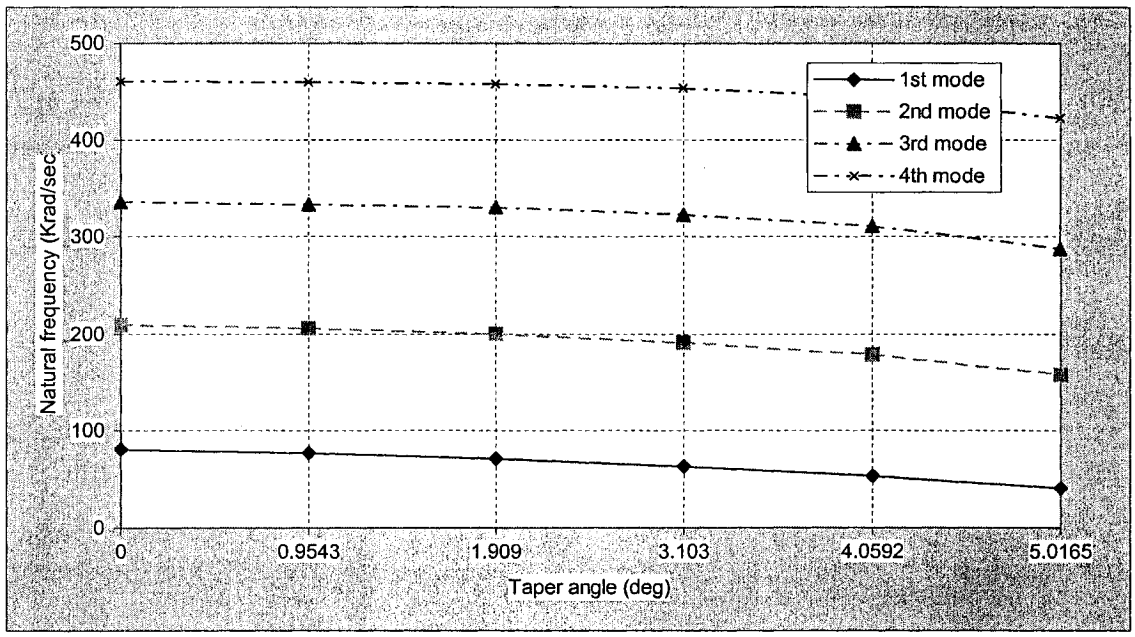

Figure 5.8 Effect of taper angle on the natural frequencies of tapered beam with simply supported boundary condition

Observation of the results in Table 5.6 and Figure 5.8 shows that increasing the taper angle leads to decreasing the natural frequencies. As discussed in Chapter 2, A_{55} is a linear function of x and D_{11} is a cubic function due to the tapered geometry property. This is similar to that of a tapered isotropic-material beam. At the same time, the change of taper angle also changes the ply stiffness, as discussed in Chapter 2. We can expect

that due to the fact that the taper angle is always small in many practical cases (less than 6°), the change of ply stiffness is small. Therefore, the majority contribution to the change of A_{55} and D_{11} is given by the reduced height of the beam, not the change of ply stiffness. From Figure 5.8, we can see that the slopes of the curves decrease very slowly at the beginning and faster along with increasing of taper angle because D_{11} is a cubic function of x.

Tables 5.7 to 5.9 give the lowest four natural frequencies for fixed-fixed, fixed-free and free-fixed supports respectively.

Table 5.7 Effect of taper angle on the natural frequencies of fixed-fixed tapered beam

Number of plies at the right section	Taper angle α°	ω_1	ω_2	ω_3	ω_4
48	0	107665	216956	339540	461511
40	0.9543	106088	214848	337831	460627
32	1.9090	103848	212447	335834	459525
22	3.1030	99432.7	207566	331838	458293
14	4.0592	93305.1	199876	324459	453209
6	5.0165	82259.2	183238	305166	435293

Table 5.8 Effect of taper angle on the natural frequencies of fixed-free tapered beam

Number of plies at the right section	Taper angle α°	ω_1	ω_2	ω_3	ω_4
48	0	32928.3	128027	261473	387429
40	0.9543	33771.7	126992	257775	384900
32	1.9090	34702.3	125528	253283	381709
22	3.1030	36209.1	123023	245465	375155
14	4.0592	38069.3	120238	236163	365211
6	5.0165	41555.9	117402	222797	346323

Table 5.9 Effect of taper angle on the natural frequencies of free-fixed tapered beam

Number of plies at the right section	Taper angle α °	ω_1	ω_2	ω_3	ω_4
48	0	32928.3	128027	261473	387429
40	0.9543	28100.1	122111	257286	384713
32	1.9090	22759.3	114669	252167	381622
22	3.1030	15597.9	101965	242696	375975
14	4.0592	9778.04	87069.9	229495	366633
6	5.0165	4207.80	64516.3	203581	343272

As can be seen from these tables, increasing the taper angle leads to decreasing the natural frequencies and frequencies decrease very slowly at the beginning and faster along with the increasing of taper angle. This tendency is as same as that of the simply supported case.

5.2.4 Effect of taper model

To study the effect of different types of taper model on the natural frequencies, the problem described in section 5.2.1 is considered. The material and the geometric properties are as described in section 5.2.1. Here, different types of tapered section (models A, B, C, D, F and M) are considered in tapered beams. It should be pointed out that for Model D, the ply orientation at the right section is $(0)_{24}$. All the 90° plies are dropped. This differs from the other models. For models A, B, C, F and M, the orientation at the right end is still $[(0/90)_6]_S$.

The lowest four natural frequencies for simply supported, fixed-fixed, fixed-free and free-fixed boundary conditions for all types of taper models and different laminate configurations are given in Tables 5.10 to 5.13. Figure 5.9 shows the frequencies of the simply supported beam with LC1 laminate configuration.

Table 5.10 Effect of taper model on frequencies of simply supported beam

		Model A	Model B	Model C	Model D	Model F	Model M
LC1	ω_1	66133.1	64620.6	65064.2	75802.2	64924.3	64911
	ω_2	186581	190983	192733	208906	192926	192816
	ω_3	308455	320675	323902	342347	324783	324566
	ω_4	428395	448323	453002	473283	454631	454338
LC2	ω_1	53393.1	51711.3	51860	51435.4	51681.9	51672.5
	ω_2	165513	167474	168002	166710	167898	167797
	ω_3	286652	296026	296975	294830	297389	297146
	ω_4	407385	425033	426404	423435	427490	427126
LC3	ω_1	70938	69182	69307.7	62671	69160.4	69139
	ω_2	195280	199550	200067	188170	200240	200080
	ω_3	319684	331779	332725	318881	333514	333208
	ω_4	441907	461599	462964	447703	464397	463985

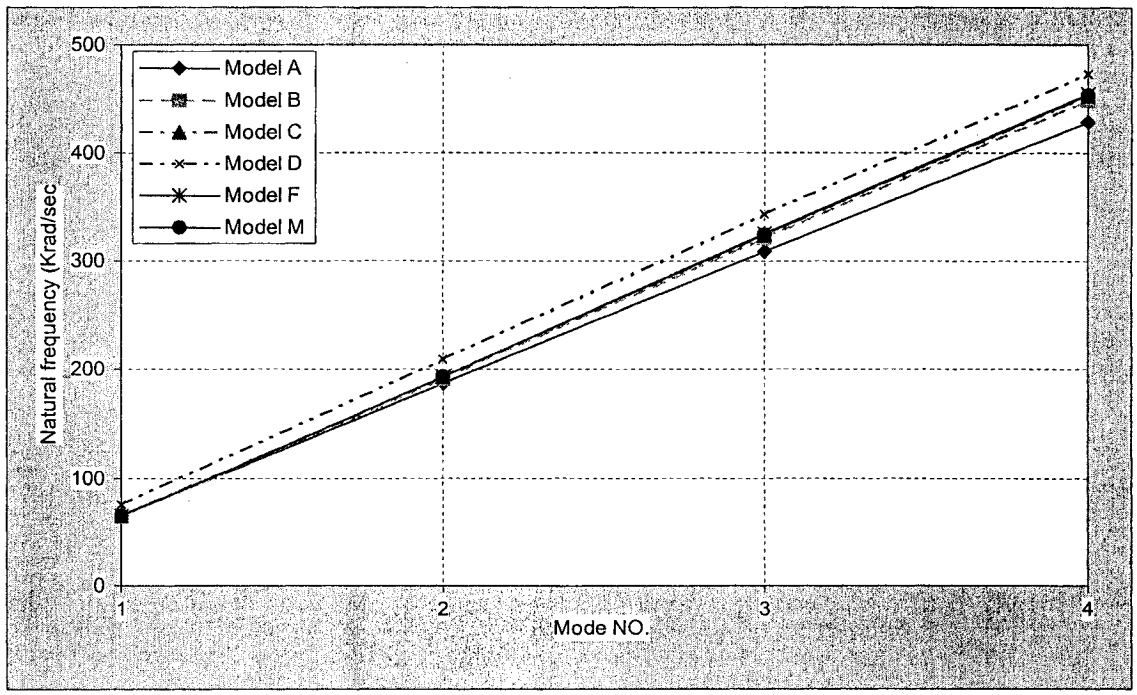

Figure 5.9 Effect of taper model on the natural frequencies for simply supported boundary condition and LC1 laminate configuration

Table 5.11 Effect of taper model on frequencies of fixed-fixed beam

		Model A	Model B	Model C	Model D	Model F	Model M
LC1	ω_1	96423.4	99369.9	100361	107187	100530	100465
	ω_2	199011	206148	208221	220511	208815	208612
	ω_3	315389	328405	331768	348552	332908	332604
	ω_4	432227	452312	457024	476396	458820	458458
LC2	ω_1	86936.9	88726	89024.8	88305.6	89035.4	88973
	ω_2	184915	190969	191586	190180	191916	191677
	ω_3	298254	309677	310663	308478	311424	311022
	ω_4	414449	432904	434285	431313	435601	435096
LC3	ω_1	100610	103433	103718	98706.6	103874	103781
	ω_2	206338	213254	213848	205020	214366	214086
	ω_3	325679	338553	339522	327420	340505	340089
	ω_4	445061	464926	466295	452059	467831	467333

Table 5.12 Effect of taper model on frequencies of fixed-free beam

		Model A	Model B	Model C	Model D	Model F	Model M
LC1	ω_1	34276.2	35621.6	36007.1	39171	35858.8	35852.2
	ω_2	116542	122287	123613	133537	123605	123498
	ω_3	233922	244276	246886	264130	247300	247050
	ω_4	354685	371589	375728	395546	376835	376494
LC2	ω_1	27575.4	28365.9	28510.1	28123.5	28367.4	28362.9
	ω_2	102565	106549	106983	105909	106866	106768.
	ω_3	212295	220811	221599	219787	221790	221493
	ω_4	331371	346201	347380	344787	348167	347709
LC3	ω_1	36350.3	37356.2	37476.4	34146	37324.8	37315
	ω_2	122184	127817	128241	120223	128245	128091
	ω_3	244027	254335	255115	242121	255562	255217
	ω_4	367483	384380	385556	370224	386692	386224

Table 5.13 Effect of taper model on frequencies of free-fixed beam

		Model A	Model B	Model C	Model D	Model F	Model M
LC1	ω_1	18532.7	17082.9	17117.3	21486.6	17055.1	17076.7
	ω_2	107202	104121	104816	119108	104922	105004
	ω_3	239135	242377	244477	264168	245013	245163
	ω_4	360474	372662	376179	396943	377416	377595
LC2	ω_1	14039.9	12897.2	12905.4	12880.3	12851.6	12868.2
	ω_2	91754.7	88572.5	88765.4	88228.6	88684.9	88757.6
	ω_3	217018	217960	218572	217057	218702	218837
	ω_4	339224	348335	349377	347003	350030	350192
LC3	ω_1	20708.7	19103.3	19110.3	16886.9	19042.7	19066.8
	ω_2	113428	110106	110261	102456	110331	110416
	ω_3	248871	251900	252476	239389	252870	253021
	ω_4	372397	384376	385404	370626	386357	386529

Figure 5.9 shows that the natural frequencies for tapered beam in which tapered section is made as model D gives the highest values for the natural frequencies. This result was expected from the geometry of the model D and the ply orientation of the particular beam. Model D has more horizontal layers in the tapered section. This can be seen from Figure 5.1. In this example, there are 48 plies in the thick section, which are dropped to 24 in the thin section. Furthermore, all the 0° plies are kept and all the 90° plies are dropped. As discussed in section 5.2.2, 0° ply has the largest bending stiffness coefficient while the 90° ply has the lowest. Therefore, for this particular beam, model D gives the highest values for the natural frequencies. If we change the orientations to $[(90/0)_{12}]_S$ and $(90)_{24}$ at the left and right sections respectively, Model D claims the lowest natural frequencies, for all the four types of boundary conditions. The frequencies are given in Table 5.14.

Table 5.14 Natural frequencies of Model D with $[(90/0)_{12}]_S$ *and* $(90)_{24}$ *configurations at the thick and thin sections*

	Simply-supported	Fixed-fixed	Fixed-free	Free-fixed
ω_1	36783.7	76191.6	27336.2	7212.58
ω_2	137498	166077	89194.2	65410.2
ω_3	254452	273393	183779	184415
ω_4	375872	388914	296775	307823

As can be seen from the above table, the natural frequency drops from 75802.2 rad/sec to 36783.7 rad/sec, more than fifty percent, for simply supported boundary condition. For fixed-fixed and fixed-free boundary conditions, the frequencies also decrease although not as much as that in the simply supported case. It drops from

21486.6 rad/sec to 7212.58 rad/sec for free-fixed case. Almost sixty-seven percent is dropped.

In this example, for the other configurations, LC2 and LC3, Model D does not have the highest natural frequency but the lowest. That is also because of the difference in the kept and dropped plies.

Moreover, the natural frequencies for models C, F and M are very close, which means that the resin near the mid-plane does not considerably affect the stiffness of the beam and this is the same observation as that obtained from the investigation of the tapered beam in the previous chapters.

5.3 Parametric study on the free vibration of tapered composite beams subjected to axial force

In this section, we will give some examples with different boundary conditions and models as those in Section 5.2, but the beams are subjected to axial forces. These axial forces are much smaller than the buckling loads of beams. As can be seen from Chapter 4 and the previous section, the results from both Ritz method and HFEM match so well. Therefore, in this section, only HFEM will be applied to the presented example problems.

5.3.1 Effect of boundary conditions

This problem is as same as that in Section 5.2.1 but the beam is subjected to compressive axial force.

Hereby, it is necessary to estimate the buckling load of this tapered composite

beam [1]. First of all, we calculate the buckling load of uniform beam having the same ply configuration as that at the thick section of this tapered beam:

$$N_{cr} = \frac{kA_{55}D_{11}m^2\pi^2}{m^2\pi^2 D_{11} + kA_{55}L^2} \tag{5.1}$$

For the uniform composite beam with ply configuration $[(0/90)_{12}]_S$, the transverse shear stiffness and bending stiffness are:

$A_{55} = 28090368\ \text{Nm}^{-1}$

$D_{11} = 2690.36\ \text{N.m}$

Then the lowest buckling load is:

$N_{cr} = 10733\ \text{KN}$

In order to ensure that the axial force applied to this tapered beam is much less than the buckling load, we limit the axial force N_x to 500 KN. It is one twentieth of N_{cr} of the uniform composite beam.

Table 5.15 gives the lowest four natural frequencies for different types of boundary conditions. The same twelve-elements and four-hierarchical-terms model is used. Figure 5.10 shows the graphical form of Table 5.15.

Table 5.15 The lowest four natural frequencies of tapered beam described in Section 5.3.1

	Simply-supported	Fixed-fixed	Fixed-free	Free-fixed
ω_1	61593.5	98354.7	32476.6	12610.1
ω_2	188422	204722	118427	100312
ω_3	318834	327146	241299	239665
ω_4	447117	451387	369519	370536

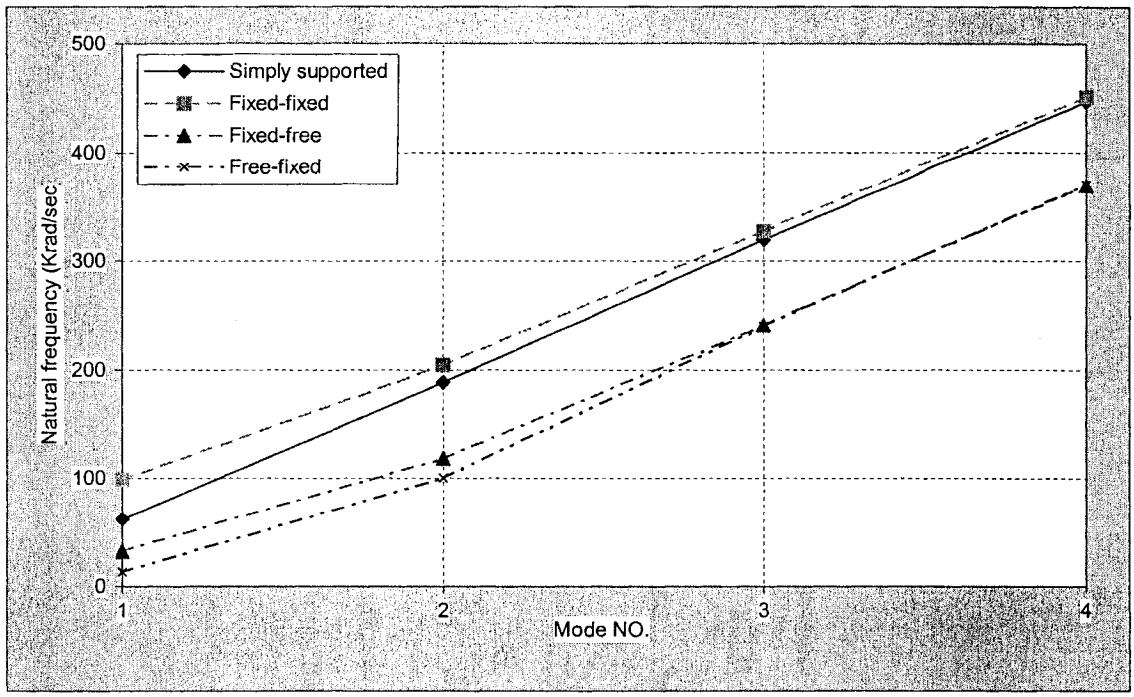

Figure 5.10 Effect of boundary condition on natural frequencies of the beam described in Section 5.3.1

Comparison between the results in Tables 5.2 and 5.15 shows that all the frequencies drop a little. The change of the boundary condition results in a considerable variation in the natural frequencies as same as those in the case without axial force. The natural frequencies for the fixed-fixed support are the highest, the second rank is for the simply supported case, the third rank is for the fixed-free case and the lowest values are for free-fixed support.

5.3.2 Effect of laminate configuration

The same problem described in section 5.2.2 is considered to investigate the effects of laminate configurations on the natural frequencies of composite beam subjected to axial force $N_x = 500\,\text{KN}$. Table 5.16 gives the lowest four natural frequencies for this problem. The 12E4T model is used.

Table 5.16 The natural frequencies of tapered beam subjected to axial force corresponding to different laminate configurations

		Simply-supported	Fixed-fixed	Fixed-free	Free-fixed
LC1	ω_1	61593.5	98354.7	32476.6	12610.1
	ω_2	188422	204722	118427	100312
	ω_3	318834	327146	241299	239665
	ω_4	447117	451387	369519	370536
LC2	ω_1	47412.3	86479.5	23289.0	5236.80
	ω_2	162640	187409	100152	83042.1
	ω_3	290815	305238	214704	212687
	ω_4	419438	427738	339970	342575
LC3	ω_1	66067.6	101794	34236.7	15226.7
	ω_2	195944	210402	123441	105965
	ω_3	327761	334900	249880	247704
	ω_4	457080	460576	379659	379667

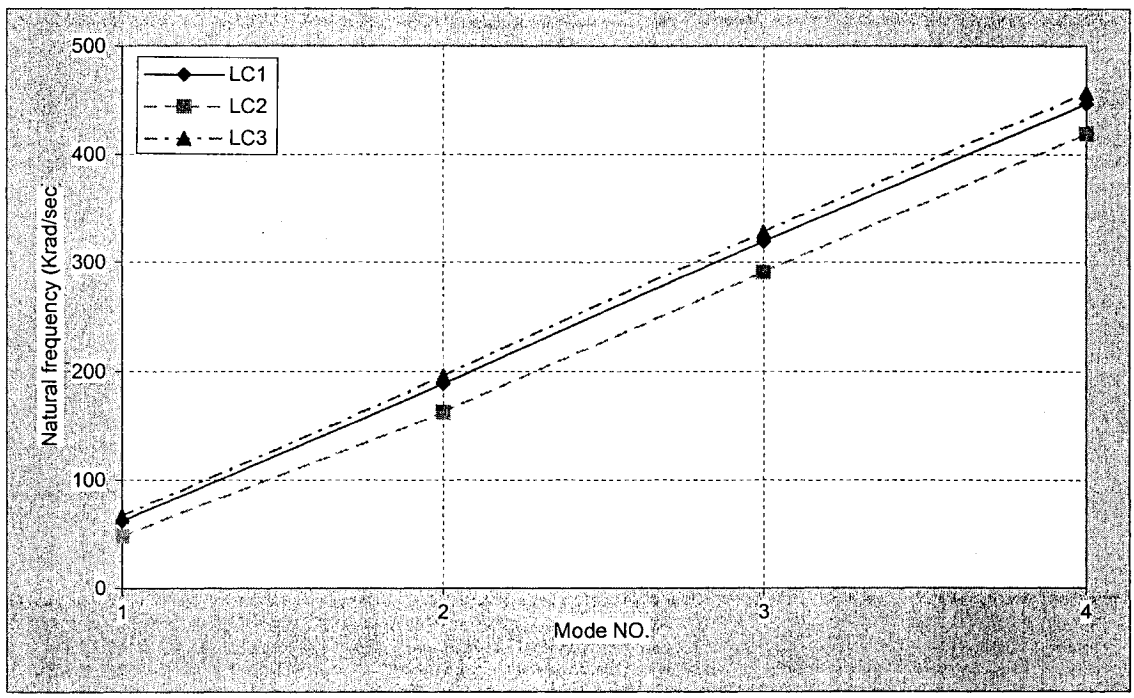

Figure 5.11 Natural frequencies of laminate configurations LC1, LC2 and LC3 subjected to axial force

It can be seen that for all the four types of boundary conditions, the natural frequencies for LC3 laminate configuration are the highest and the lowest values are

claimed by LC2 laminate configuration. The changes in natural frequencies for different configurations are due to the change in stiffness matrix for each configuration. It is similar to that in the case without axial force.

5.3.3 Effect of the taper angle

The problem given in this section is as same as that of section 5.2.3 but subjected to axial force $N_x = 500\,\text{KN}$. Taper angles have been increased from 0° (uniform) to 5.0165° to investigate the effect of taper angle on natural frequencies. Table 5.17 gives the effect of taper angle on the natural frequencies of tapered beam with simply supported boundary condition. Figure 5.11 is the graphical form of Table 5.17.

Table 5.17 Effect of taper angle on the natural frequencies of tapered beam subjected to axial force

Number of plies at the right section	Taper angle α °	ω_1	ω_2	ω_3	ω_4
48	0	78786.9	206516	332129	454905
40	0.9543	74541.7	202168	329154	453106
32	1.9090	68953.8	196552	325056	450422
22	3.1030	59391.7	185808	316654	445668
14	4.0592	48447.6	171519	303152	434938
6	5.0165	29492.2	144263	272229	404567

Observation from Table 5.17 and Figure 5.12 shows that increasing the taper angle leads to decreasing the natural frequencies. The decreasing tendency of natural frequencies is similar to that in the case without axial force, as discussed in the previous section. The slope of the curves in Figure 5.12 decreases very slowly at the beginning and faster along with the increasing of taper angle.

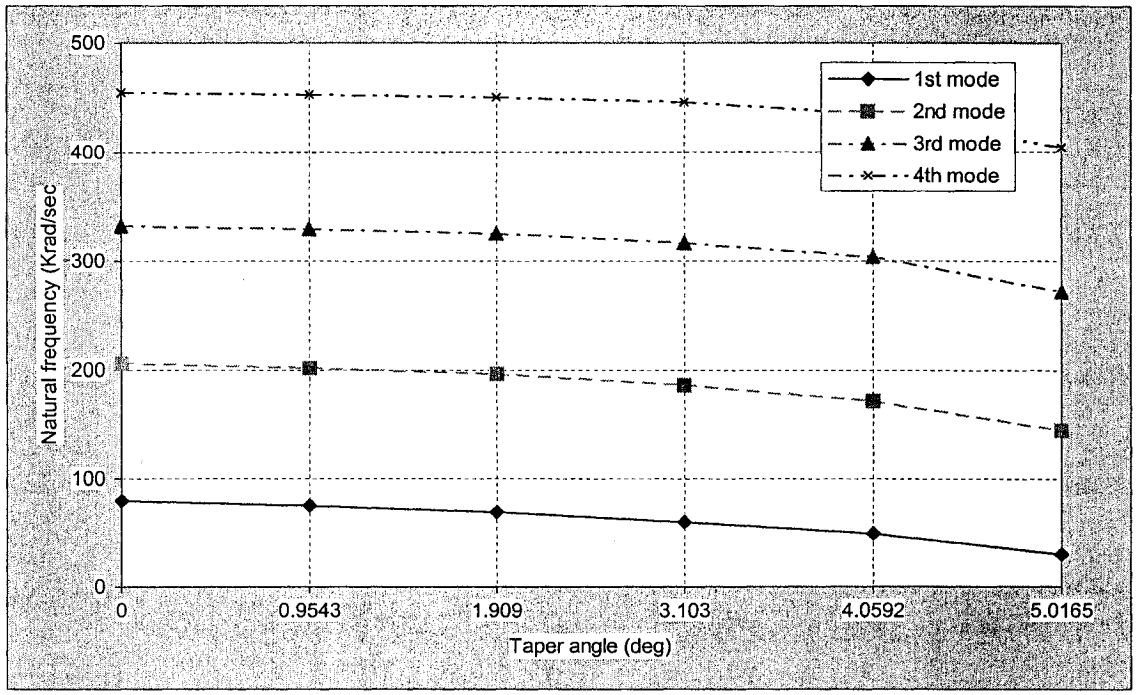

Figure 5.12 Effect of taper angle on the natural frequencies of tapered beam axial force

5.3.4 Effect of taper model

The problem given in this section is as same as that of section 5.2.3 but the beam is subjected to axial force $N_x = 500\,\text{KN}$. Here, different types of tapered section (models A, B, C, D, F and M) are considered in tapered beam.

The lowest four natural frequencies for simply supported boundary conditions for all types of taper model and different laminate configurations are given in Table 5.18 and Figure 5.13.

Table 5.18 Effect of taper model on frequencies for simply-supported beam subjected to axial force

		Model A	Model B	Model C	Model D	Model F	Model M
LC1	ω_1	62426.1	61237.2	61701.0	72989.0	61593.5	61580.0
	ω_2	181409	186386	188168	204818	188422	188312
	ω_3	301489	314587	317860	336770	318834	318615
	ω_4	419507	440626	445363	466129	447117	446822
LC2	ω_1	48692.7	47394.7	47555.4	47096.8	47412.3	47402.7
	ω_2	159592	162144	162686	161361	162640	162539
	ω_3	279092	289348	290313	288131	290815	290570
	ω_4	397996	416843	418235	415221	419438	419071
LC3	ω_1	67511.2	66054.4	66185.6	59193.7	66067.6	66045.9
	ω_2	190364	195190	195716	183518	195944	195783
	ω_3	312980	325930	326889	312767	327761	327453
	ω_4	433306	454155	455537	440002	457080	456665

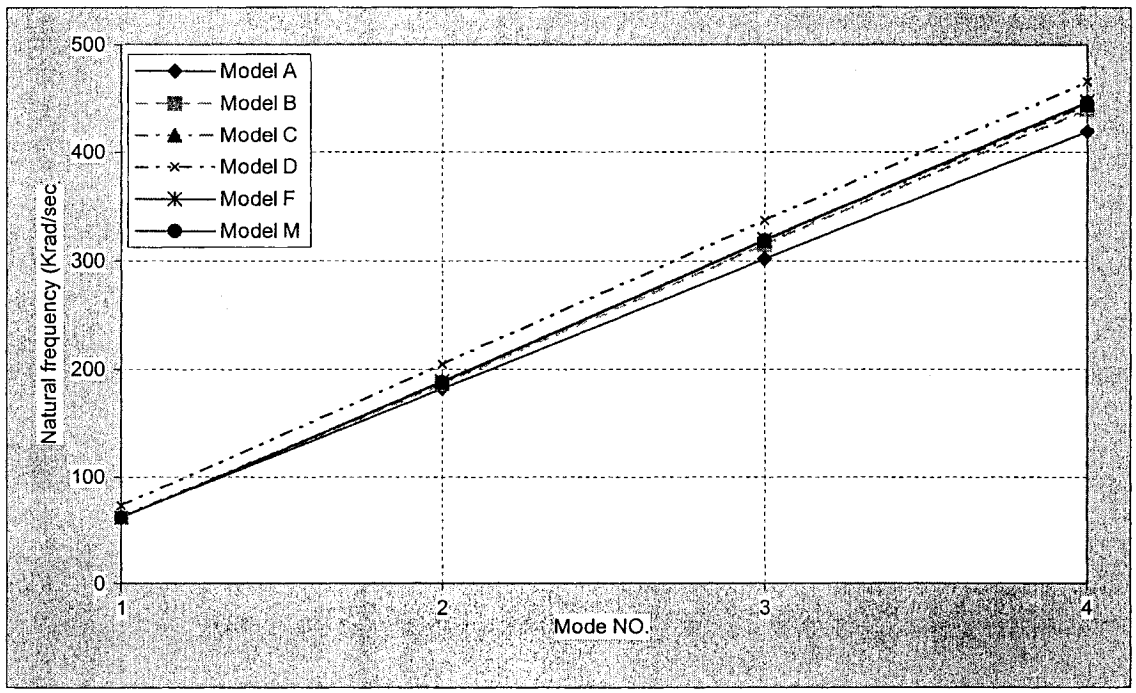

Figure 5.13 Effect of taper model on the natural frequencies corresponding to simply supported boundary conditions and LC1 laminate configuration subjected to axial force

Observation from Table 5.18 and Figure 5.13 shows that the natural frequencies for tapered LC1 beam in which tapered section is made as model D gives the highest values for the natural frequencies. It is because of the remained 0° plies and the dropped

90° plies. This conclusion is as same as that in the case without axial force, as discussed in the previous section. For the other configurations, LC2 and LC3, Model D does not have the highest natural frequency but the lowest. That is also because of the difference in the kept and dropped plies. Moreover, the natural frequencies for models C, F and M are also very close. This is the same observation that was obtained from the investigation of the tapered beam without axial force in the previous section.

5.3.5 Effect of compressive axial force

The problem given in this section is as same as that in Section 5.2.1 but the beam is subjected to compressive axial forces $N_x = 250\,\text{KN}$, $500\,\text{KN}$, $750\,\text{KN}$ and $1000\,\text{KN}$. In the next section, tensile axial force will be applied to the same beam to investigate the effect on the natural frequencies.

The lowest four natural frequencies for simply supported boundary condition for various axial forces are given in Table 5.19 and Figure 5.14.

Table 5.19 Effect of compressive axial forces on frequencies of simply supported beam

N_x	0	250 KN	500 KN	750 KN	1000 KN
ω_1	64924.3	63282.5	61593.5	59853.4	58057.0
ω_2	192926	190689	188422	186123	183790
ω_3	324783	321824	318834	315811	312754
ω_4	454631	450892	447117	443306	439456

Observation from Table 5.19 and Figure 5.14 shows that increasing the compressive axial force causes the decreasing of the natural frequencies. At the same time, the axial force has little effect on the natural frequencies. This is because the axial force we have applied is very small compared with the first buckling load of this beam

with simply supported boundary condition. Furthermore, the effects on the second, third and fourth mode frequencies are much smaller. This is because the axial force is much smaller than the second, third and fourth buckling loads.

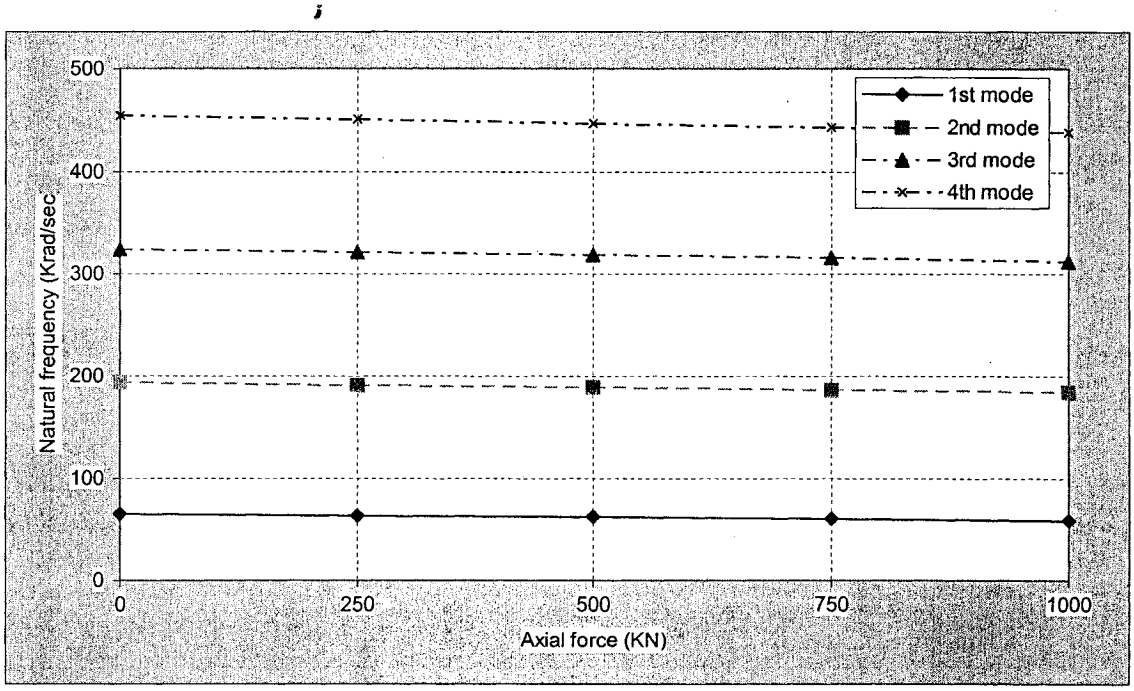

Figure 5.14 Effect of compressive axial forces on the natural frequencies of simply supported beam

We can expect that changing the boundary condition will also change the effect on the natural frequencies due to axial force.

The lowest four natural frequencies for fixed-fixed, fixed-free and free-fixed boundary conditions for various axial forces are given in Tables 5.20 to 5.22.

Table 5.20 Effect of compressive axial forces on frequencies of fixed-fixed beam

N_x	0	250 KN	500 KN	750 KN	1000 KN
ω_1	100530	99449.6	98354.7	97244.9	96119.4
ω_2	208815	206780	204722	202640	200534
ω_3	332908	330041	327146	324222	321267
ω_4	458820	455120	451387	447618	443812

Table 5.21 Effect of compressive axial forces on frequencies of fixed-free beam

N_x	0	250 KN	500 KN	750 KN	1000 KN
ω_1	35858.8	34251	32476.6	30490.3	28225.6
ω_2	123605	121060	118427	115698	112866
ω_3	247300	244325	24129	238221	235086
ω_4	376835	373200	369519	365791	362013

Table 5.22 Effect of compressive axial forces on frequencies of free-fixed beam

N_x	0	250 KN	500 KN	750 KN	1000 KN
ω_1	17055.1	15028.4	12610.1	9493.15	4345.44
ω_2	104922	102642	100312	97928.9	95490.8
ω_3	245013	242355	239665	236944	234190
ω_4	377416	373993	370536	367042	363512

Observation from Tables 5.20 to 5.22 shows that increasing the axial force causes the decreasing of the natural frequencies. At the same time, the axial force has little effect on the natural frequencies of the fixed-fixed beam. The reason is as same as that for the simply supported boundary condition. On the other hand, the first natural frequency for the free-fixed boundary condition drops a lot when $N_x = 1000\,\text{KN}$. This is because the axial force is close to the first buckling load. Meanwhile, N_x has just changed the second, third and fourth mode frequencies a little because it is much smaller than the second, third and fourth buckling loads.

5.3.6 Effect of tensile axial force

The problem given in this section is as same as the previous one but the beam is subjected to tensile axial forces $N_x = -250\,\text{KN}$, $-500\,\text{KN}$, $-750\,\text{KN}$ and $-1000\,\text{KN}$ instead of compressive axial force.

The lowest four natural frequencies for simply supported boundary condition for various axial forces are given in Table 5.23 and Figure 5.15.

Observation of Table 5.23 and Figure 5.15 shows that increasing the magnitude of the tensile axial force causes the increasing of the natural frequencies. At the same time, the axial force has little effect on the natural frequencies. This is because the axial force we have applied is not very large. Furthermore, the effects on the second, third and fourth mode frequencies are much smaller.

Table 5.23 Effect of tensile axial forces on frequencies of simply supported beam

N_x	0	-250 KN	-500 KN	-750 KN	-1000 KN
ω_1	64924.3	66522.8	68081.1	69602.1	71088.4
ω_2	192926	195134	197314	199466	201593
ω_3	324783	327712	330611	333482	336326
ω_4	454631	458335	462007	465645	469252

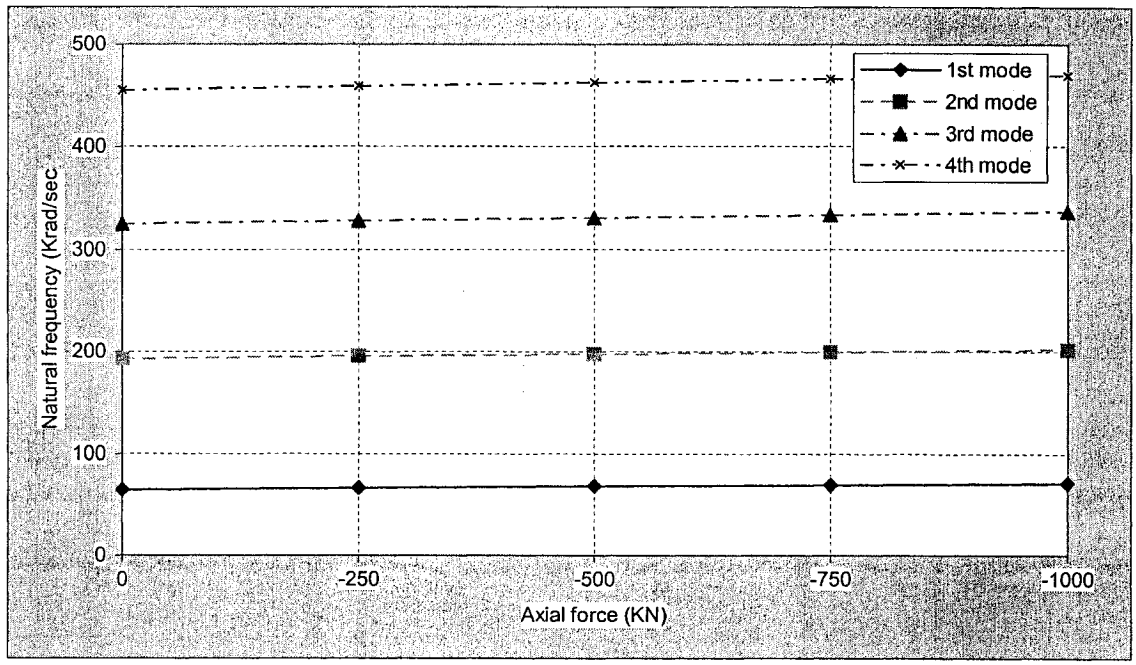

Figure 5.15 Effect of tensile axial forces on the natural frequencies of simply supported beam

The lowest four natural frequencies for fixed-fixed, fixed-free and free-fixed boundary conditions for various tensile axial forces are given in Tables 5.24 to 5.26.

Table 5.24 Effect of tensile axial forces on frequencies of fixed-fixed beam

N_x	0	-250 KN	-500 KN	-750 KN	-1000 KN
ω_1	100530	101597	102650	103691	104720
ω_2	208815	210828	212820	214791	216742
ω_3	332908	335747	338559	341346	344108
ω_4	458820	462485	466119	469720	473292

Table 5.25 Effect of tensile axial forces on frequencies of fixed-free beam

N_x	0	-250 KN	-500 KN	-750 KN	-1000 KN
ω_1	35858.8	37332.4	38695.6	39966.6	41159.4
ω_2	123605	126069	128458	130778	133034
ω_3	247300	250227	253108	255945	258741
ω_4	376835	380426	383974	387482	390951

Table 5.26 Effect of tensile axial forces on frequencies of free-fixed beam

N_x	0	-250 KN	-500 KN	-750 KN	-1000 KN
ω_1	17055.1	18822.7	20403.0	21840.2	23163.8
ω_2	104922	107156	109344	111489	113594
ω_3	245013	247642	250242	252815	255360
ω_4	377416	380805	384161	387485	390778

Observation from Tables 5.24 to 5.26 shows that increasing the magnitude of the tensile axial force causes the increasing of the natural frequencies. At the same time, the tensile axial force has little effect on the natural frequencies, even for the first mode frequency for free-fixed boundary condition. In the previous section, we have interpreted that when the compressive axial force is close to the buckling load, the beam becomes unstable and the natural frequency changes a lot. But in the case of tensile axial force, the natural frequency always increases regularly.

5.4 Conclusion and discussion

In this chapter a parametric study on the vibration of tapered composite beams has been conducted. Different types of tapered sections have been considered in tapered beams. The problems have been solved for different boundary conditions, various taper angles, different laminate configurations and various axial forces. The hierarchical finite element method and first-order shear deformation theory are imposed.

We conclude that besides the boundary conditions, the laminate configuration affects the natural frequency considerably. The 0° ply has the largest bending stiffness while the 90° ply has the lowest. This is why in Section 5.2.2 the composite beams having model D as tapered section provide the highest or lowest natural frequencies

compared to the other tapered sections. Consequently, the natural frequencies for models C, F and M are very close, because their kept and dropped plies are same and the resin near the mid-plane does not considerably affect the stiffness of the beam. Increasing the taper angle decreases the value of natural frequencies. The compressive axial force decreases the natural frequencies a little unless it is close to the buckling load. At the same time, the tensile axial force always increases the natural frequencies regularly.

Chapter 6

Conclusions and future work

In the present thesis an advanced finite element formulation has been developed for vibration analysis of tapered composite beams with and without axial force. The effect on the laminate stiffness of the composite beam caused by the taper angle has been considered. Different configurations of tapered beams, including mid-plane tapered as well as internally tapered beams have been investigated. The study of the vibration response has been conducted using Ritz method, conventional finite element formulation and hierarchical finite element method for both uniform-thickness and tapered composite beams based on both classical laminate theory and first-order shear deformation theory.

The taper angle of composite beam changes not only the geometric properties but also the stiffness of the oblique plies. Consequently, the mechanical behavior of tapered composite beam differs from that of uniform beam. The effect on the ply stiffness can be ignored if the taper angle is very small. Along with the increasing of the taper angle, this influence is not negligible.

Considering the effect of taper angle, the constitutive equations of motion of tapered composite beam with and without axial force have been derived. Then, based on these differential equations, the Ritz method, and the conventional and hierarchical FEM have been applied for mid-plane and internally tapered beams.

The conventional finite element model for the beam structure considers two degrees of freedom per node, viz. displacement and slope so as to satisfy the geometric boundary conditions. It was shown that the conventional finite element model for beams has some disadvantages: large number of elements are needed to achieve accurate results. Furthermore, the conventional FEM also faces the problem of shear lock for Timoshenko beam.

The hierarchical formulation enhances the capability of the element by making the degree of the approximating function to tend to infinity. Based on the classical laminate theory, the four cubic displacement modes used in the conventional formulation are retained and additional trigonometric terms are used. Based on the first-order shear deformation theory, the linear displacement and rotation modes are kept and trigonometric terms are added to both displacement and rotation modes.

The programming, involving symbolic and numerical computations, is done using MATLAB® software. At the end of each formulation, appropriate problems have been solved and the results are validated with the exact solutions if available. In the analysis of vibration, comparisons between the results obtained using Ritz method, conventional

formulation and hierarchical formulation are inherent in all the problems. To elaborate on the analysis in the present thesis, a parametric study using all the three types of formulations is provided.

The parametric study is carried out for the tapered composite beams with and without axial force to see the effects of various changes in the laminate parameters on the natural frequencies. These changes include the change in the boundary conditions, change in the laminate configuration, change in the taper angle, change in the type of internal taper and finally change in the axial force. The work done in the present thesis has provided some conclusions on the performance of the advanced finite element formulation, and manufacturing and design of the tapered composite beams. The important and principal conclusions are:

- The accuracy can be obtained more efficiently and rapidly by increasing the number of degrees of freedom in the element rather than increasing the number of elements of the same or fewer degrees of freedom. At the same time, it is necessary to increase the number of elements besides increasing the number of hierarchical terms.
- The advanced formulation uses fewer elements to obtain accurate results which itself leads to less expensive computational processes. This result is very important in vibration analysis especially in the computation of higher frequencies.

- In general, the Euler-Bernoulli beam element needs less number of elements to arrive at an accurate result whereas the Timoshenko beam element uses more elements to give an accurate result. This conclusion is valid for both conventional and advanced finite element formulations.
- The stiffness of the tapered composite beam depends on the geometric properties and the kept plies. The tapered beam model D (staircase-dispersed), could be the stiffest or weakest model according to different laminate configurations, hence this model gives the highest or lowest natural frequencies for all types of boundary conditions and geometries. In another words, we need to consider the composition of different models and laminate configurations in order to control the natural frequencies.
- The tapered beams designed using model C (overlapped- grouped), model F and model M are very similar in term of stiffness. This is because the kept and dropped plies are same and the dropped resin pocket or layers in these models are close to the mid-plane. The tapered beam model A usually is the least-stiff model.

The study on the vibration of the tapered laminates with and without axial force can be continued in the future based on the following recommendations:

1. The advanced finite element formulation presented in this thesis can be extended for the analysis of the forced vibration response of different types of laminated beams.

2. The advanced finite element formulation could be extended for the stress analysis, vibration and buckling of tapered laminated composite plates.
3. The effect of damping can be considered in the free and forced vibrations of tapered composite beams and plates.
4. The study in this thesis can be applied to design optimization of tapered composite laminates.

References

[1] Reddy, J.N., Mechanics of Laminated Composite Plates – Theory and Analysis, 1997, CRC Press, U.S.A.

[2] Whitney, J.M., Structural Analysis of Laminated Anisotropic Plates, 1987, Technomic Publishing Company, Lancaster, Pa.

[3] Bertholet, J.M., Composite Materials – Mechanical Behavior and Structural Analysis, 1999, Springer Verlag, New York.

[4] Jones, R. M., Mechanics of Composite Materials, 1975, Scripta Book Co., Washington.

[5] Krishnaswamy, S., Chandrashekhara, K. and Wu, W. Z. B., "Analytical Solutions to Vibration of Generally Layered Composite Beams", Journal of Sound and Vibration, Vol.159 (1), 1992, pp. 85-99.

[6] Noor, Ahmed K., "Free Vibration of Multilayered Composite Plates", AIAA Journal, Vol. 11, 1973, pp. 1038-1039.

[7] Miller, A. K. and Adams, D. F., "An analytic Means of Determing the Flexural and Torsional Resonant Frequencies of Generally Orthotropic Beams", Journal of Sound and Vibration, Vol.41, 1975, pp. 433-449.

[8] Teoh, L. S. and Huang, C. C., "Vibration of Beams of Fiber Reinforced Material", Journal of Sound and Vibration, Vol.51 (22), 1997, pp. 467-473.

[9] Chen, A. T. and Yang, T.Y., "Static and Dynamic Formulation of a Symmetrically Laminated beam Finite Element for a Microcomputer", Journal of Composite Materials, Vol.19, 1985, pp. 459-475.

[10] Chandrashekhara, K., Krishnamurthy, K. and Roy, S., "Free Vibration of

Composite beams including Rotary Inertia and Shear Deformation", Composite Structures, Vol. 14, 1990, pp. 269-279.

[11] Abramovich, A., "Shear Deformation and Rotary Inertia Effects of Vibrating Composite Beams", Composite Structures, Vol. 20, 1992, pp. 165-173.

[12] Banerjee, J. R., "Frequency equation and mode shape formulae for composite Timoshenko beams", Composite Structures, Volume 51, Issue 4, 2001, pp. 381-388.

[13] Banerjee, J. R., "Free Vibration of Axially Loaded Composite Timoshenko Beams using the Dynamic Stiffness Matrix Method", Composite Structures, Vol. 69(2), 1998, pp. 197-208.

[14] Cortinez, V. H. and Piovan, M. T., "Vibration And Buckling of Composite Thin-Walled Beams with Shear Deformability", Journal of Sound and Vibration, Volume 258, Issue 4, 5, 2002, pp. 701-723.

[15] Hodges, Dewey H., Atilgan, Ali R., Fulton, Mark V. and Rehfield, L.W., "Free Vibration Analysis of Composite Beams", Journal of the American Helicopter Society, Vol. 36 (3), 1991, pp. 36-47.

[16] Khedeir, A. A. and Reddy, J. N., "Free Vibration of Cross-ply Laminated Beams with Arbitrary Boundary Conditions", International Journal of Engineering, Vol.32 (12), 1994, pp. 1971-1980.

[17] Chandrashekhara, K. and Bangera, K. M., "Free Vibration of Composite Beam using a Shear Flexible Beam Element", Computers and Structures, Vol. 43(4), 1992, pp. 719-727.

[18] Eisenberger, M., Abramovich, H. and Shulepov, O., "Dynamic Stiffness Analysis of Laminated Beam Using a First Order Shear Deformation Theory", Composite

Structures, Vol. 31, 1995, pp. 265-271.

[19] Hjela, P. and Teboub, Y., "Free Vibration of Generally Layered Composite Beams using Symbolic Computations", Composite Structures, Vol. 33 (3), 1995. pp. 123-134.

[20] Singh, M. P. and Abdelnasser, A. S., "Random Response of Symmetric Cross-Ply Composite Beams with Arbitrary Boundary Conditions", AIAA Journal, Vol. 30(4), 1992, pp. 1081-1088.

[21] Zappe, J. A., and Lesieutre, G. A., "Vibration Analysis of Laminated Beams using an Iterative Smeared Laminate Model", Journal of Sound and Vibration, Vol. 199(2), 1997, pp. 275- 284.

[22] Farghaly, S. H. and Gadelrab, R. M., "Free Vibration of a Stepped Composite Timoshenko Cantilevered Beam", Journal of Sound and Vibration, Vol. 187 (5), 1995, pp. 886-896.

[23] Rao, S. R. and Ganesan, N., "Dynamic Response of Non-Uniform Composite Beams", Journal of Sound and Vibration, Vol. 200(5), 1997, pp. 563-577.

[24] Nabi, M. S. and Ganesan, N., "A Generalized Element for the Free Vibration Analysis of Composite Beams", Computers and Structures, Vol. 51(5), 1994, pp. 607-610.

[25] Karabelis, D. L. and Beskos, D. E., "Static, Dynamic and Stability Analyses of Structures Composed of Tapered Beams", Computers and Structures, Vol. 16(6), 1983, pp. 731-748.

[26] Tong, X., Tabarrok, B. and Yeh, K. Y., "Vibration Analysis of Timoshenko Beams with Non-homogeneity and Varying Cross-section", Journal of Sound and

Vibration, Vol. 186 (5), 1995, pp. 821-835.

[27] He, K., Hoa, S. V. and Ganesan, R., "The Study of Tapered Laminated Composite Structures: a review", Composites Science and Technology, Vol. 60(14), 2000, pp. 2643-2657.

[28] Abd EL-Maksoud, Mohamed A, "Dynamic Analysis and Buckling of Variable-Thickness Laminated Composite Beams using Conventional and Advanced Finite Element Formulations", M.A.Sc. Thesis, 2000, Concordia University.

[29] Zabihollah, Abolghassem. "Vibration and Buckling Analysis of Tapered Composite Beams Using Conventional and Advanced Finite Element Formulations", M.A.Sc. Thesis, 2003, Concordia University.

[30] Peano, A. G., "Hierarchies of Conforming Finite Elements for Plane Elasticity and Plate Bending", Computers and Mathematics with Applications, Vol. 2, 1976, pp. 211-224.

[31] Babuska, I., Szabo, B. A., and Katz, I. N., "The p-version of the Finite Element Method", SIAM Journal of Numerical Analysis, Vol. 18(3), 1981, pp. 515-545.

[32] Cook, R.D., Malkus, D. S. and Plesha, M. E., Concepts and Applications of Finite Element Analysis, 1989, Wiley Publishing Company, New York.

[33] Zienkiewicz, O. C., The Finite Element Method, 1979, McGraw-Hill, New York.

[34] Reddy, J.N., An Introduction to the Finite Element Method, 1993, McGraw-Hill, New York.

[35] Nickel, R. and Secor, G., "Convergence of Consistently Derived Timoshenko Beam Finite Elements", International Journal of Numerical Methods in Engineering, Vol.5, 1972, pp. 243-253.

[36] Dawe, D. J., "A Finite Element for the Vibration Analysis of Timoshenko Beams", Journal of Sound and Vibration, Vol.60 (1), 1978, pp. 11-20.

[37] Thomas, J. and Abbas, A. H., "Finite Element Model for Dynamic Analysis of Timoshenko Beam", Journal of Sound and Vibration, Vol. 41 (3), 1975, pp. 291-299.

[38] Thomas, J. L. and Dokumaci, E., "Improved Finite Element for Vibration Analysis of Tapered Beams", Aeronautical Quarterly, Vol. 24, 1973, pp. 39-46.

[39] To, C. W. S., "Higher Order Tapered Beam Finite Element for Vibration Analysis", Journal of Sound and Vibration, Vol. 63 (1), 1979, pp. 33-50.

[40] Cleghorn, W. L. and Tabarrok, B., "Finite Element Formulation of a Tapered Timoshenko Beam for Free Vibration Analysis", Journal of Sound and Vibration, Vol.152 (3), 1997, pp. 461-470.

[41] Shi, G., Lam, K. Y. and Tay, T. E., "On Efficient Finite Element Modeling of Composite Beams and Plates Using Higher Order Theories and an Accurate Composite Beam Element", Composite Structures, Vol. 41(2), 1998, pp. 159-165.

[42] Ramtekkar, G. S., Desai, Y. M., and Shah, A. H., "Natural Vibration of Laminated Composite Beams by using Mixed Finite Element Modeling", Journal of Sound and Vibration, Vol. 257(4), 2002,pp. 635-651.

[43] Rao, S. R., and Ganesan, N., "Dynamic Response of Tapered Composite Beams Using Higher Order Shear Deformation Theory", Journal of Sound and Vibration, Vol.187 (5), 1995, pp. 737-756.

[44] Han, W. and Petyt, M., "Linear Vibration Analysis of Laminated Rectangular Plates using the Hierarchical Finite Element Method – I: Free Vibration Analysis", Computers and Structures, Vol. 61, 1996, pp. 705-712.

[45] Han, W. and Petyt, M, "Linear Vibration Analysis of Laminated Rectangular Plates using the Hierarchical Finite Element Method – II: Forced Vibration Analysis", Computers and Structures, Vol. 61, 1996, pp. 713-724.

[46] Han, W. and Petyt, M., "Geometrically Non-Linear Vibration Analysis of Thin, Rectangular Plates using the Hierarchical Finite Element Method – I: The Fundamental Mode of Isotropic Plates", Computers and Structures, Vol. 63, 1997, pp. 295-308.

[47] Han, W. and Petyt, M., "Geometrically Non-Linear Vibration Analysis of Thin, Rectangular Plates using the Hierarchical Finite Element Method – II: 1st Mode of Laminated Plates and Higher Modes of Isotropic and Laminated Plates", Computers and Structures, Vol. 63, 1997, pp. 309-318.

[48] Rebeiro, P. and Petyt, M., "Non-Linear Vibration of Plates by the Hierarchical Finite Element and Continuation Methods", International Journal of Mechanical Sciences, Vol. 41, 1999, pp. 437-459.

[49] Rebeiro, P. and Petyt, M., "Non-Linear Vibration of Composite Laminated Plates by the Hierarchical Finite Element Method", Composite Structures, Vol. 46, 1999, pp. 197-208.

[50] Rebeiro, P. and Petyt, M., "Non-Linear Vibration of Beams with Internal Resonance by the Hierarchical Finite Element Method", Journal of Sound and Vibration, Vol. 224, 1999, pp. 591-624.

[51] West, L. J., Bardell, N. S., Dunsdon, J. M. and Loasby, P. M., "Some Limitations Associated with the use of K-Orthogonal Polynomials in Hierarchical Versions of the Finite Element Method", Structural Dynamics: Recent Advances (editors, Ferguson, N. S., Wolfe, H. F. and Mei, C.), The Institute of Sound and Vibration Research,

Southampton, 1997, pp. 217-227.

[52] Houmat, A., "An Alternative Hierarchical Finite Element Formulation Applied to Plate Vibration", Journal of Sound and Vibration, Vol. 206, 1997, pp. 201-215.

[53] Leung, A. Y. T., and Chan, J. K. W., "Fourier p-elements for the Analysis of Beams and Plates", Journal of Sound and Vibration, Vol. 212, 1998, pp. 179-185.

[54] Krahula, J. L., and Polhemus, J. F., "Use of Fourier Series in the Finite Element Method", AIAA Journal, Vol. 6, 1968, pp. 726-728.

[55] Barrette, M., Berry, A., and Beslin, O., "Vibration of Stiffened Plates Using Hierarchical Trigonometric Functions ", Journal of Sound and Vibration, Vol. 235(5), 2000, pp. 727-747.

[56] Nigam, Amit, "Dynamic Analysis of Composite Beams using Hierarchical Finite Element Method", M.A.Sc. Thesis, 2002, Concordia University.

[57] Poceski, A., Mixed finite element method, 1992, Springer-Verlag, New York.

[58] Ochoa, O.O. and Reddy, J.N., Finite element analysis of composite laminates, 1992, Kluwer Academic Publishers, Boston.

[59] Chen, H., "Failure Analysis of Laminated Composite Beams". M.A.Sc. Thesis, 2001, Concordia University.

[60] Shames, I. H. and Dym, C. L., Energy and Finite Element Methods in Structural Mechanics, 1985, McGraw-Hill, New York.

[61] Matthews, F. L., Davies, G. A. O., Hitchings, D. and Soutis, C., Finite Element Modeling of Composite Materials and Structures, 2000, CRC Press, Boca Raton, FL.

[62] Weaver, W. Jr., Timoshenko, S. P. and Young, D. H., Vibration Problems in Engineering, 1990, Wiley Publishing Company, New York.

[63] Kim, D. H., Composite Structures for Civil and Architectural Engineering, 1995, E & FN Spon, U. S. A.

[64] Botting, A. D., Vizzini, A. J. and Lee, S.W., "Effect of ply-drop configuration on delamination strength of tapered composite structures", AIAA Journal, Vol. 34(8), 1996, pp. 1650-1656.

[65] Meirovitch, L. and Bahruh, H., "On the inclusion principle for the hierarchical finite element method", International Journal of Numerical Methods in Engineering, Vol. 19, 1983, pp. 281-291.

[66] Petyt, Maurice, Introduction to Finite Element Vibration Analysis, 1990, Cambridge University Press, New York.

[67] Cheung, Y. K. and Leung, A. Y. T., Finite Element Methods in Dynamics, 1991, Kluwer Academic Publishers, New York.

[68] Altenbach, H., Altenbach, J. and Kissing, W., Mechanics of composite structural elements, 2004, Springer, New York.

[69] Decolon, Christian, Analysis of composite structures, 2002, Taylor & Francis, New York.

[70] Hyer, M.W., Stress analysis of fiber-reinforced composite materials, 1998, WCB McGraw-Hill, Boston.

[71] Tenek, L.T. and Argyris, J., Finite element analysis for composite structures, 1998, Kluwer Academic Publishers, Boston.

Appendix

Taper models of laminated composite beam

Model A

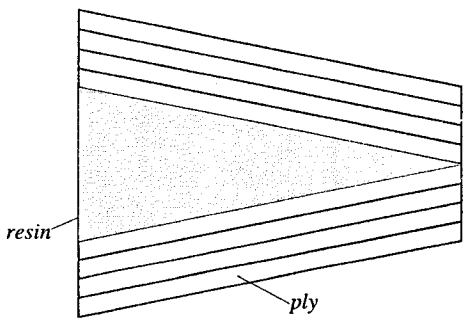

Model B

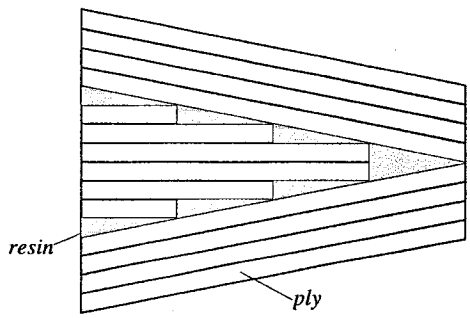

Model C

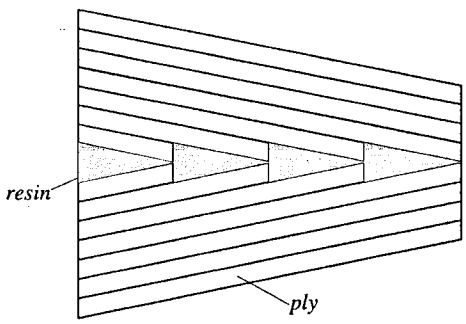

Model D

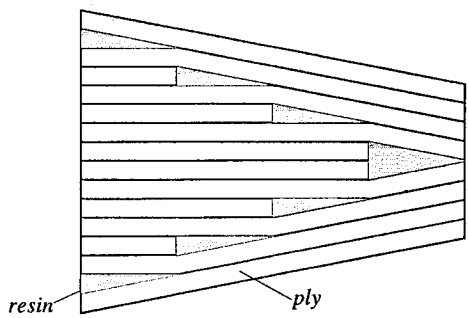

Model F

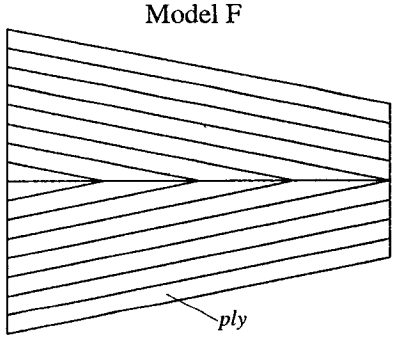

Model M